CAPACITY RATING OF THE LOS ALAMOS CANYON ARCH BRIDGE

2005 FINAL REPORT
LA-UR-05-2670

Prepared for:

University of California
Los Alamos National Laboratory
Utilities and Infrastructure
NWIS-UI, MS-K718
Los Alamos, NM 87545

Prepared by:

David V. Jáuregui, PhD
Nguyenngoc Tuyen, MS
Kenneth R. White, PhD, PE

New Mexico State University
Department of Civil Engineering
Hernandez Hall, Box 30001, MS 3CE
Las Cruces, NM 88003

May 2005

ABSTRACT

CAPACITY RATING OF THE LOS ALAMOS CANYON ARCH BRIDGE

by

David V. Jáuregui, PhD
Nguyenngoc Tuyen, MS
Kenneth R. White, PhD, PE

New Mexico State University
Las Cruces, New Mexico, 2005

The Omega Bridge is a riveted steel arch bridge built in the early 1950s to cross the Los Alamos Canyon and connect the town of Los Alamos, NM to technical areas of the Los Alamos National Laboratory (LANL). With just one other immediate route through the canyon, the Omega Bridge is a major crossing for LANL business. The alternate route is approximately two miles long on a curvy, steep grade which is not a suitable option for emergency vehicles such as fire trucks.

In the early 1990s, the Omega Bridge was rehabilitated due to the poor condition of the deck and increased traffic demands which resulted in several changes to the original structure. This report provides the load rating results of the bridge as affected by the rehabilitation according to the Load Factor Rating (LFR) Method specified by the American Association of State Highway and Transportation Officials (AASHTO). Attention is given to the superstructure elements including the floor system (stringers, floor beams, and spandrel beams); columns (pier, skewback, and arch columns); and two-hinge, parabolic arch rib. Live loads used to rate the bridge components include

the AASHTO HS-20 design truck; AASHTO legal loads (Type 3, Type 3-3, and Type 3S2); and “emergency-one titan fire truck” specified by LANL.

Of the three floor system components, the floor beams were found to control the capacity rating; the stringers and spandrel beams all had rating factors exceeding one at the inventory and operating level. Several floor beams had inventory rating factors less than one for design and fire truck loading; however, the operating ratings for these two trucks as well as all the rating factors under legal loads were larger than one. Because of the uncertainty of the riveted connection stiffness at the column ends, two separate models were developed to obtain the column rating factors. Smaller rating factors resulted when the column connections were assumed to be rigid rather than pinned due to beam-column behavior. All the pier and skewback columns were found satisfactory since their rating factors were larger than one. The rating factors for several arch columns at inventory level under design, legal, and fire truck loading were all less than one; however, they were all larger than one at the operating level for all five trucks. Unlike the rating factors of the columns, the rating factors of the arch rib were not much different between the two separate connection models (i.e., rigid and pinned). All rating factors for the arch rib exceeded one indicating that the arch rib capacity was satisfactory.

In summary, the Omega Bridge was found to be in satisfactory structural condition and no load posting was necessary. Furthermore, the operating ratings for all

superstructure components under the fire truck were larger than one indicating that the bridge was safe for the passing of the emergency vehicle. However, there were some concerns for the floor beams and the arch columns at the inventory rating level. As a result, more frequent inspection of the critical floor beams and arch columns than the two-year interval is recommended as well as traffic monitoring for overloads.

TABLE OF CONTENTS

LIST OF TABLES

LIST OF FIGURES

CHAPTER 1

BRIDGE BACKGROUND

1.1 Introduction

The Los Alamos Canyon Bridge (also called the Omega Bridge) is a riveted, steel arch bridge that carries north and south bound traffic on Diamond Drive (NM 501) over the Los Alamos Canyon between the town of Los Alamos, New Mexico and technical areas of the Los Alamos National Laboratory (LANL). With just one other immediate route through the canyon, the Omega Bridge is a major laboratory crossing with an average daily traffic (ADT) of approximately 23,000 vehicles / day and average daily truck traffic (ADTT) of approximately 500 vehicles / day. About 14% of the ADT occurs during the morning hour from 7 am to 8 am (south bound) and evening hour from 5 pm to 6 pm (north bound) as LANL employees commute to and from work. As shown in Figure 1.1, the alternate route runs through the canyon on West Road, which entails approximately 3.1 km (1.9 miles) of additional travel on a steep grade. For emergency vehicles such as fire trucks, the West Road detour is not a suitable option for obvious reasons. Hence, the primary objective of the study reported herein was to determine the current capacity level of the Omega Bridge, so that more reliable decisions could be made by the LANL regarding the safety of the bridge under modern traffic loads. To achieve this objective, a conventional rating analysis was performed according to the Load Factor Rating (LFR) Method specified in the American Association of State Highway and Transportation Officials (AASHTO) *Manual for Condition Evaluation of Bridges* (2000).

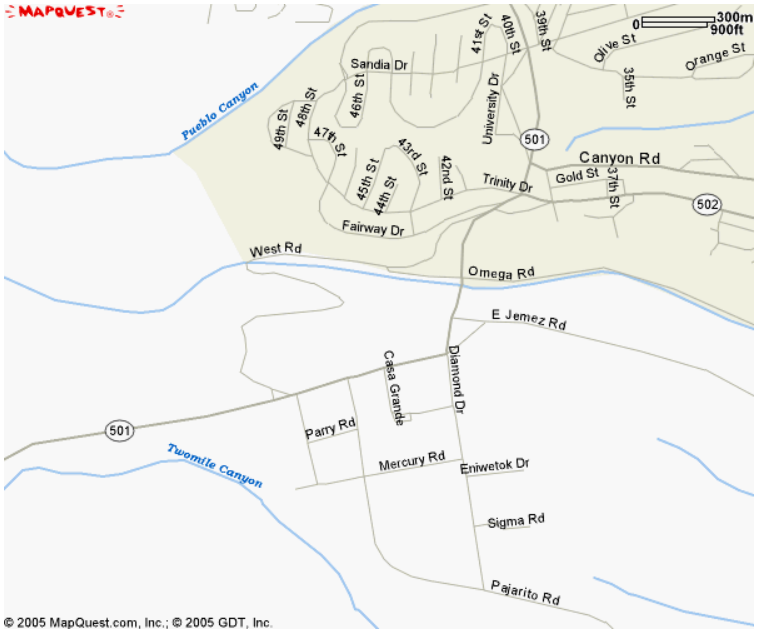

Figure 1.1 Location of Omega Bridge and West Road detour.

The Omega Bridge was designed by Finney and Turnispeed, fabricated by the American Bridge Company, and erected by the Vinson Construction Company in 1951. As shown in Figure 1.2, the bridge is 820 ft. long with a 442.5-ft. arch span and six 62-ft. approach spans (there are three approach spans at each end of the bridge).

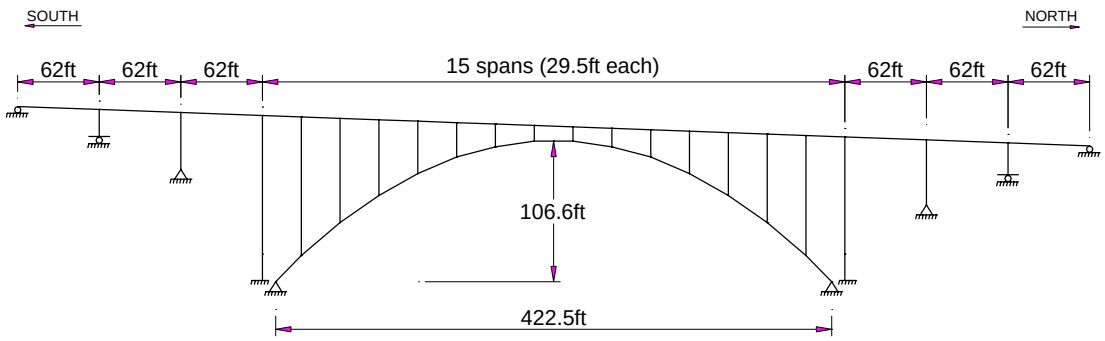

Figure 1.2 Elevation view of the Omega Bridge.

The bridge was originally designed for H-20 vehicular live load based on the ASD (Allowable Stress Design) Method specified in the 1944 AASHO (American Association of State Highway Officials) Specifications. Normal weight concrete with a compressive strength of 3000 psi and Grade 40 reinforcement was used for the deck; for the superstructure, ASTM A7 (F_y = 33 ksi) steel was used. Composite action, by means of mechanical shear connectors, was not provided between the deck and the superstructure in the original design. The cross-section of the bridge floor system before its major repair in 1992 had an overall width of 51'–3 ½", which included a 39'–9" wide roadway and a 7'–6" wide pedestrian walkway (see Figure 1.3). The roadway had no shoulders and four lanes, each having a width of 9'–11 ¼"; the narrow lanes caused significant delays to traffic flow over the bridge, especially during peak traffic hours. The walkway was separate from the steel superstructure and consisted of a pre-cast concrete double tee supported by a steel bracket secured to the west spandrel beam. Figure 1.3 shows the walkway after it was repaired in 1983; in the original cross-section, the reinforced concrete deck simply extended past the west spandrel beam to carry pedestrian traffic. For reasons discussed later, the original cantilever deck overhang was replaced with the walkway configuration shown in Figure 1.3. Starting from 1983, the floor system remained as shown in the figure until it was rehabilitated in 1992.

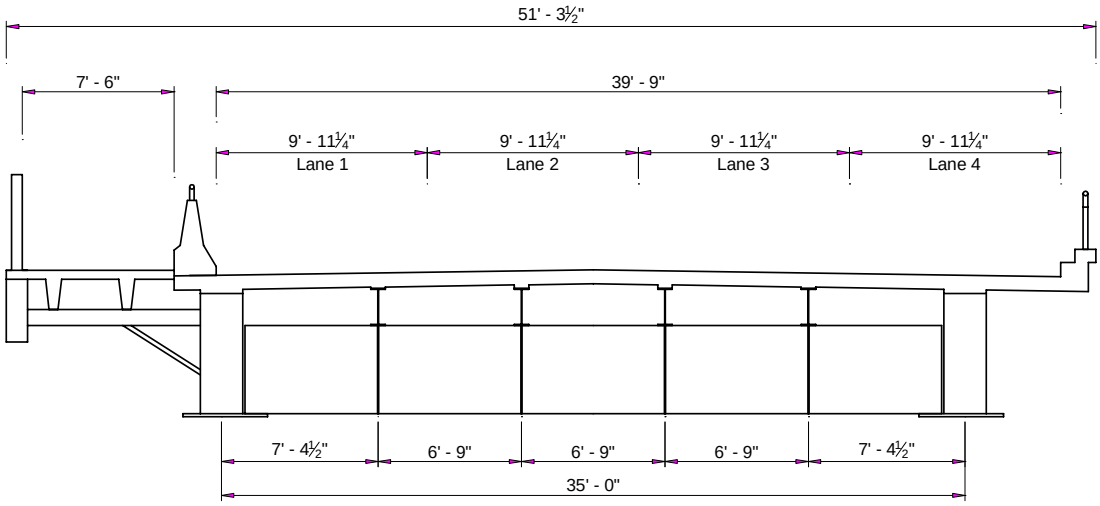

Figure 1.3 Cross-section of floor system before rehabilitation in 1992.

1.2 Past Inspection and Evaluation Studies

Since the early 1970s, several engineering studies have been performed by various consultants related to the physical condition and structural integrity of the Omega Bridge (Merrick & Company, 1989). The first significant study of the bridge was carried out by HNTB (Howard Needles Tammen & Bergendoff) Corporation in 1973, which included an in-depth bridge inspection and a structural analysis of the deck and steel superstructure. The major observations made from the inspection were (1) the overall structure was in good condition; (2) the number of missing rivets was minimal; (3) the test strength of the steel was more characteristic of ASTM A36 steel (F_y = 36 ksi) rather than ASTM A7 steel (F_y = 33 ksi) as specified in the design; and (4) the use of de-icing salts coupled with the poor concrete casting techniques used in the original construction was deteriorating the deck. From the structural analysis, HNTB Corporation found that (5) the deck was overstressed by 29% under the

existing dead loads and H-20 live loading; (6) the steel members were also overstressed but to a lesser degree than the deck; (7) the H-20 vehicular live load used in the original design was consistent with the type of truck loads currently (i.e., 1973) traveling over the bridge; and (8) the member stresses would increase under the HS-20 vehicular live load specified for new bridge designs.

Approximately 10 years after the investigation by HNTB Corporation, two studies were performed by Holmes and Narver in 1983 with assistance from New Mexico State University (NMSU) which focused on assessing the structural condition of the original deck and pedestrian walkway. The first major deficiency identified for the study was that the deck was structurally adequate only for H-15 vehicular live load, although the records showed that the original design had been based on H-20 vehicular live load. As a result, significant repair or total replacement of the deck was recommended. The second major deficiency found was that the overhanging portion of the deck which served as the walkway was improperly constructed, causing excessive sag and concern for public safety. Consequently, construction plans were drawn up by Holmes and Narver to replace the walkway, which was completed in 1983 (see Figure 1.3).

As noted above, the previous investigations of the Omega Bridge concluded that the deck was deteriorated and overstressed. Accordingly, a study was performed in 1988 by Merrick & Company to come up with various alternatives along with construction

cost estimates for rehabilitating the bridge. Based on information provided in that rehab study, the LANL opted to replace the entire deck and to retrofit the remaining components of the floor system to meet the current AASHTO and NMSHTD (New Mexico State Highway and Transportation) standards. The following year, Merrick & Company continued the rehabilitation project starting with a feasibility study of three deck replacement alternatives including a normal-weight concrete deck; a light-weight concrete deck; and a light-weight, concrete filled steel grid deck. Using a three-dimensional structural analysis program, the level of stress in the bridge members under dead load and HS-20 vehicular live load (plus impact) was evaluated for the three deck replacement alternatives. The analysis showed that the light-weight concrete deck alternative resulted in the lowest member stresses and thus, would require the least work to retrofit. Ultimately, Merrick and Company decided on a light-weight, reinforced concrete deck with stay-in-place metal decking.

In 1992, the floor system of the Omega Bridge was rehabilitated, resulting in the cross-section shown in Figure 1.4. The rehabilitation increased the width of the cross-section from 51'–3 ½" to 55'-6" and the roadway from 39'–9" to 44'–0" in order to provide four 11' – 0" wide traffic lanes (the original lanes had a width of 9'–11 ¼"). Other major rehabilitation work done on the bridge included: (1) light-weight concrete with a 28-day compressive strength of 4.5 ksi was used for the deck; (2) shear studs were installed on the interior stringers and spandrel beams to provide composite action with the deck; (3) cover plates were added to the interior stringers

and spandrel beams for additional moment capacity; and (4) exterior stringers supported by outrigger beams were added on both sides of the bridge width. A more detailed description of the Omega Bridge is provided in Chapter 2.

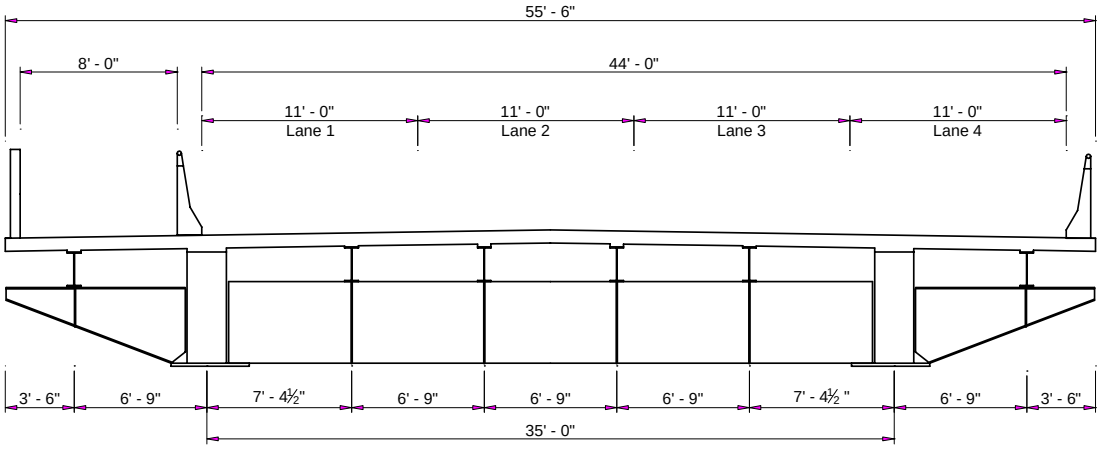

Figure 1.4 Cross-section of floor system after rehabilitation in 1992.

Since the early 1980s, NMSU has conducted regular in-depth inspections of the Omega Bridge every 2 or 3 years in accordance with NBIS (National Bridge Inspection System) Standards. The most recent inspection was completed in the summer of 2003; both the superstructure and substructure were rated as “fair” during that inspection. No major deficiencies were found with the superstructure, only isolated areas of corrosion on the arch ribs, spandrel beams, and bracing members. Cleaning and painting of these rusted areas was recommended within five years. During the substructure inspection, minor cracking, scaling, and spalling (with evidence of leaching) was discovered in the concrete abutments and piers; the most significant deterioration was found at the skewback concrete columns and footings, which had cracks up to ¼” wide with moderate leaching and spalling. At the time of

the inspection, major repairs were being made to seal the cracks in the substructure. Overall, the inspection found no major deficiencies which would influence the load rating of the Omega Bridge. Ultimately, the physical condition of the Omega Bridge observed from the inspection was documented in virtual reality format. This inspection record was referenced frequently throughout the AASHTO load rating analysis of the bridge and proved to be an extremely helpful aid, particularly for interpretation of the as-built construction plans.

CHAPTER 2

BRIDGE DESCRIPTION

2.1 Floor System

The floor system includes a reinforced concrete slab, six stringers, 28 floor beams and two spandrel beams. Figure 2.1 shows the cross-section while Figure 2.2 shows the overall plan view of the bridge floor system. As shown in Figure 2.1, the total width of the bridge deck is 55'–6" (out-to-out) and includes a 44'–0" roadway with four traffic lanes (each lane has a width of 11'–0") and an 8'–0" sidewalk on the west side. The slab concrete is light-weight with a density of w_c = 120 pcf and a 28-day compressive strength of f_c' = 4500 psi. The thickness of the slab is t_s = 7.25" which includes a 0.5-in. integral wearing surface. The transverse reinforcement consists of top and bottom mats of #5 bars placed at a spacing of 6.5". The longitudinal reinforcement consists of a top mat of #3 bars spaced at 9" and a bottom mat of #4 bars spaced at 6" or 9" as shown in Figure 2.1.

Bridge appurtenances include a sidewalk railing; west and east guardrails; fencing and light poles; and electric and steam utilities. The dead load estimates for these accessories given in Table 2.1 were furnished by the LANL based on the original design and rehabilitation drawings and subsequently field verified. These dead weights were increased by 4% to account for miscellaneous details. With the exception of the fencing, the weights of the accessories were distributed over the entire length of the bridge. The fencing is located on the 150-ft. center portion of the

bridge length on each side of the bridge width and was thus, distributed only over that region of the bridge. Details of the stringers, floor beams, and spandrel beams are discussed in subsequent sections.

Table 2.1 Weight estimate of bridge appurtenances.

Sidewalk Railing 4-L4"X3"X5/16"=4(7.2plf)=28.8plf 1-5WF16 @3.54'/9.83'=5.76plf 1-5C6.7=6.7plf 1-Plate 9.1875"X0.3125"=9.74plf 1-Base Plate 10"X1"X10.5"X1/9.83'=3.03plf 1-Base Plate 10"X3/4"X10.5"X1/9.83'=2.27plf 1-Base Plate 8"X5/8"X8"X1/9.83'=1.15plf 2-Conn Plate 2X5"X3/8"X3.875"@1/9.83'=0.42plf 6-Conn Plate 6X3.25"X3/8"X3.875"@1/9.83'=0.82plf 4-Anchors 4X1"DiaX 8.25"X1/9.83'=0.75plf Subtotal=59.44plf **West Guardrail** 1-Pipe 4" Dia=10.79plf 1-Plate ½"X10"X4.25"@1/8.33'=0.72plf 1-Plate ½"X5.5"X8.5"@1/8.33'=0.80plf 1-Bent Plate 18.25"X1/4"X12"@1/8.33'=1.86plf 1-Anch Bolt ½" DiaX 8.5"@1/8.33'=0.06plf Subtotal=14.23plf **East Guardrail** 2-Pipe 3.5"Dia=18.22plf 1-Plate ½"X1.83'X4"@1/8.33'=1.50plf 1-Plate ½"X5.5"X9"@1/8.33'=0.84plf 1-Bent Plate 18.25"X1/4"X12"@1/8.33'=1.86plf 1-Anch Bolt ½" DiaX 8.5"X1/8.33'=0.06plf 1-Splash Plate ¼"X9"=7.66plf Subtotal=30.14plf **Fencing** 4-Pipe 2"Dia @ 150'=2190lbs 1-Pipe 3" Dia @ 12/10' X 150'=1364.4lbs 1-Fencing 0.1483"X6/1'X12'X150'=635.35lbs 2-Conn Plate 2X0.375"X8"X8"@1/10'X150'=204.00lbs 2-Bent Plate 2X0.25"X13"X6"@1/10'X150'=165.75lbs Subtotal=4559.5lbs (one side – distributed on center 150' of bridge) Subtotal=9119.0lbs (both sides – distributed on center 150' of bridge)	**Light Pole** 6-Poles 5" Ave Dia X26.5'X1/814.5'=2.85plf 6-Poles 5" Ave Dia X25.25'X1/814.5'=2.72plf 12-Light Arms 3" DiaX 8'X1/814.5'=0.89plf 12-Lamps (Assume 15lbs each)X1/814.5'=0.22plf 2-Conduit 2" Dia=7.30plf Subtotal=13.98plf **Electric Utility** 3-Conduit 2" Dia=10.95plf 2-Conduit 5" Dia=29.24plf 1-Conduit 1.25" Dia=2.27plf Subtotal=42.46plf **Steam Utility** 1-Steam Pipe 10"Dia=40.48plf 1-CondensatePipe 4"Dia + π(1.913"X1.913")/144in^{2}X62.4pcf =14.98plf+4.98plf=19.96plf 1-Asbestos Insulation π {[(8.375")^2 - (5.375")^2]/144}153pcf=137.69plf 1-Asbestos Insulation π {[(4")^2 - (2.25")^2]/144}153pcf =36.51plf Hangars—Assume 10% of pipe=4.05plf Subtotal=238.69plf

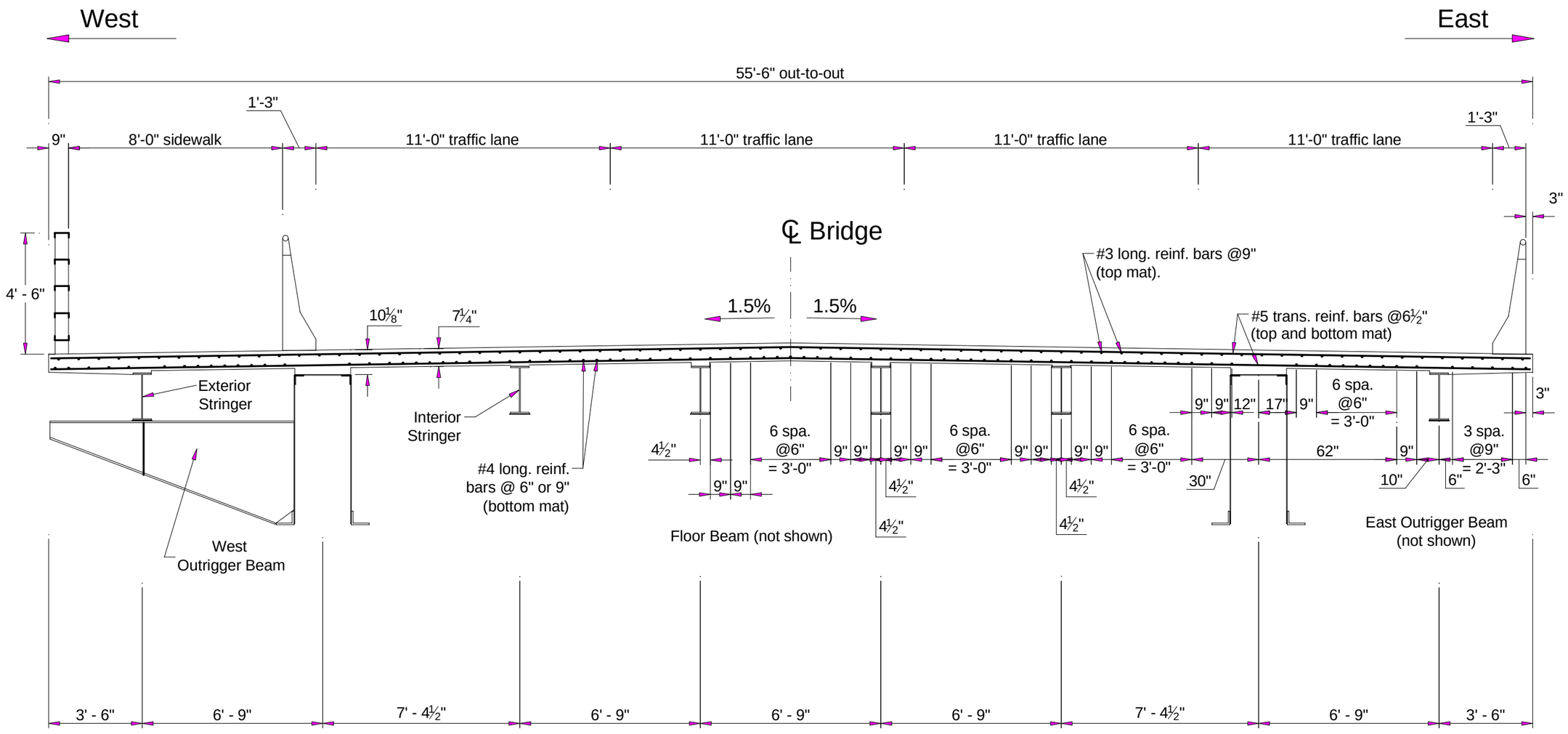

Figure 2.1 Cross-section of the floor system.

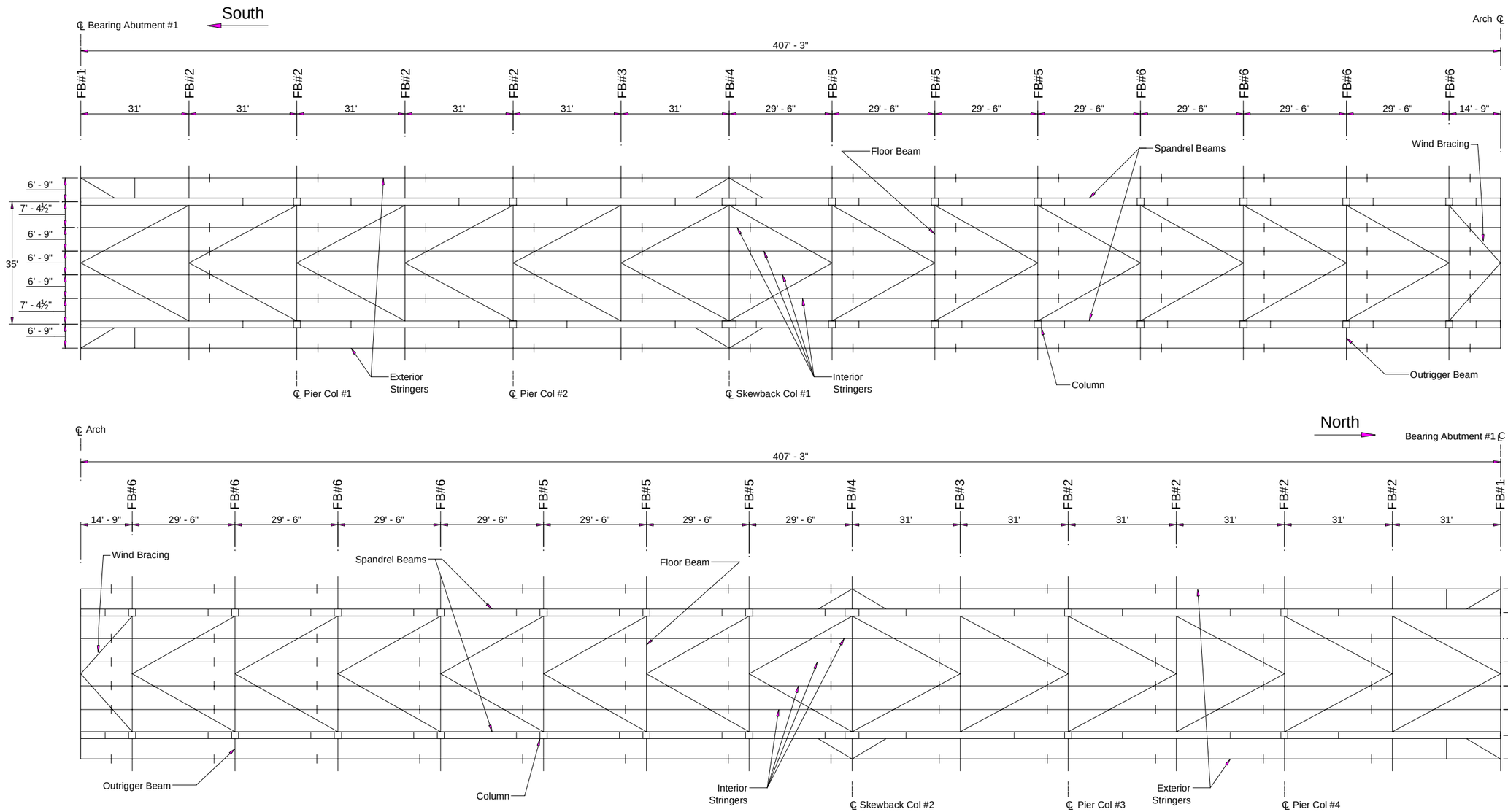

Figure 2.2 Overall plan view of floor system.

2.1.1 Stringers

Each stringer is a continuous beam supported at the locations of the floor beams over a total of 27 spans as shown in Figure 2.2. The 12 spans on the approach to the arch (six on both the north and south ends) each have a length of 31’–0” while the remaining 15 spans over the arch have a length of 29’–6”.

The two exterior stringers are W21x62 sections (ASTM A36 steel) with no cover plates, which were installed during the 1992 retrofit. Shear studs are distributed only in the first span on the north and south ends of the stringers as shown in Figure 2.3. Therefore, only the positive moment regions in the end spans are composite; the remaining length of the stringers is non-composite. The stud spacing is 9” over a distance of 10’–6” from each end and changes to 11” over the remaining distance of 19’–3”. The studs terminate 3” from the centerline of the outrigger beams.

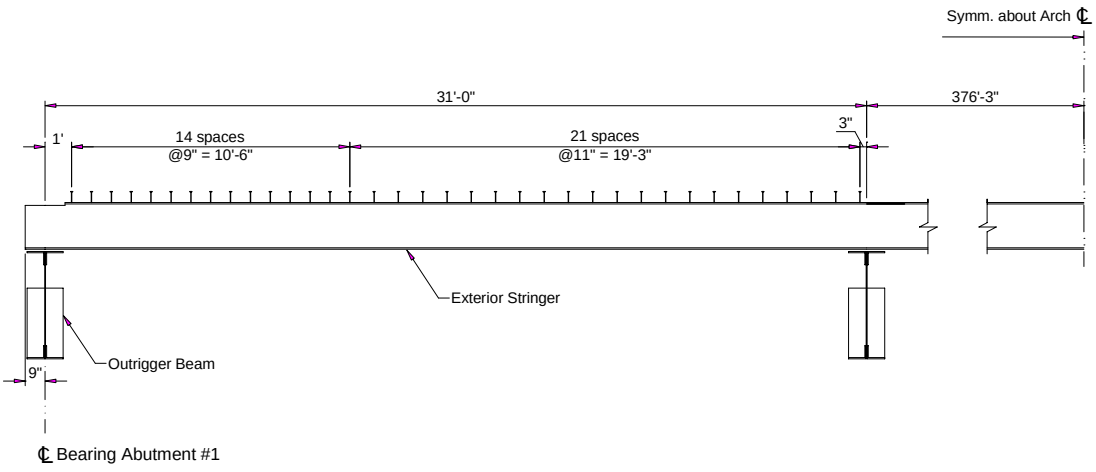

Figure 2.3 Exterior stringer layout.

The four interior stringers are W21x62 sections (ASTM A7 steel), which were installed when the bridge was originally built in 1951. Shear studs are provided only in the positive moment regions of the first and sixth spans and in the negative moment regions at the floor beam locations above the pier and skewback columns on the approach to the arch as shown in Figure 2.4. The spacing of the shear studs is most dense (i.e., @ 7") in the negative moment regions over the floor beams. In the positive moment regions, the studs are spaced similar to that of the exterior stringer with the exception of the 7" spacing close to the first interior floor beam. Cover plates of ASTM A7 steel with dimensions of $^{3}/_{8}$"x7"x14'–0" were provided in the original design in the end spans (both top and bottom flanges) starting at a distance of 6 ft. from the centerline of the abutment bearings. During the 1992 retrofit, new cover plates of ASTM A36 steel with dimensions of $^{3}/_{8}$"x9"x8'–0" were provided at the location of the floor beams having column support (on the bottom flange only).

According to Article 10.38.3 in the AASHTO Standard Specifications (2002), the effective flange width of the concrete deck acting composite with the steel stringers shall be the smaller of the following quantities: (1) one-forth the span length of the girder; (2) the distance center-to-center of the girders; and (3) twelve times the least thickness of the slab. For both the interior and exterior stringers, criterion (2) controlled; therefore, the effective flange width for the stringers was taken as 81". Ignoring the thickness of the haunch, the section properties of the exterior and interior stringers were computed.

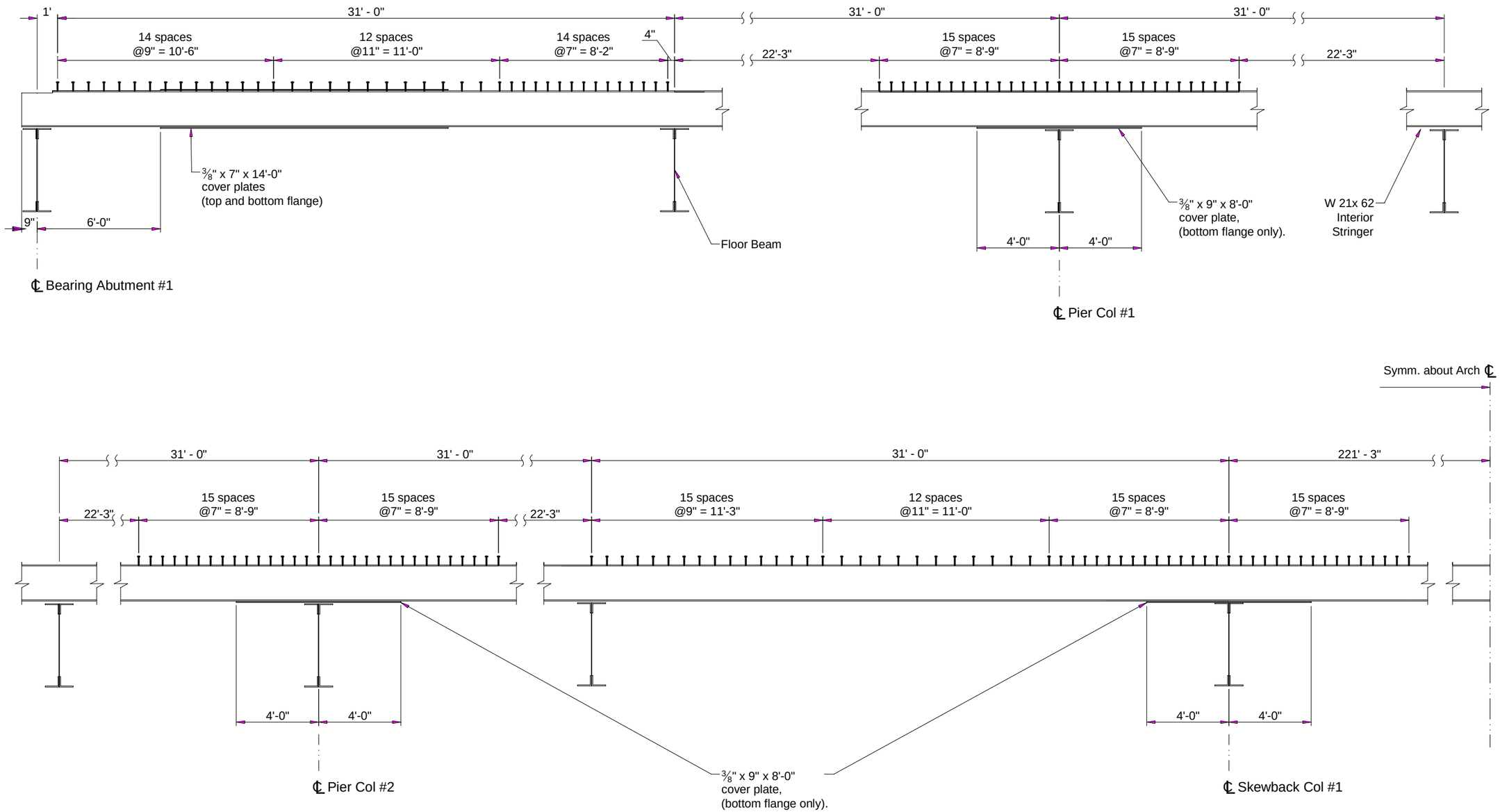

Figure 2.4 Interior stringer layout.

2.1.1.1 Exterior Stringers

As shown in Figure 2.3, the exterior stringers are composite with the deck only for positive moment in the first 31'–0" span at the bridge ends; an 81" effective deck width acts as the concrete compression flange of the composite section. Non-composite and composite section properties for the exterior stringers (ignoring the steel reinforcement) are given in Figure 2.5. The figure also shows the section dimensions and the neutral axis location (labeled N.A.).

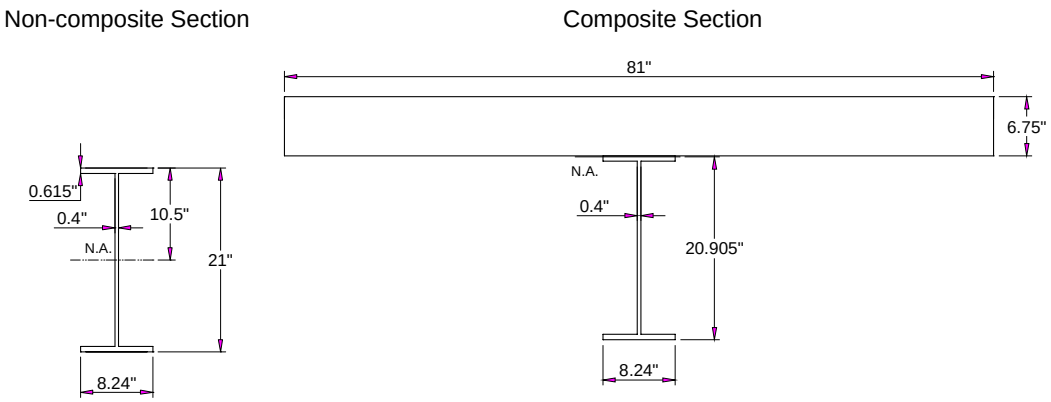

Non-composite Properties			Composite Properties		
A (in^2)	I (in^4)	S_t, S_b (in^3)	I (in4)	S_{ct} (in^3)	S_{cb} (in^3)
18.3	1330	126.67	4180	43780	200

Figure 2.5 Positive moment region of the exterior stringer.

In the exterior stringers, the shear studs are provided only within the end spans as shown in Figure 2.3. Therefore, the negative moment region at the first interior floor beam support is a non-composite section; the positive and negative moment regions

over the remaining length of the exterior girders are also non-composite. Non-composite section properties for those regions are given in Figure 2.5.

2.1.1.2 Interior Stringers

In the positive moment regions in the first and sixth spans, an 81" effective deck width acts as the concrete compression flange of the composite section; the compression steel reinforcement in the deck slab is ignored. In the negative moment regions above the pier columns, above the approach columns, the reinforced concrete slab is subject to tension. In accordance with Article 10.50.2 of the AASHTO Standard Specifications (2002), the concrete was assumed not to carry tension. Thus, only the steel reinforcement contributes to the stiffness and strength of the composite section. Within the effective width of the slab, there are nine #3 bars in the top mat and ten #4 bars in the bottom mat. Non-composite and composite section properties for the interior stringers are given in Figure 2.6 through 2.8.

In the positive moment region of the first span, 7"x$^{3}/_{8}$" cover plates are provided on both the top and bottom flanges as shown in Figure 2.6. In the positive moment region of the sixth span, cover plates are not provided as in the first span (see Figure 2.7).

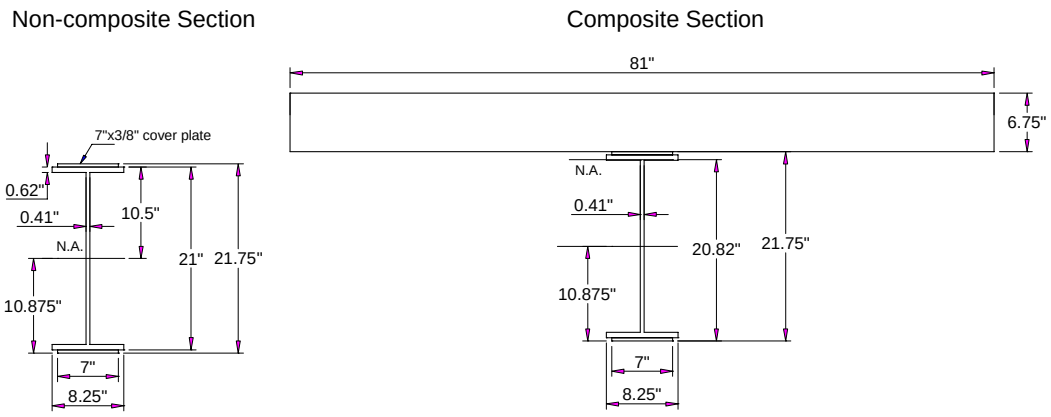

Non-composite Properties			Composite Properties		
A (in^2)	I (in^4)	S_t, S_b (in^3)	I (in^4)	S_{ct} (in^3)	S_{cb} (in^3)
23.77	1943	178.69	5519	5918	265

Figure 2.6 Positive moment region of interior stringers (in first span).

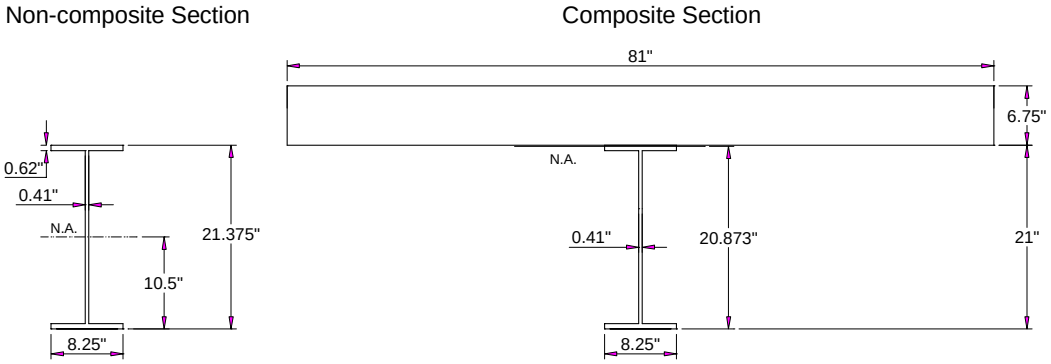

Non-composite Properties			Composite Properties		
A (in^2)	I (in^4)	S_t, S_b (in^3)	I (in^4)	S_{ct} (in^3)	S_{cb} (in^3)
18.52	1344	128	4217	33290	202

Figure 2.7 Positive moment region of interior stringers (in sixth span).

In the negative moment region at floor beam locations over the pier columns, a cover plate is provided on the bottom flange only (see Figure 2.8). In the remaining positive and negative moment regions of the interior girders, neither shear studs nor cover plates are provided. Section properties of these non-composite regions are given in Figure 2.7.

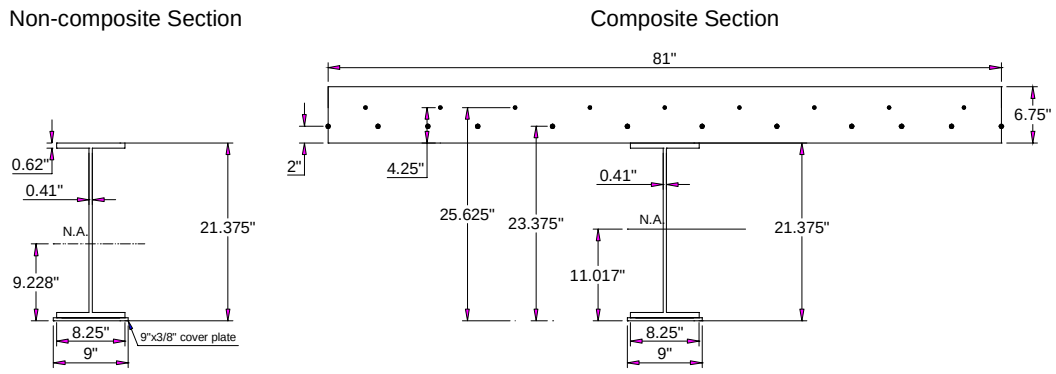

Non-composite Properties				Composite Properties		
A (in^2)	I (in^4)	S_t (in^3)	S_b (in^3)	I (in^4)	S_{ct} (in^3)	S_{cb} (in^3)
21.9	1670	137.5	180.9	2256	217.85	204.82

Figure 2.8 Negative moment region of interior stringers (at pier columns).

2.1.2 Floor Beams

There are two built-up sections used for the floor beams; one section corresponds to the floor beams labeled FB#1 and FB#6 while the other section corresponds to the floor beams labeled FB#2 through FB#5 (see Figure 2.2 for floor beam labels).

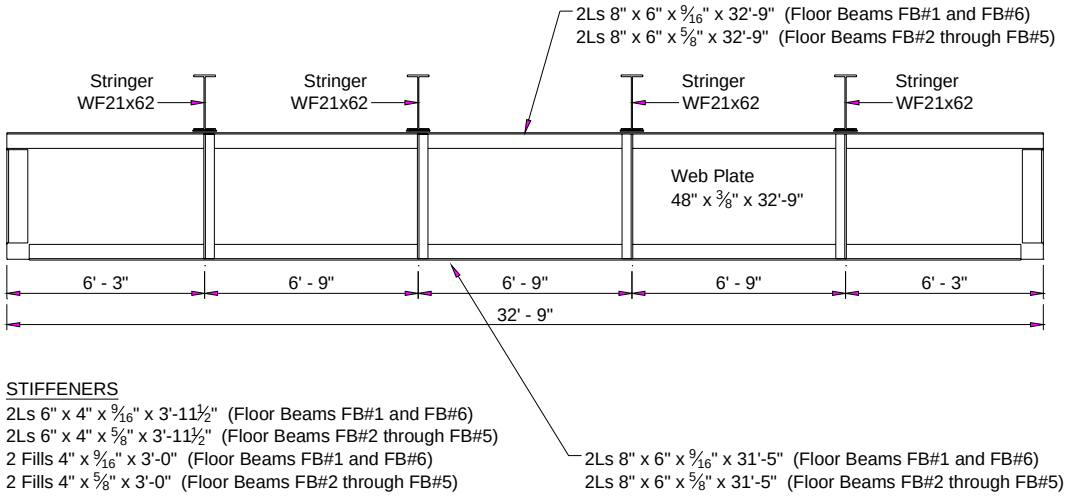

Figure 2.9 Floor beam elevation view.

As shown above in Figure 2.9, there are four web stiffeners at the stringer locations. Each stiffener consists of two angles (6"x 4"x3'–$11^1/_2$") and two fill plates (4"x3'–0") arranged symmetrically about the web plate. The cross-section of the floor beams consists of two angles (8"x6"x32'–9") at the top; two angles (8"x6"x31'–5") at the bottom; and a web plate (48"x$^3/_8$"x32'–9"). The only difference between the two floor beam sections is the thickness of the angles and fill plates; the thickness is $^9/_{16}$" for the floor beams labeled FB#1 and FB#6 and $^5/_8$" for the floor beams labeled FB#2 through FB#5. The span length of the floor beam is 35 ft. (center-to-center of

spandrel beams). Dimensions and properties for the two floor beams sections are given in Figure 2.10.

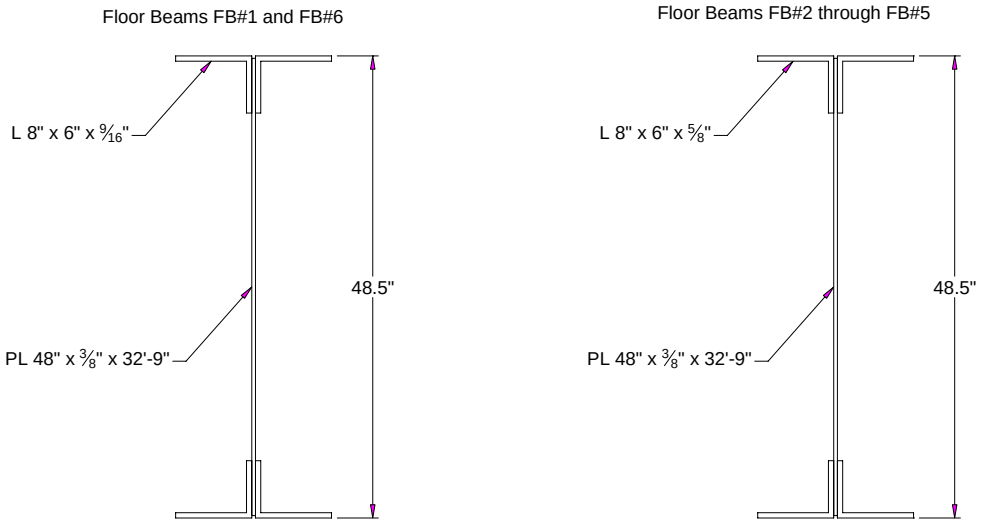

Floor Beams FB#1 and FB#6			**Floor Beams FB#2 through FB#5**		
A (in^2)	I (in^4)	S_t, S_b (in^3)	A (in^2)	I (in^4)	S_t, S_b (in^3)
48.4	19320	796.7	51.6	20960	864.2

Figure 2.10 Floor beam sections.

2.1.3 Spandrel Beams

Each spandrel beam (located on the west and east side of the bridge width) is a continuous beam supported at the abutments and the column locations over a total of 21 spans. The three approach spans on the north and south end of the bridge length are 62 ft each and the remaining 15 spans over the arch are 29.5 ft each. As shown in Figure 2.11, shear studs were installed over half the length of the three approach spans (i.e., 93 ft. on both ends of the bridge). The stud spacing is 1'–3" over the first 31'–0" and 12.5" over the remaining 62'–0". Bottom flange cover plates are provided at the location of the first interior floor beam from the abutments (see Figure 2.11).

According to Article 10.38.3 of the AASHTO Standard Specifications (2002), the effective flange width of the concrete deck acting composite with the steel spandrel beam shall not exceed the following quantities: (1) one-forth the span length of the girder; (2) the distance center-to-center of the girders; and (3) twelve times the least thickness of the slab. Hence, the effective flange width of the deck acting composite with the spandrel beam was controlled by criterion (3), which amounted to 81". The cross-section of the spandrel beam consists of two angles (8"x6"x$^{3}/_{4}$") on the bottom; two angles (4"x4"x$^{3}/_{8}$") on the top; two web plates (66"x$^{3}/_{8}$" each); and a top flange plate (25"x$^{3}/_{8}$"). The thickness of the haunch (2.87 in.) and the steel reinforcement was included in the calculation of the composite section properties in both the positive and negative moment regions. The dimensions and properties of the spandrel beam sections are given in Figures 2.12 and 2.13.

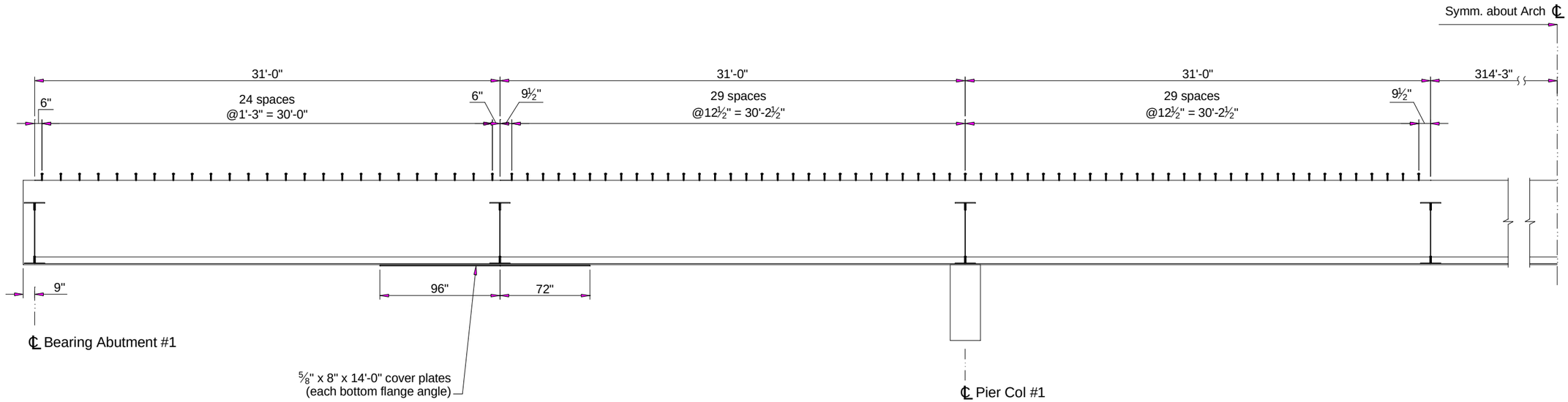

Figure 2.11 Spandrel beam layout.

As shown in Figure 2.11, shear studs were installed in the positive moment region of the end spans. Cover plates were also provided on the bottom flange angles of the section during the 1992 retrofit. However, analysis showed that the critical section for bending moment occurred at the end of the cover plates and thus, the cover plates were ignored. Within the 81" effective width of the slab, there are nine #3 bars in the top mat and eight #4 bars in the bottom mat. Section properties for the spandrel beam in the positive moment region are given in Figure 2.12.

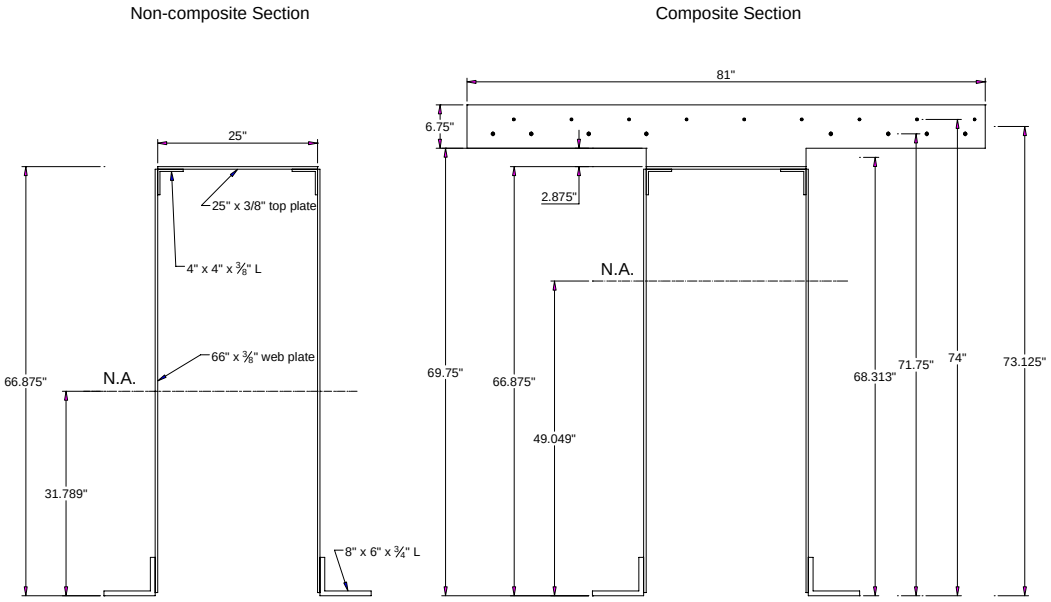

Non-composite Properties				Composite Properties		
A (in^2)	I (in^4)	S_t (in^3)	S_b (in^3)	I (in^4)	S_{ct} (in^3)	S_{cb} (in^3)
84.545	54300	1548	1708	114200	6406	2328

Figure 2.12 Positive moment region of spandrel beam.

In the negative moment region at the pier columns closest to the abutments, shear studs were installed on the spandrel beams to provide composite action. In negative flexure, the concrete slab is subject to tension which leads to cracking; thus, only the reinforcement in the concrete slab contributes to the stiffness and strength of the cross-section. Section properties for the spandrel beam in the negative moment region are given in Figure 2.13.

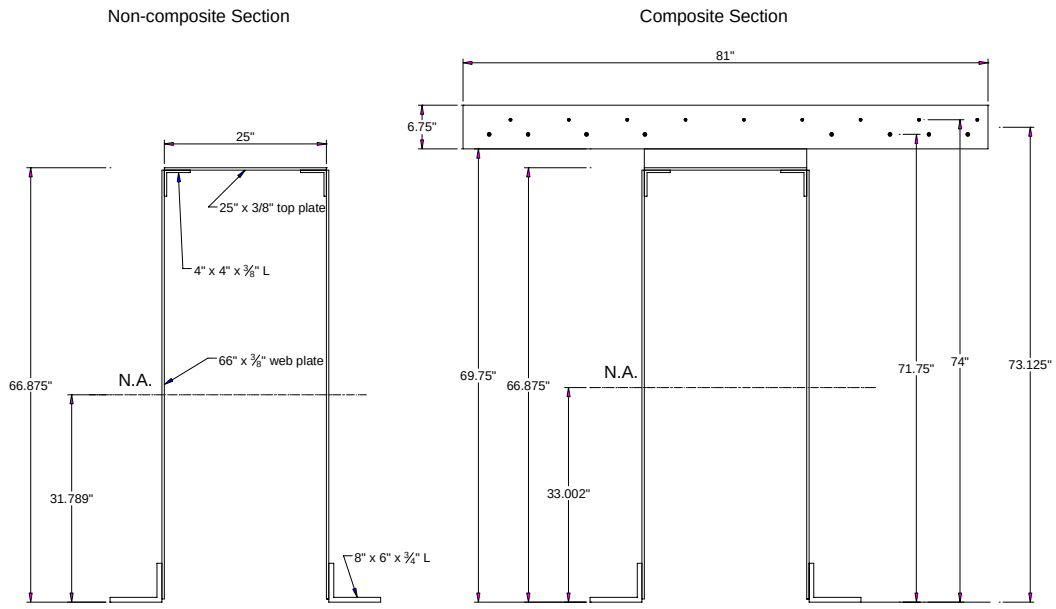

Non-composite Properties				Composite Properties		
A (in^2)	I (in^4)	S_t (in^3)	S_b (in^3)	I (in^4)	S_{ct} (in^3)	S_{cb} (in^3)
84.545	54300	1548	1708	58490	1727	1772

Figure 2.13 Negative moment region of spandrel beam.

Since shear studs were not installed in the positive moment regions of the remaining spans and in the remaining negative moment regions at the column locations, the spandrel beam sections in these regions are non-composite. Non-composite section properties of the spandrel beam can be found in Figures 2.12 and 2.13.

2.2 Columns

Each spandrel beam lies in the arch rib plane and is supported by four pier columns, 14 arch columns and two skewback columns as shown in Figure 2.14. All pier columns have a riveted connection to the spandrel beam and a pinned support at the base. The top ends of the skewback and arch columns also are riveted to the spandrel beam. The base of the skewback columns are fixed to a concrete foundation while the bottom ends of the arch columns are riveted to the arch rib.

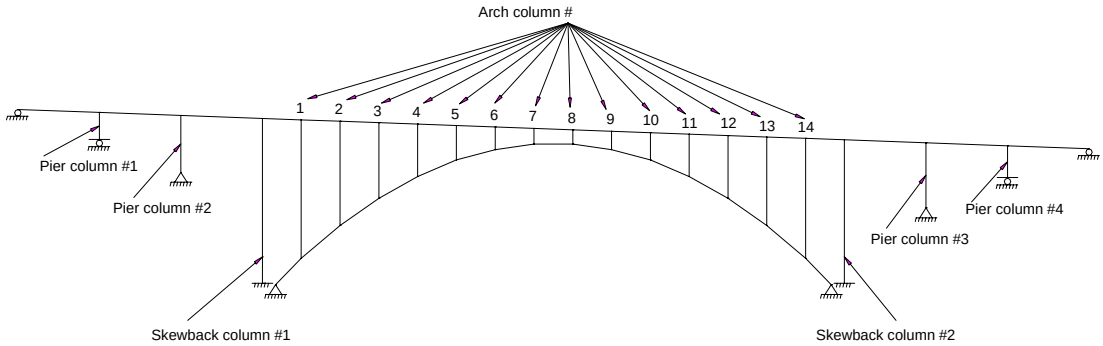

Column	Label	Length (ft)
Pier column #1	N2	18.4
Pier column #2	N3	41.2
Skewback column #1	N4	103.1
Arch column #1	N5	99.1
Arch column #2	N6	73.1
Arch column #3	N7	51.4
Arch column #4	N8	34.2
Arch column #5	N9	20.5
Arch column #6	N10	11.7
Arch column #7	N11	6.9

Column	Label	Length (ft)
Arch column #8	N12	5.8
Arch column #9	N13	8.5
Arch column #10	N14	15.1
Arch column #11	N15	26.7
Arch column #12	N16	41.7
Arch column #13	N17	61.2
Arch column #14	N18	85
Skewback column #2	N19	86.8
Pier column #3	N20	47.4
Pier column #4	N21	22.1

Figure 2.14 Column layout.

Figure 2.14 also shows the labels and lengths of the columns; the column lengths were taken as the distances between the centers of gravity of the connections at the column ends. The dimensions as well as the section properties of the column sections are given in Figures 2.15 and 2.16.

2.2.1 Pier and Arch Columns

The cross-section of the pier and arch columns are identical which consists of four 4”x4”x$^1/_2$" angles and four 24”x$^1/_2$" plates as shown in Figure 2.15.

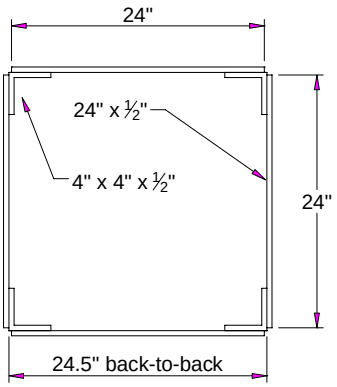

Pier/Arch Column Properties		
A (in^2)	I (in^4)	r (in)
63	6762	10.36

Figure 2.15 Cross-section of pier and arch columns.

2.2.2 Skewback Columns

The cross-section of the skewback columns consists of eight 4”x4”x$^1/_2$" angles, three short plates (24”x$^1/_2$”), and two long plates (48”x$^1/_2$”) as shown in Figure 2.16. The moment of inertia and radius of gyration are given for the in-plane and out-of-plane axes.

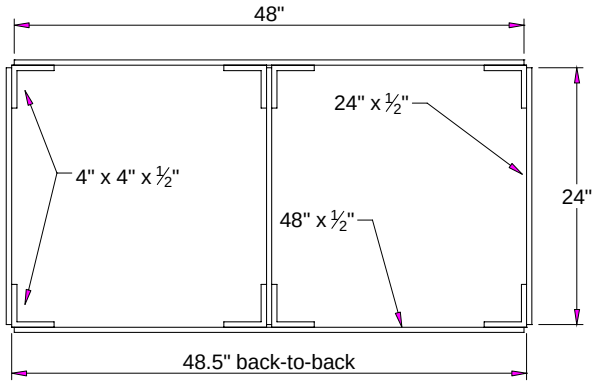

Skewback Column Properties				
A (in^2)	I_o (in^4)	r_o (in)	I_i (in^4)	r_i (in)
114	12950	10.658	31680	16.670

Figure 2.16 Cross-section of skewback columns.

2.3 Arch Ribs

Each arch rib, which was original built in 1951, is a two-hinge parabolic arch with a span of 422.5 ft. and a rise of 106.6 ft. as shown in Figure 2.17. The steel used for the arch ribs is ASTM A7. The transverse distance between the two arch ribs is equal to 25 ft. and the support locations of the east and west arch are at the same elevation. Furthermore, each arch rib is symmetrical about its centerline.

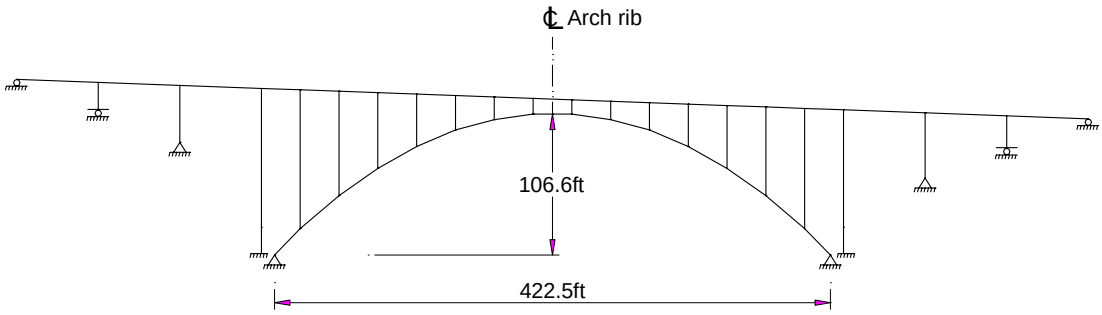

Figure 2.17 Arch rib span and rise.

The dimensions and properties of the arch section are given in Figure 2.18. As shown in the figure, the built-up cross section consists of eight flange angles (8”x8”x$^{3}/_{4}$"); two exterior web plate stiffener angles (6”x4”x$^{3}/_{4}$"); two interior web plate stiffener angles (4”x4”x$^{3}/_{8}$"); two web plates (71$^{1}/_{2}$”x$^{1}/_{2}$”) and two flange plates (48”x$^{3}/_{4}$”). The center-to-center distance between the two web plates is 26” while the center-to-center distance between the top and bottom flange plates is 72.75”. The section properties given in Figure 2.18 are for the in-plane bending axis.

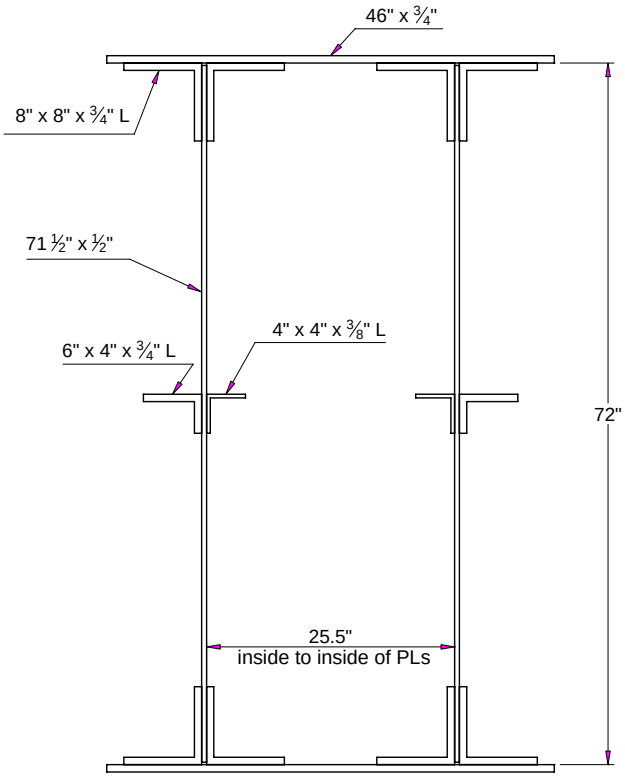

Arch Rib Properties			
A (in^2)	I (in^4)	r (in)	S_t, S_b (in^3)
252	227100	30.02	6179

Figure 2.18 Cross-section of the arch rib.

CHAPTER 3

BRIDGE RATING USING AASHTO

3.1 Introduction

In general, load rating may be defined as the process by which the magnitude of load a bridge can safely carry is determined (based on a structural capacity analysis). Rating calculations should take into account the existing dimensions and properties of the bridge as observed during the most recent inspection. Accordingly, load ratings should be re-examined as part of every inspection cycle and updated if necessary to account for any notable changes in the loading and/or condition of the bridge (AASHTO, 1994; AASHTO, 2003). Types of events that may occur during the service life of a bridge that can ultimately influence its load rating (i.e., safe load capacity) include: installation of a new deck wearing surface; replacement of a bridge deck; section loss of a bridge member due to deterioration and/or corrosion; retrofit of a bridge member; changes in vehicular live loads and/or traffic demand; and widening of a bridge roadway. In the case of the Omega Bridge, rehabilitation work was completed by Merrick & Company in the early 1990s (to comply with the AASHTO standards current at the time) which resulted in several changes to the original structure; the reader is referred back to Chapter 1 for a discussion of the rehab. The study reported herein provides the load rating of the Omega Bridge as affected by this rehabilitation and according to the latest AASHTO standards.

There are three AASHTO procedures available for the load rating of highway bridges: Allowable Stress Rating (ASR); Load Factor Rating (LFR); and Load and Resistance Factor Rating (LRFR). The ASR and LFR methods are covered in the AASHTO Manual for Condition Evaluation of Bridges (1994) which is consistent with the AASHTO Standard Specification for Highway Bridges (2002). The AASHTO Manual for Condition Evaluation and Load and Resistance Factor Rating (LRFR) of Highway Bridges (2003) together with the AASHTO LRFD Bridge Design Specifications (2004) describes the rating procedures pertinent to the LRFR method. The new LRFR Manual (AASHTO, 2003) also includes the ASR and LFR methods as an appendix so that all three rating methods are available in a single document.

In this study, the Omega Bridge is evaluated based on the LFR method which is the customary rating approach used in many states in the U. S; only a few states have adopted the LRFR approach. Attention is given to the superstructure elements including the stringers, floor beams, spandrel beams, columns (including the pier, skewback, and arch columns), and arch rib. In the new LRFR manual (AASHTO, 2003), it is stated that “stringer-supported concrete deck slabs that are carrying normal traffic satisfactorily need not be routinely evaluated for load capacity”. This statement is supported by test data which has shown that concrete bridge decks resist wheel loading primarily by internal arching or membrane action rather than flexure as assumed in design. In fact, a steel-free deck slab design has been developed in

Canada which is based on arching behavior. Therefore, significant reserve strength exists in concrete decks having top and bottom steel reinforcing mats that are designed according to the AASHTO Standard Specifications based on flexure. However, punching shear failure under wheel loads should be checked in deck areas where severe spalling and deterioration has occurred. Aside from concrete decks, the new LRFR manual (AASHTO, 2003) also argues that the load carrying capacity of substructure components need not be checked during each inspection cycle unless there is evidence of distress and/or questionable stability. In these situations, the load capacity of the substructure may govern that of the whole bridge and thus, should be evaluated. In the case of the Omega Bridge, both the concrete deck and the substructure were found to be structurally sound during the 2003 inspection conducted by NMSU and were therefore not evaluated in this study.

3.2 Rating Procedures

3.2.1 Allowable Stress and Load Factor Rating (ASR and LFR)

The ASR and LFR methods use the following basic equation to determine the rating factor for a bridge component or connection subjected to a single load effect (i.e., axial force, flexure, or shear):

$$RF_{ASR,\,LFR} = \frac{C - A_1 D}{A_2 L(1+I)}$$

where $RF_{ASR,\,LFR}$ = ASR or LFR rating factor; C = nominal member capacity; A_1 = dead load factor; D = nominal dead load effect; A_2 = live load factor; L = nominal

live load effect caused by rating vehicle; and I = live load impact factor. The rating factor is the ratio of the available to required live-load capacity and thus, is a direct measure of the safe live-load capacity of a bridge. If less than one, then the live load effects caused by the rating vehicle exceed the capacity minus the dead load effects. Separate rating factors are computed for the different bridge components (i.e., slab, superstructure, and substructure) and different load effects (i.e., moment, shear, axial force, etc.). The individual member with the smallest rating factor is the weak link and thus, controls the load rating of the bridge as a whole. Bridge members or connections under combined loading such as axial-bending or shear-bending should be evaluated taking into account the interaction of load effects. In such cases, the load rating should be based on the appropriate interaction equation rather than the basic equation given above which applies only to members subjected to an individual load effect as mentioned earlier (Minervino et al., 2004).

Load ratings are computed at an inventory and operating level compliant with the ASR and LFR methods. The inventory rating represents the magnitude of load that a bridge can safely carry for an indefinite period of time whereas the operating rating denotes the absolute maximum load that may be permitted on a bridge but with appropriate restrictions (AASHTO, 1994; AASHTO, 2003). In the ASR method, the dead load and live load factors (i.e., A_1 and A_2, respectively) are taken as unity while the nominal capacity is determined based on an allowable stress which depends on the rating level. For steel bridge members in tension or flexure, for example, the

allowable stresses are 55% of the yield stress for inventory and 75% for operating. In the LFR method, A_1 is taken as 1.3 regardless of the rating level whereas A_2 is taken as 1.3 and 2.17 for inventory and operating, respectively. The nominal capacity, C, is independent of the rating level and is computed according to the AASHTO Standard Specifications.

The inventory and operating ratings represent the multiple of the load effects caused by the rating vehicle that a highway bridge can safely carry. For example, an inventory rating of 1.0 for an HS-20 truck indicates that the bridge safely can carry unlimited passes of a vehicular load that causes load effects equal to those caused by the HS-20 truck. An operating rating of 1.67, on the other hand, indicates that the bridge can safely carry a load that causes live load effects equal to 1.67 times that of an HS-20 truck but on a periodic not continual basis. Safe load capacities are typically given in terms of the design loading which is the customary reporting format specified for the National Bridge Inspection Standards (NBIS) and Bridge Management Systems (BMS). Hence, inventory and operating ratings of 1.0 and 1.67, respectively, for an HS-20 truck would be reported as HS-20 and HS-32. Alternatively, load ratings may be reported in terms of the weight (in tons) of the rating vehicle. For the example given above, this results in an inventory rating of 36 tons and an operating rating of 60 tons.

3.2.2 Load and Resistance Factor Rating (LRFR)

The same limit states design philosophy used to develop the LRFD Bridge Design Specifications was extended to the evaluation of existing bridges in the new LRFR manual (AASHTO, 2003). The load rating equation used in LRFR for members under discrete loading is given as:

$$RF_{LRFR} = \frac{\phi_c \phi_s \phi R_n - \gamma_{DC} DC - \gamma_{DW} DW}{\gamma_L LL(1+IM)}$$

where RF_{LRFR} = LRFR rating factor; ϕ_c, ϕ_s = condition and system factor, respectively; ϕR_n = design resistance of member (ϕ = LRFD resistance factor and R_n = nominal member resistance); γ_{DC}, γ_{DW}, γ_L = load factors for structural components and attachments (DC), wearing surfaces and utilities (DW), and live load (L), respectively; DC, DW, LL = nominal dead load effect due to structural components and attachments, dead load effect due to wearing surfaces and utilities, and live load effects, respectively; and IM = dynamic load allowance. Dead loads for the LRFR method are separated into two categories: component / attachment loads (DC) and wearing surface / utility loads (DW). The two loads have different dead load factors (i.e., γ_{DC} = 1.25 and γ_{DW} = 1.50) in recognition of the lower degree of variability of the component dead loads compared to that of the wearing surface. The condition factor, ϕ_c, accounts for the larger uncertainty in the resistance of deteriorated members (and the possibility for future deterioration) which ranges from 0.85 (poor condition) to 1.0 (satisfactory condition). It is important to note that this factor does not account for any observed changes in the physical dimensions of the member (i.e.,

section loss). The system factor, ϕ_s, relates to the degree of redundancy inherent in a bridge system; that is, the capability of the bridge to redistribute load in the event of damage or failure to one or multiple members. Like the condition factor, the system factor ranges from 0.85 to 1.0 with the higher value corresponding to redundant structures (e.g., multiple girder bridges). As in the LFR approach, the nominal member resistance (R_n) is computed according to the applicable design specifications which in the LRFR approach is the LRFD Bridge Design Specifications.

The factored live load effect of the LRFR rating equation represents the largest discrepancy with LFR. First of all, the LRFR dynamic load allowance (IM) is a fixed value, whereas the LFR impact factor (I) varies with span length. Also impacting the live load effects are the distribution factors for moment and shear; the AASHTO LRFD Bridge Design Specifications introduced new empirical equations that yield more accurate estimates of live-load distribution. The LRFD-based distribution factors consider span length, girder spacing, girder stiffness, and slab thickness, whereas the LFD-based distribution factors consider only the girder spacing. For interior girders, distribution factors for moment and shear are considered separately in LRFD. This is not the case for LFD where the same distribution factor is used for both moment and shear. For exterior beams, the LRFD distribution factors are determined by either modifying the distribution factors for the interior beam or by employing the lever rule; only the lever rule is applied in computing exterior beam

distribution factors in LFD. The LRFD-based distribution factors also account for support skew and rigid intermediate diaphragms.

A major difference in the live load effect lies in the type of vehicle used in the analysis; LRFR employs the HL-93 design load while LFR employs the HS-20. The HL-93 consists of an HS-20 design truck (or design tandem) combined with the design lane load of 0.64 klf. Conversely, the LFR method considers the HS-20 truck and lane load separately which yields smaller live load forces (undistributed and unfactored) compared to LRFR. One last parameter that influences the live load effects is the live load factor. In LRFR, the live load factor (γ_L) is 1.75 for the Strength I check and 1.35 for the Strength II check. Note that Strength I and II in LRFR is the same as inventory and operating rating in LFR. Under legal loads, the live load factor ranges from 1.4 to 1.8 depending on the Average Daily Truck Traffic (ADTT). Separate live load factors are also specified for permit loads depending on the permit type, frequency of crossing, loading condition, ADTT, and permit weight. In LFR, the live load factors for legal and permit loads are usually taken to be equal to those at inventory and operating levels, respectively, under design loads; that is, A_2 = 2.17 for legal loads and 1.3 for permit loads. Further discussion of capacity rating under design, legal, and permit loads are given in the next section.

3.3 Design, Legal, and Permit Load Rating

The live loads applied in the rating process can be broken down into three types: design, legal, and permit loads. The new LRFR manual (AASHTO, 2003) explicitly defines a tiered approach to load rating which starts with a design load rating, followed by a legal load rating, and ending with a permit load rating. Design load rating provides a measure of the safe load capacity of existing bridges according to new bridge design standards. As mentioned in Chapter 1, the Omega Bridge was originally designed for H-20 truck loading by Allowable Stress Design (ASD) based on the 1944 AASHO Specifications. The structure was later rehabilitated in 1992 using Load Factor Design (LFD) to conform to HS-20 vehicular loading. Figure 3.1 shows the axle weights and longitudinal spacing for the H-20 and HS-20 design trucks; the transverse distance between wheel lines (not shown) is equal to 6 ft.

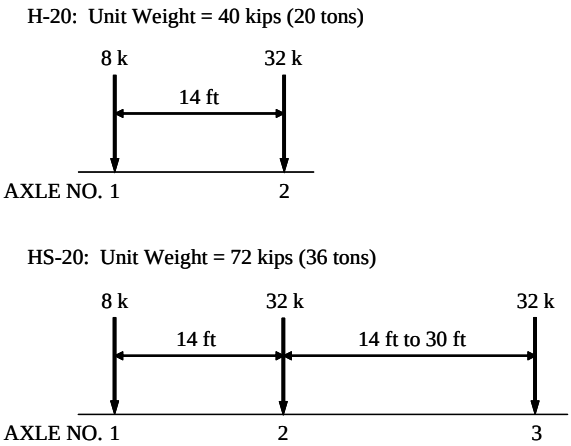

Figure 3.1 AASHTO design trucks.

The AASHTO Standard Specifications uses the HS-20 truck or lane loading (equal to 0.640 kips/ft), whichever produces the maximum effect (AASHTO, 1994). In the new LRFR manual (AASHTO, 2003), the live load model adopted by the AASHTO LRFD Bridge Design Specifications is designated as HL-93 which combines rather than separates the HS-20 truck and the 0.640 klf lane load. As mentioned earlier, the safe load capacities of highway bridges are customarily reported at the inventory and operating levels under design loading. A major difference between LFR and LRFR is in the use of these design load ratings as a screening check for legal loads. Legal load ratings provide information necessary to the posting of loads or the rehabilitation of the structure. Figure 3.2 shows the legal loads (designated as Type 3, 3S2, and 3-3) adopted by AASHTO which are suitable for posting purposes. Similar to the H-20 and HS-20 design trucks, the wheel line spacing is 6 ft.

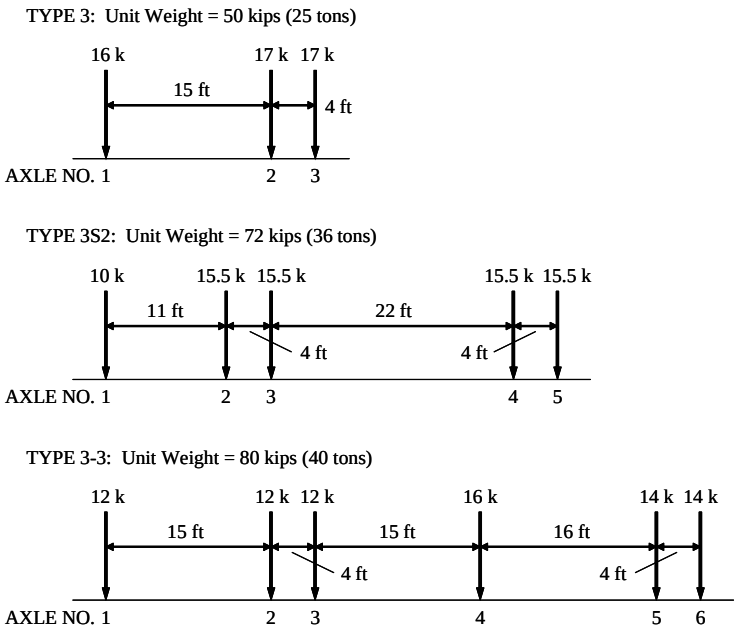

Figure 3.2 AASHTO legal loads.

In LRFR, an inventory rating greater than one (computed based on HL-93 design loading) indicates that the bridge has adequate capacity to carry all AASHTO legal loads as well as "exclusion" vehicles currently allowed to routinely travel on highways in various states in the U. S. The group of state "exclusion" vehicles is defined in the AASHTO LRFD Bridge Design Specifications (AASHTO, 2003). In LFR, bridges that have an inventory rating greater than one must still be checked for legal loads due to the lighter design load (i.e., HS-20 < HL-93).

For the evaluation of the Omega Bridge presented herein, the LFR method was used to arrive at inventory and operating ratings for five different vehicular loads which included the AASHTO HS-20 design truck; AASHTO Type 3, 3S2, and 3-3 legal loads; and "Emergency-One Titan" fire truck. The axle configuration of the fire truck is shown in Figure 3.3; unlike the AASHTO design and legal loads, the wheel line spacing is 7.2 ft. This truck was included at the request of the Los Alamos National Laboratory to assess the structural capacity of the Omega Bridge under emergency response vehicles.

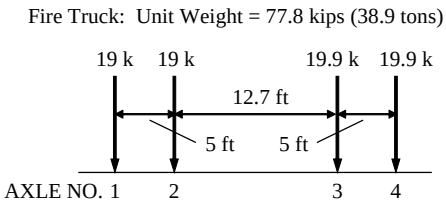

Figure 3.3 "Emergency-One Titan" fire truck.

An LFR inventory rating greater than one indicates the Omega Bridge has adequate capacity to carry unlimited passes of the rating vehicle. In cases where the Omega Bridge passes only the operating level check (i.e., inventory rating < 1, operating rating > 1), the bridge is still safe to carry the rating vehicle but additional inspection and traffic monitoring may be warranted. The practice of bridge posting varies widely from agency to agency and may be enforced at the inventory rating, operating rating, or somewhere between (Taly, 1998). Federal regulations require that bridges be posted only when legal loads fail the operating rating check (AASHTO, 2003).

Although only five loads were considered in this study, the rating analysis and results provided in this report provide the basis for future evaluations under other legal loads, such as state legal vehicles having heavier gross weights and axle configurations significantly different than those of the AASHTO legal loads. Load rating analysis conducted under permit loads or loads that exceed legal loads is referred to as permit load rating. Highway bridges should only be evaluated under permit loads if shown that they can safely carry the legal loads. Under no circumstances should a vehicle be permitted to cross a bridge which fails the operating rating check (i.e., operating rating < 1).

CHAPTER 4

LOAD RATING OF FLOOR SYSTEM

This chapter covers the load rating of the three floor system components; the stringers (section 4.1), floor beams (section 4.2), and spandrel beams (section 4.3). A description of the rating model for each element is first provided followed by a discussion of the capacity evaluation using the Load Factor Rating (LRF) method. Rating factors were determined for the bridge members based on flexure using the equation

$$RF = \frac{M_R - A_1 M_D}{A_2 M_L}$$

where RF = rating factor (RF_i for inventory or RF_o for operating); M_R = flexural capacity of the member; A_1 = dead load factor = 1.3; M_D = bending moment due to dead load; A_2 = live load factor = 2.17 (for inventory rating) or 1.3 (for operating rating); and M_L = bending moment due to live load (equal to the bending moment caused by a wheel line of the live load vehicle times the distribution, multiple presence, and impact factors). As mentioned in Chapter 3, the live loads used to rate the bridge components include the traditional AASHTO HS-20 truck loading; standard AASHTO rating vehicles (Type 3, Type 3-3, and Type 3S2); and Emergency-One Titan Fire Truck. The rating analysis complies with the 2nd Edition of the AASHTO Manual for Condition Evaluation of Bridges (2000) including the 2003 Interim Revisions and the 17th Edition of the AASHTO Standard Specifications for Highway Bridges (2002). A full listing of the rating calculations for AASHTO

HS-20 truck loading is provided in the appendix for the stringers (Appendix A1), floor beams (Appendix A2), and the spandrel beams (Appendix A3).

4.1 Stringers

4.1.1 Description of Rating Model

For purpose of analysis, the stringers were modeled as continuous beams supported at the floor beam locations. There are a total of 27 spans over the length of the stringers; the span length is 31 ft in the six approach spans at each end of the bridge and 29.5 ft in the 15 interior spans over the arch. Figure 4.1 shows the rating models for the approach spans of the interior and exterior stringers starting from the south end of the bridge; the floor beam support locations are labeled N1, N2, N3, etc.

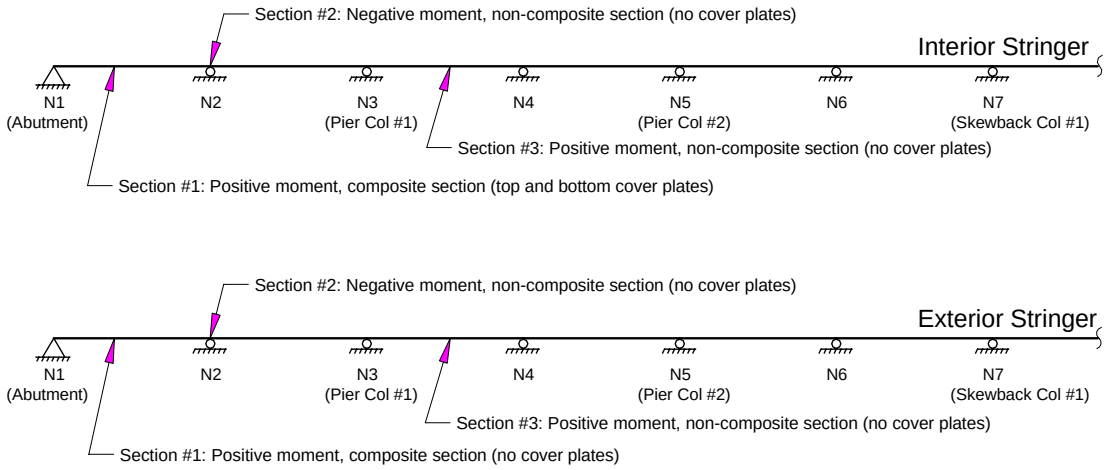

Figure 4.1 Rating models of stringers (with critical sections).

As shown in the figure, the floor beams are assumed to provide unyielding support to the stringers in the vertical direction. This model assumes that the vertical stiffness

provided by the floor beams (and spandrel beams) to the stringer is completely rigid (i.e., the stringers do not deform vertically at the floor beam locations). In actuality, the support stiffness has a finite spring constant which depends not only on the position of the stringer above the floor beam but also on the position of the floor beam relative to the length of the spandrel beam. In the end, a spring constant of infinity was chosen to simplify the analytical model which results in smaller positive moments within the spans and larger negative moments at the floor beam locations. Furthermore, the torsional stiffness of the stringer to floor beam connections and that of the floor beams themselves was ignored. The section properties were also assumed constant (i.e., prismatic) along the entire length of the stringer based on non-composite action. This assumption ignores the change in stiffness between composite and non-composite regions as well as between areas with and without cover plates. Incidentally, structural analysis showed no significant difference in the results between the non-prismatic and prismatic models.

For the interior stringer, the total dead load was w_{Di} = 556 plf which includes the self-weight of the stringer (66.1 plf); the tributary weight of the slab (456 plf); and the tributary weight of the integral wearing surface (33.8 plf). The total dead load that acts on the east exterior stringer was w_{De} = 609 plf, which includes the self-weight of the stringer (65.1 plf); the tributary weight of the slab (465 plf); the tributary weight of the integral wearing surface (33.8 plf); and the weights of the barrier and utilities (45.9 plf). According to Article 3.23.2.2 of the AASHTO Standard Specification

(2002), the moment distribution factor for an interior stringer (DF_{int}) in bridges having two or more traffic lanes is

$$DF_{int} = \frac{S}{5} = \frac{6.75}{5} = 1.23$$

where S equals the stringer spacing in feet. For an exterior stringer, AASHTO Article 3.23.2.3 states that the moment distribution factor "shall be determined by applying to the stringer or beam the reaction of the wheel load obtained by assuming the flooring to act as a simple span between stringers or beams" (AASHTO, 2002). This approach, also referred to as the lever rule, resulted in a moment distribution factor equal to unity (i.e., $DF_{ext} = 1.00$) assuming the deck spanned from the top edge of the spandrel beam. When the deck was assumed to span from the centerline of the spandrel beam, a value of $DF_{ext} = 1.19$ was computed. AASHTO (2002) also specifies a lower bound for DF_{ext} of

$$DF_{ext} = \frac{S}{4 + 0.25S} = \frac{6.75}{4 + 0.25(6.75)} = 1.19$$

where S (the distance between the exterior and adjacent interior stringer) is between six and 14 feet; thus, the distribution factor for the exterior stringer was taken as $DF_{ext} = 1.19$. AASHTO Article 3.8.2.1 requires that vehicular live loads be increased a maximum of 30% to account for dynamic, vibratory, and impact effects using the equation

$$I = \min\left(\frac{50}{L+125}, 0.30\right) = \min\left(\frac{50}{31 \text{ or } 29.5+125}, 0.30\right) = \min(0.32, 0.30) = 0.30$$

where I is the impact factor and L is the loaded span length in feet (i.e., 31 ft for approach spans and 29.5 ft for arch spans). The same moment distribution and impact factors for the AASHTO HS-20 truck loading were also used to evaluate the bridge members under the standard AASHTO rating vehicles and the Emergency-One Titan Fire Truck.

Taking into account the moment envelopes for dead load and vehicular live load as well as the varying flexural capacity of the stringers, three critical sections were identified along the length of the interior and exterior stringers (labeled Section #1, Section #2, and Section #3 in Figure 4.1). As discussed in Chapter 2, the stringers are composite in some areas and non-composite in others. Furthermore, ASTM A36 steel (F_y = 36 ksi) was used for the exterior stringers while ASTM A7 steel (F_y = 33 ksi) was used for the interior stringers. Cover plates were also provided in some regions of the interior stringers. The first critical section (Section #1) is located in the positive moment region of the end span as shown in Figure 4.1 where the interior and exterior stringers are both composite. However, cover plates were provided on the top and bottom flanges of the interior stringers only. The second (Section #2) and third (Section #3) critical sections are located in the negative moment region at the floor beam support location N2 and the positive moment region of the third span, respectively, where both the interior and exterior stringers have no cover plates and

are non-composite. The load rating analysis at these critical sections of the stringers is discussed next.

4.1.2 Load Factor Rating Analysis

The magnitudes of the dead load moment (M_D), live load moment (M_L), flexural capacity (M_R) and rating factors for the interior and exterior girders are reported in Tables 4.1 and 4.2, respectively. The moment values given for dead load and live load are unfactored; furthermore, the distribution and impact factors are included in the live load moments as mentioned previously. Note that the dead load moments for the exterior stringer are larger than those for the interior stringer mainly due to the added weight of the barrier and utilities. The live load moments, on the other hand, are slightly larger for the interior stringer since it had a larger distribution factor than the exterior stringer (i.e., $DF_{int} = 1.23 > DF_{ext} = 1.19$). The flexural capacity of the stringers was governed by the plastic moment capacities of the composite section (AASHTO Article 10.50) at Section #1 and the non-composite section (AASHTO Article 10.48) at Section #2 and Section #3.

Table 4.1 Moment values and rating factors for interior stringer.

Critical Section		Section #1	Section #2	Section #3
Dead Load Moment (M_D), kip-ft		41.6	56.3	23.4
Live Load Moment (M_L), kip-ft	HS-20	190	139	147
	TYPE 3	153	107	121
	TYPE 3S2	147	146	94.6
	TYPE 3-3	122	121	84.2
	FIRE	184	156	139
Flexural Capacity (M_R), kip-ft		1070	401	401
Inventory Rating Factor (RF_i)	HS-20	2.46	1.09	1.16
	TYPE 3	3.05	1.41	1.42
	TYPE 3S2	3.19	1.03	1.80
	TYPE 3-3	3.84	1.25	2.03
	FIRE	2.55	0.97	1.23
Operating Rating Factor (RF_o)	HS-20	4.11	1.81	1.94
	TYPE 3	5.10	2.36	2.36
	TYPE 3S2	5.33	1.72	3.01
	TYPE 3-3	6.41	2.09	3.38
	FIRE	4.25	1.62	2.05

Table 4.2 Moment values and rating factors for exterior stringer.

Critical Section		Section #1	Section #2	Section #3
Dead Load Moment (M_D), kip-ft		45.6	61.6	25.6
Live Load Moment (M_L), kip-ft	HS-20	184	135	143
	TYPE 3	149	104	117
	TYPE 3S2	142	142	91.7
	TYPE 3-3	118	119	81.6
	FIRE	178	151	135
Flexural Capacity (M_R), kip-ft		888	433	433
Inventory Rating Factor (RF_i)	HS-20	2.07	1.21	1.29
	TYPE 3	2.57	1.57	1.58
	TYPE 3S2	2.69	1.15	2.01
	TYPE 3-3	3.23	1.39	2.26
	FIRE	2.14	1.08	1.37
Operating Rating Factor (RF_o)	HS-20	3.46	2.02	2.15
	TYPE 3	4.29	2.62	2.63
	TYPE 3S2	4.49	1.92	3.35
	TYPE 3-3	5.40	2.33	3.77
	FIRE	3.58	1.80	2.28

The plastic capacity at Section #1 of the interior stringer is about 20% larger than that of the exterior stringer largely because cover plates were provided for the interior stringer. Conversely, the plastic capacity of the non-composite section (i.e., $M_R = ZF_y$ where Z is the plastic section modulus of the W-section) at Sections #2 and #3 of the interior stringer is smaller than that of the exterior stringer due to the difference in the grade of steel. Both stringers satisfied the compact section requirements at Sections #1 through #3 needed to develop the plastic moment capacity.

Based on the rating factors given in Tables 4.1 and 4.2, the negative moment region (i.e., Section #2) of the stringers controlled the load rating; the rating values at this location are repeated in Table 4.3. As shown in the table, all the rating factors (with the exception of RF_i for the interior stringer for the FIRE truck) exceeded one.

Table 4.3 Rating factors at negative moment region (Section #2) of stringers.

Stringer		**Interior**		**Exterior**	
Rating Factor		**RF_i**	**RF_o**	**RF_i**	**RF_o**
Live Load	**HS-20**	1.09	1.81	1.21	2.02
	TYPE 3	1.41	2.36	1.57	2.62
	TYPE 3S2	1.03	1.72	1.15	1.92
	TYPE 3-3	1.25	2.09	1.39	2.33
	FIRE	0.97	1.62	1.08	1.80

Recall that the rating model assumed that the stringer was a continuous beam rigidly supported by the floor beams (i.e., no vertical deformation occurs at the support locations). In actuality, however, the floor beams deform vertically as a function of the flexural spring constant which will reduce the magnitude of the support reactions.

This, in turn, will decrease the negative moment in the stringers at the floor beam locations and increase the positive moment between floor beams. Hence, the rigid support assumption results in conservative rating factors for the negative moment region (i.e., Section #2) which controlled the capacity of the stringers. However, the same assumption has the opposite effect on the rating factors (i.e., overestimates) in the positive moment regions (i.e., Sections #1 and #3). This is not so much a concern at Section #1 (composite section) which had much larger rating factors compared to Section #3 (non-composite section).

The stiffness effect of the floor beam / spandrel beam system on the stringer moments could be better evaluated by three-dimensional finite element analysis and experimental field testing of the Omega Bridge. It was also assumed that the W-section in the non-composite regions completely resisted the bending moment with no contribution from the concrete deck. Although there is no definite connection (i.e., shear studs) in these areas, research has shown that some level of interaction somewhere between a true non-composite and composite section may exist due to friction and mechanical interlock which will aid the negative moment section (Section #2) and positive moment section (Section #3) to carry more load than estimated based on AASHTO provisions. The participation of the deck in regions without shear connectors, however, must be evaluated by field testing.

4.2 Floor Beams

4.2.1 Description of Rating Model

As shown in Figures 4.2 and 4.3, the floor beams were modeled as simple-supported spans with an overhang on either side (representing the outrigger beam). Figure 4.2 corresponds to the floor beams located in the approach spans and Figure 4.3 corresponds to those located in the arch spans (labeled FB#2 and FB#6, respectively, in Figure 2.2).

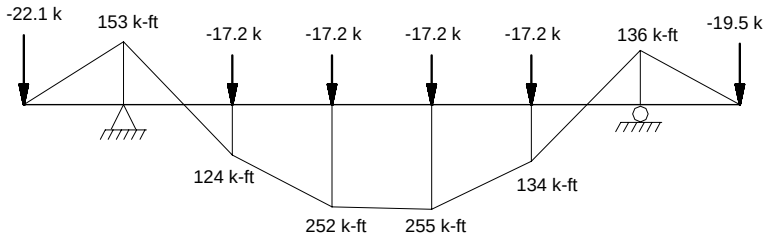

Figure 4.2 Distribution of dead load on floor beam FB#2 of approach span and moment diagram.

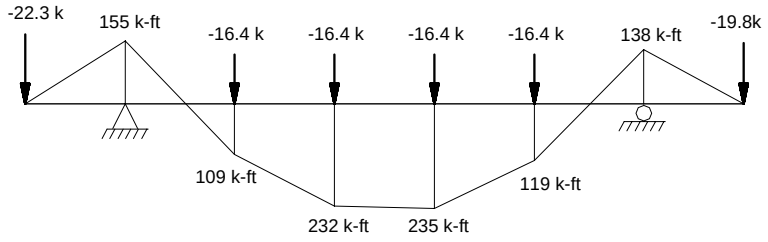

Figure 4.3 Distribution of dead load on floor beam FB#6 of arch span and moment diagram.

The floor beams were assumed to be rigidly supported by the spandrel beams and dead load was applied as six concentrated loads coincident with the stringer locations.

The two forces at the ends of the overhang include the weight of the exterior stringers, the deck slab (based on the exterior tributary flange width), the barriers and utilities. The four interior forces include the weight of the interior stringers and the deck slab (based on the interior tributary flange width). All forces were calculated by summing up the total weight over the distance between floor beams (i.e., 31 ft for the approach spans or floor beam FB#2 and 29.5 ft for the arch spans or floor beam FB#6). The distribution of dead load on floor beam FB#6 is different from that of FB#2 for two reasons. First, the spacing between the floor beams in the arch spans is 1.5 ft shorter than the floor beam spacing in the approach spans which explains the larger dead loads at the interior stringer locations of FB#2. Second, there is a fencing load that acts only on the arch span floor beams which explains the slightly larger dead loads at the exterior stringer locations of FB#6. The dead load moment diagrams are shown in Figures 4.2 and 4.3; the analysis also included the self-weight of the floor beams (equal to a uniform load of about 0.180 k/ft).

Figure 4.4 illustrates the analytical model used to determine the live load forces from an HS-20 truck on floor beam FB#2. The top sketch of the figure shows the cross-section of the floor system loaded with three HS-20 trucks (centered about the bridge centerline); the loading of three lanes controlled the capacity rating of the floor beams. The distance between wheel lines for each HS-20 truck is 6 feet and the distance between adjacent trucks is 4 feet as specified by AASHTO Article 3.7. In addition, AASHTO Article 3.12 specifies a reduction in live load of 10% for three

loaded traffic lanes to account for the improbability that the maximum loading in the three lanes occurs simultaneously. Note that there is no reduction for one or two loaded traffic lanes and a 25% reduction is permitted for four loaded traffic lanes due to the higher improbability of having each lane under maximum truck loading.

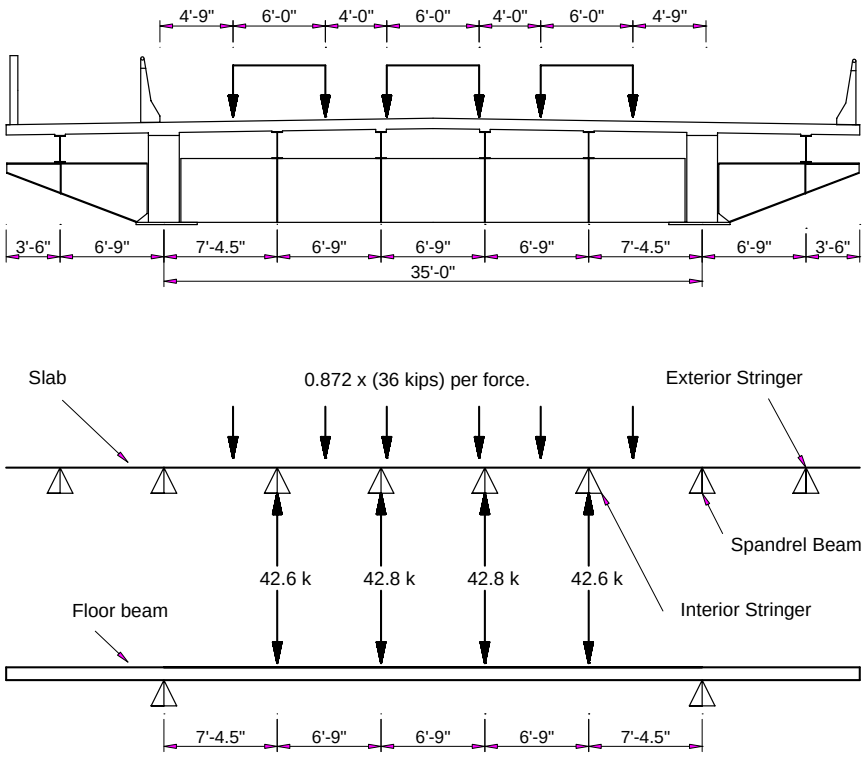

Figure 4.4 Distribution of HS-20 live load on floor beam FB#2.

The critical floor beam FB#2 in the approach spans was located one bay from the abutment (i.e., at support location N2 in Figure 4.1). The live load forces acting on this critical floor beam were determined by first calculating the fraction of the HS-20 truck that acts on the deck slab directly over the floor beam. This percentage or longitudinal distribution factor equaled 0.872 for an HS-20 truck (see Figure 4.4)

which is the ratio of the maximum reaction at floor beam support N2 (see Figure 4.1) determined from the stringer analysis to the total weight of a single line of HS-20 truck wheels or 36 kips.

Next, the distributed wheel line loads of (0.872 x 36 kips) were applied to the deck slab which was modeled as a continuous beam rigidly supported by the stringers and the spandrel beams as shown in Figure 4.4. Deck section properties were computed assuming a rectangular section with a height equal to the slab thickness and width equal to the floor beam spacing. With this model, the reactions at the four interior stringers were computed (equal to 42.6 kips and 42.8 kips) which represented the HS-20 live load forces applied to floor beam FB#2. The sum of the interior stringer reactions is smaller than the total load applied to the floor beam (i.e., 2 x 42.6 kips + 2 x 42.8 kips = 170.8 kips < 6 x 0.872 x 36 kips = 188.4 kips) since load is also distributed transversely to the spandrel beams. It is important to note that this modeling approach deviates from AASHTO Article 3.23.3 which ignores the transverse distribution of wheel loads and thus, results in larger bending moments. However, the AASHTO-based model assumes that live load is entirely distributed to the spandrel beams by the floor beams rather than through the deck slab and the floor beams, an unrealistic and conservative assumption. Furthermore, the torsional stiffness of the spandrel beam was ignored so that under live-load forces (transferred from the interior stringers), the floor beam model is a simple-supported beam with overhangs and rigidly supported by the spandrel beams. Consideration of the torsional

stiffness would decrease the bending moment carried by the floor beam, which could be evaluated by three-dimensional finite element analysis and field testing.

A similar approach was taken to determine the live load forces on the floor beams under the AASHTO standard rating vehicles and the fire truck. In Figures 4.5 and 4.6, the live load forces and corresponding moment diagrams for floor beams FB#2 and FB#6, respectively, under the different vehicular loads are given. As shown in the figures, floor beam FB#2 had larger live load forces than floor beam FB#6 mainly due to the larger longitudinal distribution factor.

Similar to the stringer analysis, the same dynamic impact factor was applied to each truck load using the span length of the floor beam from center-to-center of the spandrel beams (L = 35 feet), which amounted to

$$I = \min\left(\frac{50}{L+125}, 0.30\right) = \min\left(\frac{50}{35+125}, 0.30\right) = \min(0.31, 0.30) = 0.30$$

as specified in AASHTO Article 3.8.2.1. The use of three lanes of trucks, which has a multiple presence factor of 0.9, also controlled for the various trucks. As mentioned previously, the first floor beam from the abutment was critical in the approach spans while the eight floor beams located on the center of the bridge were equally as critical in the arch spans (see Figure 2.2). For each floor beam, the location under the third stringer from the east spandrel beam controlled the load rating; specific details of the load rating analysis are given next.

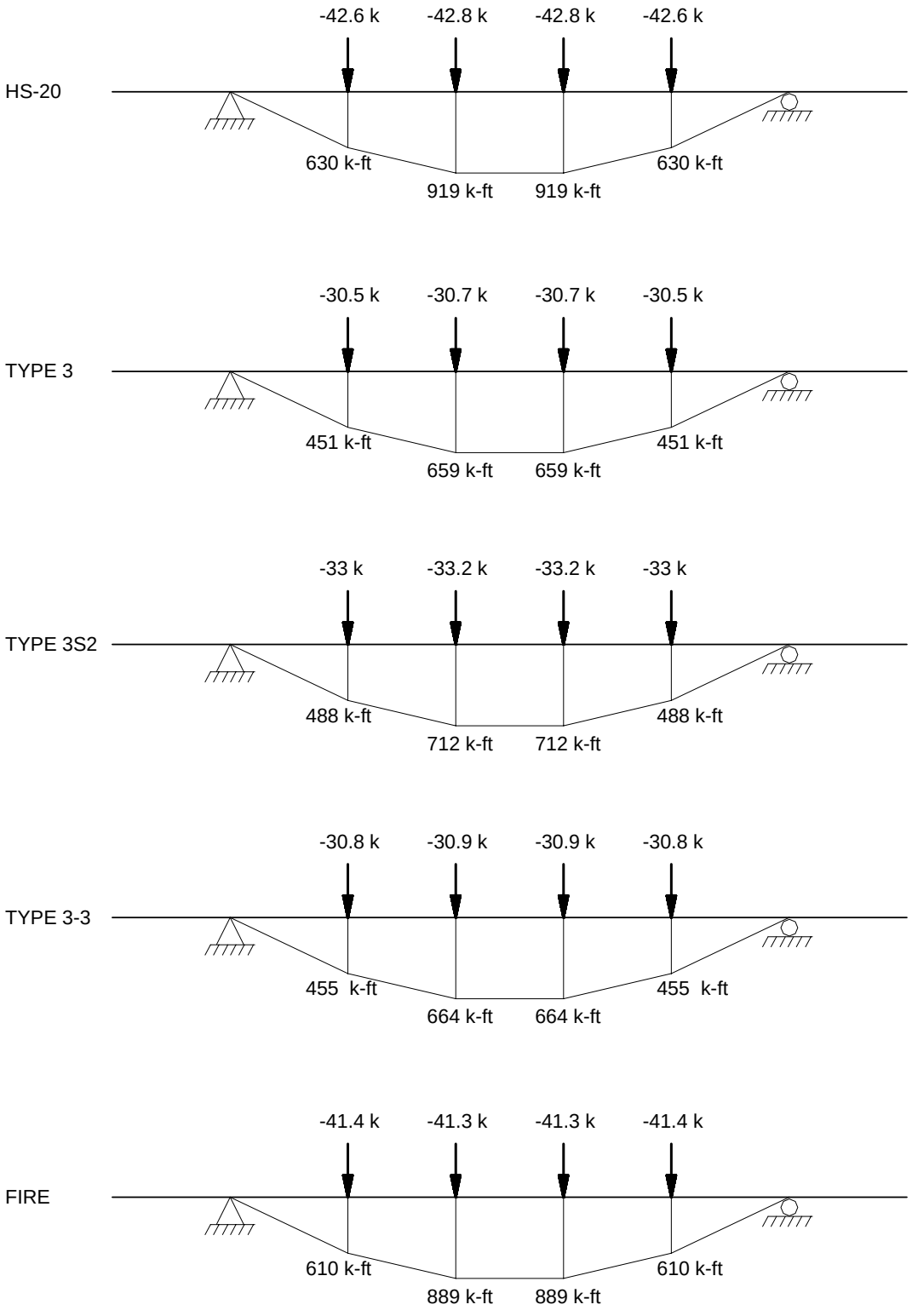

Figure 4.5 Distribution of live loads on floor beam FB#2 and moment diagrams.

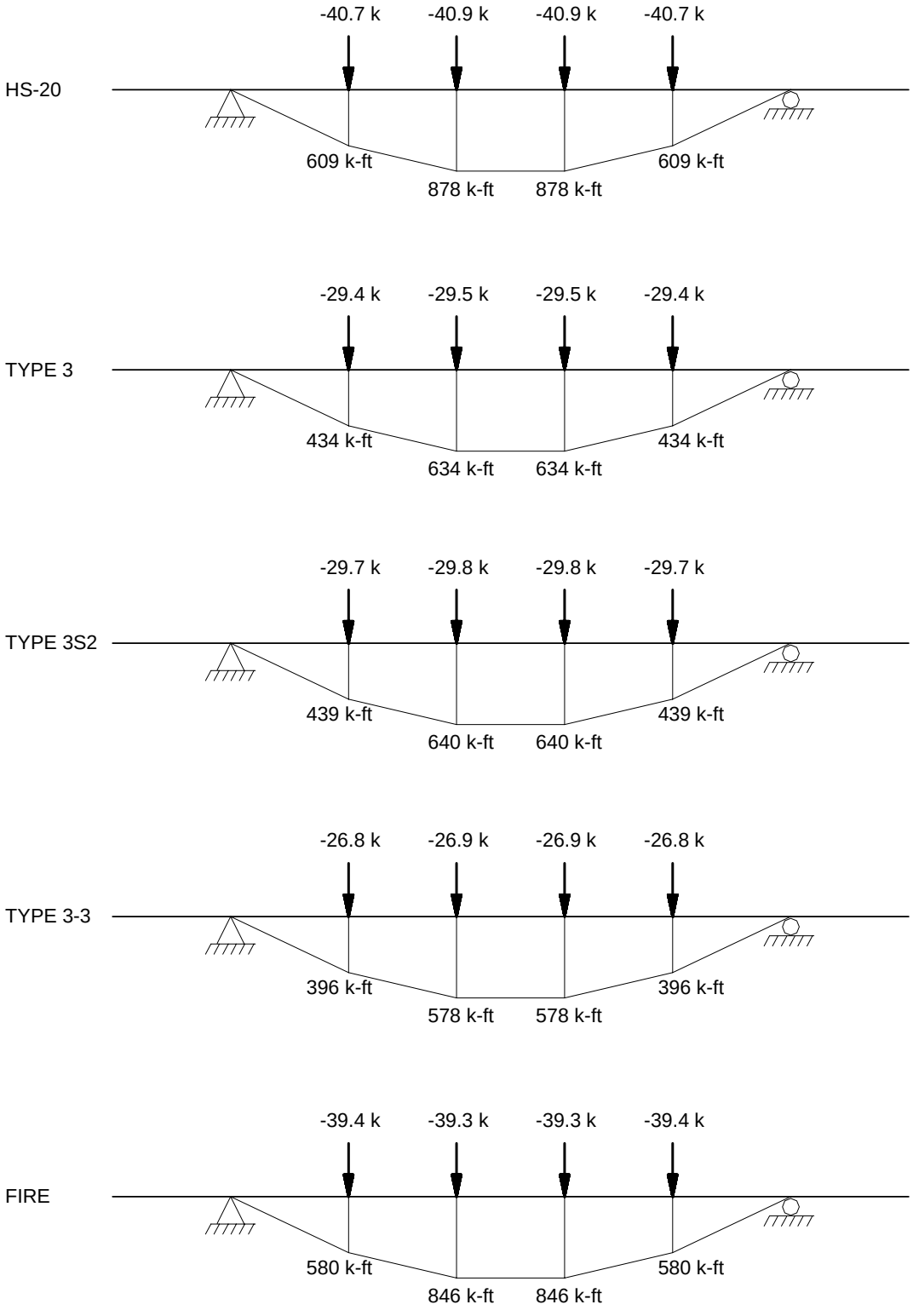

Figure 4.6 Distribution of live loads on floor beam FB#6 and moment diagrams.

4.2.2 Load Factor Rating Analysis

The dead load moment, live load moment, flexural capacity, and rating factors for floor beams FB#2 and FB#6 are reported in Table 4.4. The dead and live load moments are unfactored; in addition, the live load moment has not been reduced to account for multiple lane loading. As shown in Appendix A2, the compression flange of the floor beams failed the size requirements for a compact and non-compact section specified in the 17th Edition of the AASHTO Standard Specifications (2002) which classified the flange as a slender element. For a section having this type of structural element, the flexural capacity is less than the yield moment since the stress is elastic when buckling occurs; the computation of moment strength for sections with slender elements requires an elastic buckling analysis. When the compression flange was evaluated based on the 16th Edition of the AASHTO Standard Specification (1996), however, floor beam FB#2 failed the compact section requirements but satisfied those for a non-compact section at both the inventory and operating rating level. Floor beam FB#6, which had a flange thickness 1/16” smaller than floor beam FB#2, also satisfied the non-compact section requirements but only at the operating rating level. Based on these findings, the floor beams were considered as non-compact sections for purposes of computing the flexural capacity; floor beam FB#2 had a slightly larger flexural capacity because of its 1/16” larger flange thickness. Cases where the compression flange of floor beam FB#6 did not quite satisfy the requirements in the 16th AASHTO Standard Specification (1996) for a non-compact section are designated by an asterisk (*) in Table 4.4.

Table 4.4 Moment values and rating factors for floor beams.

Floor Beam		FB#2	FB#6
Dead Load Moment (M_D), kip-ft		255	235
Live Load Moment (M_L), kip-ft	**HS-20**	1080	1030
	TYPE 3	771	741
	TYPE 3S2	833	749
	TYPE 3-3	776	675
	FIRE	1040	990
Flexural Capacity (M_R), kip-ft		2380	2190
Inventory Rating Factor (RF_i)	**HS-20**	0.88	0.85*
	TYPE 3	1.22	1.17*
	TYPE 3S2	1.13	1.16*
	TYPE 3-3	1.21	1.29
	FIRE	0.91	0.88*
Operating Rating Factor (RF_o)	**HS-20**	1.46	1.41
	TYPE 3	2.04	1.96
	TYPE 3S2	1.89	1.94
	TYPE 3-3	2.03	2.15
	FIRE	1.51	1.47

*Non-compact section requirements for compression flange not satisfied.

Table 4.4 shows comparable rating factors between the two floor beams; floor beam FB#2 controlled the capacity for two AASHTO rating vehicles (Type 3S2 and Type 3-3) while floor beam FB#6 controlled for the remaining live loads. The critical rating values, which were calculated based on the 16th AASHTO Standard Specification (1996), are repeated in Table 4.5. It is important to note that the rating factors would have been approximately 10% smaller than those given in Tables 4.4 and 4.5 had no transverse distribution of live load been assumed as specified in AASHTO Article 3.23.3. As mentioned previously, it is more realistic that some of the live load will transfer directly to the spandrel through the slab and the remainder will transfer

through the floor beam; this approach results in smaller live load moments and thus, larger rating factors.

Table 4.5 Critical rating factors for floor beams.

Rating Factor		RF_i	RF_o
Live Load	**HS-20**[a]	0.85	1.14
	TYPE 3[a]	1.17	1.96
	TYPE 3S2[b]	1.13	1.89
	TYPE 3-3[b]	1.21	2.03
	FIRE[a]	0.88	1.47

[a]Controlled by floor beam FB#6.
[b]Controlled by floor beam FB#2.

In addition, the torsional stiffness of the spandrel beam was ignored, which if accounted for would also possibly decrease the bending moment in the floor beam and further increase the rating factor; finite element analysis and field testing is recommended to better evaluate this behavior. Another aspect of the floor beam evaluation of interest is the new compression flange requirements which are more stringent that those specified in the original design of the Omega Bridge.

4.3 Spandrel Beams

4.3.1 Description of Rating Model

The spandrel beam has a total of 21 spans; there are three 62-ft approach spans at each end of the bridge and fifteen 29.5-ft intermediate spans above the arch. Two separate models were developed to evaluate the capacity of the spandrel beam. In the first model (designated BEAM model), the spandrel beam was idealized as a continuous beam supported at the abutments and the pier, skewback, and arch columns as shown in Figure 4.7. This model assumes that the columns provide rigid support stiffness to the spandrel beam in the vertical direction but no flexural stiffness.

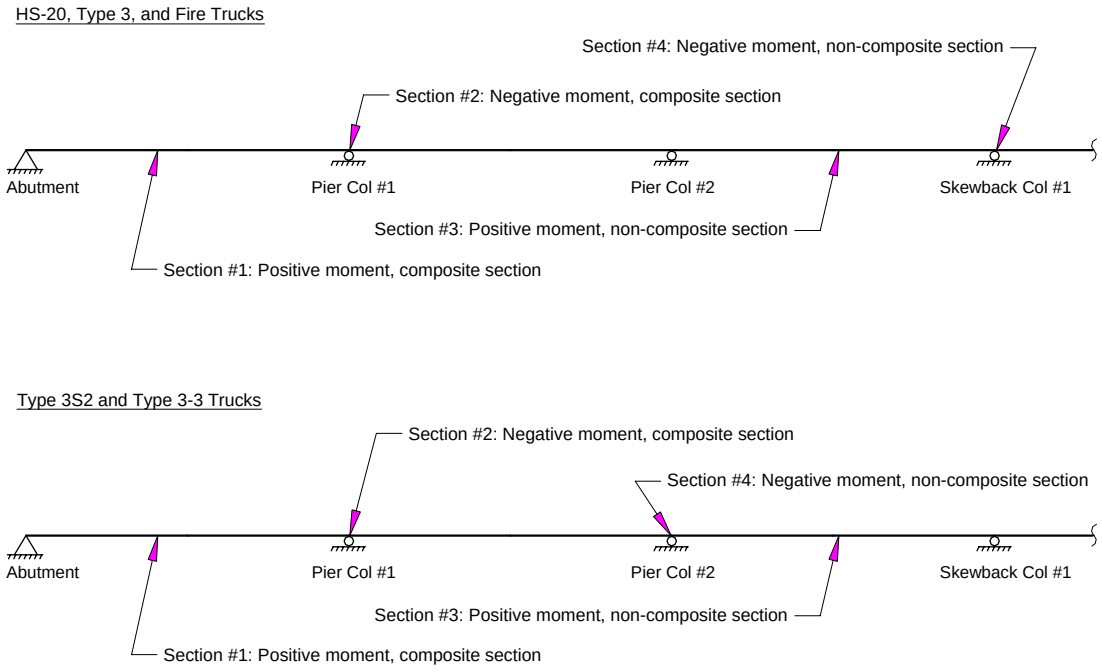

Figure 4.7 BEAM rating model of spandrel beam (including critical sections).

In the second model (designated FRAME model), the entire structure in the arch rib plane was modeled including the spandrel beam, columns, and arch as shown in Figure 4.8.

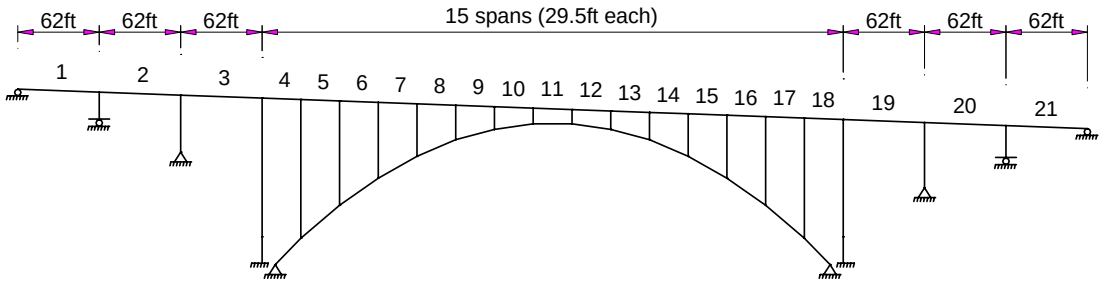

Figure 4.8 FRAME rating model of spandrel beam (including span numbers).

Spandrel-to-column and column-to-arch connections were modeled as rigid and both the axial and flexural stiffness of the columns and arch were considered. For the most part, the FRAME model shown in Figure 4.8 resulted in larger negative moments in the spandrel beam at the column locations and smaller positive moments between the columns compared to the BEAM model (see Figure 4.7). Furthermore, axial forces in the spandrel were below 15% of the yield force as required by AASHTO Article 10.48.1.1(d) for flexural members; otherwise, beam-column analysis would be necessary.

Similar to the stringer analysis, the section properties of the spandrel beam in both models were assumed prismatic (based on non-composite action) along the entire length of the bridge. Again, this assumption ignores the change in stiffness between

composite and non-composite regions as well as between areas with and without cover plates, but does not significantly influence the bending moments of the BEAM model. The FRAME model, on the other hand, is affected since the moments are more dependent on the relative flexural stiffness of the spandrel beam compared with the columns and arch. However, the use of non-composite instead of composite section properties for the spandrel will result in larger negative moments at the column locations, which is the more critical scenario.

The major portion of the dead load that acts on the spandrel beam amounts to w_{D1} = 2770 plf which includes the self-weight of the spandrel beam (302 plf) and the tributary weights of the slab (1910 plf), integral wearing surface (139 plf), floor beams (162 plf), stringers (198 plf), and wind bracing (55.7 plf). Although the load is mostly distributed to the spandrel beam as concentrated forces coming from the floor beams, the discrete point loads at the floor beam locations were assumed to be uniformly distributed over the spandrel's length. This approach simplifies the analysis but does not significantly affect the dead load moments. As shown in Figure 2.1, the vehicle traffic lanes are not symmetrical about the bridge centerline but are situated on the eastern side of the bridge width; there is a sidewalk for pedestrians on the west side of the traffic lanes. With this layout, the spandrel beam located on the east side of the bridge width is the most heavily loaded and thus, controls the capacity. In addition to dead load w_{D1}, the eastern spandrel beam is also subjected to an additional dead load of w_{D2} (equal to 307 plf) for barriers and utilities, and w_F (equal to 40.4 plf) for

fencing. While the dead loads w_{D1} and w_{D2} act over the entire length of the spandrel, the fencing load w_F acts only on the center 150 ft.

Based on Article 3.8.2.1 of the 17th AASHTO Standard Specification (2002), the live load impact factor amounted to

$$I = \min\left(\frac{50}{L+125}, 0.30\right) = \min\left(\frac{50}{62+125}, 0.30\right) = \min(0.27, 0.30) = 0.27$$

for the spandrel beam (L = 62 ft); this dynamic amplification factor was applied to all the trucks. The distribution factors for bending moment were determined using the lever rule as specified in AASHTO Article 3.23.2.3 for exterior beams and live load reduction as specified in AASHTO Article 3.12.1 for multiple loaded traffic lanes; the results for the different trucks are tabulated in Table 4.6.

Table 4.6 Live load distribution for spandrel beam.

Number of Loaded Traffic Lanes	AASHTO Vehicles			FIRE Truck		
	Moment Distribution Factor (DF)	Multiple Presence Factor (m)	DF x m	Moment Distribution Factor (DF)	Multiple Presence Factor (m)	DF x m
1	1.11	1	1.11	1.09	1	1.09
2	1.93	1	1.93	1.86	1	1.86
3	2.46	0.9	2.22	2.31	0.9	2.08
4	2.71	0.75	2.04	N/A	0.75	N/A

As shown in the table, the FIRE truck had unique moment distribution and multiple presence factors since the wheel line spacing is 7.2 ft rather than the 6 ft specified for the AASHTO vehicles. In addition, a maximum of four traffic lanes could be loaded

with the AASHTO vehicles compared to only three lanes for the FIRE truck because of the wheel line spacing. In the end, when the moment distribution and multiple presence factors were combined, the critical case turned out to be three traffic lanes for all the trucks.

Figure 4.7 shows the four critical sections (labeled Section #1 through Section #4) that were identified by analysis based on the moment envelopes for dead load and live load for the different trucks. The first (Section #1) and second (Section #2) critical sections are located in the positive moment region in the first approach span and the negative moment region at the first pier column, respectively. For these two sections, the spandrel beam is composite with the deck. The third critical section (Section #3) is located in the positive moment region of the third approach span where the spandrel is non-composite. The fourth critical section (Section #4) is located in a negative moment, non-composite region of the spandrel beam. However, the critical section is at the skewback column for the HS-20, Type 3, and FIRE trucks and at the second pier column for the Type 3S2 and Type 3-3 trucks. The load rating analysis at these critical sections is discussed next.

4.3.2 Load Factor Rating Analysis

Tables 4.7 and 4.8 compare the rating factors for the four critical sections (see Figure 4.7) of the spandrel beam based on the BEAM and FRAME models, respectively. The smallest rating factors are noted by an asterisk (*).

Table 4.7 Moment values and rating factors of spandrel beam (BEAM model).

Critical Section		Section #1	Section #2	Section #3	Section #4
Dead Load Moment (M_D), kip-ft		930	1223	613	750
Live Load Moment (M_L), kip-ft	HS-20	1867	1154	1382	1252
	TYPE 3	1397	822	1045	896
	TYPE 3S2	1438	952	1031	894
	TYPE 3-3	1269	1026	892	952
	FIRE	1823	1166	1322	1263
Flexural Capacity (M_R), kip-ft		6403	4749	4256	4256
Inventory Rating Factor (RF_i)	HS-20	1.17	1.19	1.15 (*)	1.21
	TYPE 3	1.57	1.67	1.53 (*)	1.69
	TYPE 3S2	1.52	1.44 (*)	1.55	1.53
	TYPE 3-3	1.73	1.34 (*)	1.79	1.44
	FIRE	1.20	1.18 (*)	1.21	1.20
Operating Rating Factor (RF_o)	HS-20	1.96	1.98	1.93 (*)	2.02
	TYPE 3	2.62	2.78	2.55 (*)	2.82
	TYPE 3S2	2.54	2.40 (*)	2.58	2.56
	TYPE 3-3	2.88	2.23 (*)	2.99	2.40
	FIRE	2.01	1.96 (*)	2.01	2.00

Table 4.8 Moment values and rating factors of spandrel beam (FRAME model).

Critical Section		Section #1	Section #2	Section #3	Section #4
Dead Load Moment (M_D), kip-ft		927	1231	560	881
Live Load Moment (M_L), kip-ft	HS-20	1872	1145	1386	1097
	TYPE 3	1399	816	1049	785
	TYPE 3S2	1439	941	1036	1010
	TYPE 3-3	1271	1009	900	930
	FIRE	1824	1157	1327	1105
Flexural Capacity (M_R), kip-ft		6403	4749	4256	4256
Inventory Rating Factor (RF_i)	HS-20	1.17	1.19	1.17 (*)	1.31
	TYPE 3	1.57	1.67	1.55 (*)	1.83
	TYPE 3S2	1.52	1.45 (*)	1.57	1.46
	TYPE 3-3	1.72	1.35 (*)	1.81	1.58
	FIRE	1.20	1.18 (*)	1.23	1.30
Operating Rating Factor (RF_o)	HS-20	1.96	1.99	1.96 (*)	2.18
	TYPE 3	2.62	2.79	2.59 (*)	3.05
	TYPE 3S2	2.54	2.42 (*)	2.62	2.43
	TYPE 3-3	2.88	2.26 (*)	3.02	2.64
	FIRE	2.01	1.97 (*)	2.05	2.16

The dead load moments, live load moments (with the impact, distribution, and multiple presence factors included), and flexural capacities for the spandrel beam are also reported in Tables 4.7 and 4.8 at the four critical sections. Recall from Chapter 2 that the critical location for Section #1 was at the end of the cover plates due to the analysis assumptions. The support conditions and stiffness of the spandrel, columns, and arch rib all affect where the critical section occurs. In the end, the conservative decision was made to take the critical section at the end of the cover plates.

Between the BEAM and FRAME models, there was very little discrepancy in the analytical results at Sections #1 through #2 as shown in Tables 4.7 and 4.8. This behavior is reasonable since the pier column at Section #2 (i.e., Pier Column #1) is subjected to axial loading and no bending moment in both models since the base of this column is supported by a rocker bearing. More notable differences occurred in the bending moments at locations further away from the abutment at Section #3 (dead load moment) and Section #4 (dead and live load moments). Hence, these two locations are more affected by the stiffness of the riveted connections between the columns (i.e., Pier Column #2 and Skewback Column #1) and the spandrel beam. This is because the second pier column has a pinned base support while the skewback column has a fixed based support. As a result, bending moment develops in the columns when the column connections to the spandrel beam are modeled as rigid.

The flexural capacity of the spandrel beam was governed by the yield moment capacities of the composite section (AASHTO Article 10.50) at Sections #1 and #2 and the non-composite section (AASHTO Article 10.48) at Sections #3 and #4. Although the spandrel met the compact requirements for a composite section in the positive moment region (Section #1), the yield moment controlled the capacity as indicated by AASHTO Article 10.50.1.1 since the spandrel was non-compact (due to the web slenderness) in the negative moment pier region (Section #2). For the non-composite sections in the positive and negative moment regions (i.e., Sections #3 and #4), the spandrel was also non-compact for the web and thus, governed by the yield moment capacity. The web slenderness actually failed the unstiffened web requirement but satisfied the stiffened web requirement for a non-compact section. Since the webs of the spandrel beam were interconnected by diaphragm plates, the non-compact requirements were considered to have been met which based the capacity on the yield moment.

In accordance with AASHTO Article 10.50(c), the yield moment capacities of the positive and negative composite sections (i.e., Sections #1 and #2, respectively) were computed considering non-composite action (i.e., the steel spandrel beam acting alone) under dead load and composite action under live load. Thus, for these two sections, the rating factors are computed as follows

$$RF = \frac{M_R - \left(\frac{A_1 M_D}{S_{nc}}\right) S_c}{A_2 M_L} = \frac{F_y S_c - \left(\frac{A_1 M_D}{S_{nc}}\right) S_c}{A_2 M_L}$$

where S_{nc} and S_c are the section moduli at the extreme tension fiber of the steel spandrel for the non-composite and composite sections, respectively. By replacing S_c by S_{nc} in the above equation, the rating factors for the positive and negative non-composite sections (i.e., Sections #3 and #4, respectively) are determined as shown below

$$RF = \frac{M_R - \left(\frac{A_1 M_D}{S_{nc}}\right) S_{nc}}{A_2 M_L} = \frac{F_y S_{nc} - A_1 M_D}{A_2 M_L}$$

Based on the smaller rating factors shown in Tables 4.7 and 4.8, the BEAM model resulted in a lower capacity level for the spandrel beam compared to the FRAME model. In both models, Section #2 (where the spandrel beam is composite and subjected to negative moment) controlled the capacity under the Type 3S2, Type 3-3, and FIRE truck loads. For the HS-20 and Type 3 truck loads, Section #3 (where the spandrel beam is non-composite and subjected to positive moment) controlled the spandrel beam capacity. The rating factors at these two sections for the BEAM model are repeated in Table 4.9 which shows all values larger than 1; the smallest rating factors are those for the HS-20 and FIRE trucks.

Table 4.9 Rating factors at Sections #2 and #3 of spandrel beam (BEAM model).

Rating Factor		RF_i	RF_o
Live Load	HS-20[a]	1.15	1.93
	TYPE 3[a]	1.53	2.55
	TYPE 3S2[b]	1.44	2.40
	TYPE 3-3[b]	1.34	2.23
	FIRE[b]	1.18	1.96

[a]Controlled by Section #3.
[b]Controlled by Section #2.

It is recommended that a three-dimensional finite element model be developed and field testing be performed to further evaluate the spandrel. One particular improvement that could be made is with the moment distribution factor. Recall that the AASHTO distribution factor was determined based on the lever rule. In many cases, this approach overestimates the load carried by exterior beams and thus, results in low rating factors. A better estimate of the load distribution to the spandrel beam could help improve its capacity rating. In addition, the actual stiffness of the spandrel-to-column connections as well as that of the column supports in the approach spans could be better evaluated. In the FRAME model, the base support was assumed to be pinned for the pier columns and fixed for the skewback column. Another parameter that could be evaluated is the spandrel beam stiffness properties. Both the BEAM and FRAME models assumed prismatic section properties based on non-composite action. The bending moments in the spandrel depend on its stiffness relative to the columns and arch rib. Finally, finite element analysis and field testing allows the overall three-

dimensional behavior of the bridge to be evaluated opposed to the two-dimensional models used in this study that are commonly used in design.

CHAPTER 5

LOAD RATING OF COLUMNS

5.1 Description of Rating Model

As discussed earlier in Chapter 2, there are four pier columns, 14 arch columns and two skewback columns in each arch rib plane of the Omega Bridge as shown in Figure 5.1. All the columns have a riveted connection to the spandrel beam at their top end; however, the columns have different support conditions at their bottom end (see Figure 5.1). Pier columns #1 and #4, which are located closest to the abutments, are supported by rocker bearings (i.e., rollers) while pier columns #3 and #4 are pin supported at their bases. The two skewback columns, #1 and #2, are both fixed at their bottom ends. For the 14 arch columns, labeled #1 through #14, the base connections with the arch rib are riveted.

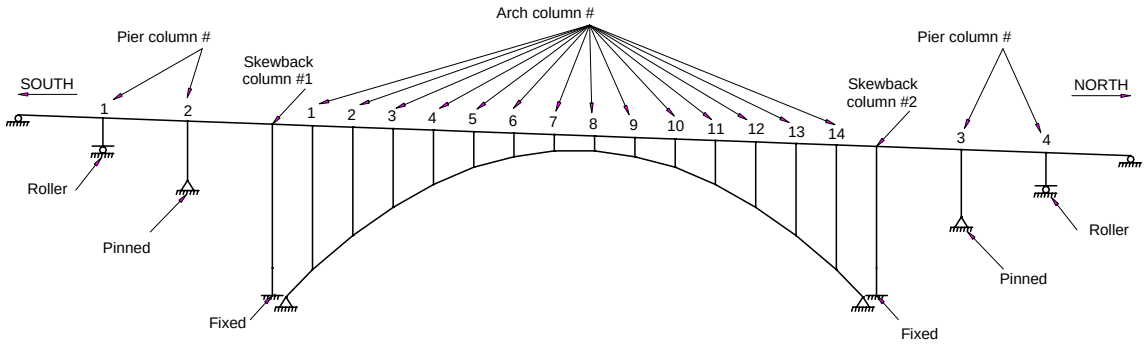

Figure 5.1 BEAM-COLUMN rating model of pier, skewback, and arch columns.

As mentioned above, the column-spandrel beam connections as well as the connections between the arch columns and the arch rib are all riveted; however, two

separate design details were used to make these connections. Based on a review of these details, it is anticipated that the connections will provide semi-rigid stiffness somewhere between a true hinge (i.e., no moment transfer and independent rotation of connecting members) and a fully rigid connection (i.e., full moment transfer and upholding original angle between connecting members). Due to the uncertainty of the rotational connection stiffness at the column ends, two separate models were developed to evaluate the capacity of the columns. In the first model (designated BEAM-COLUMN model), all the riveted column connections with the spandrel beam and the arch rib as well as the base connections of the skewback columns were idealized as rigid connections as shown in Figure 5.1. This modeling approach simulates frame behavior and therefore, produces both bending moment and axial compression in the vertical members. Under combined axial load and bending, the vertical members are evaluated as beam-columns according to AASHTO Article 10.54.2. In the second model (designated COLUMN model), all the riveted connections as well as the base support of the skewback columns were discretized as hinged connections as shown in Figure 5.2.

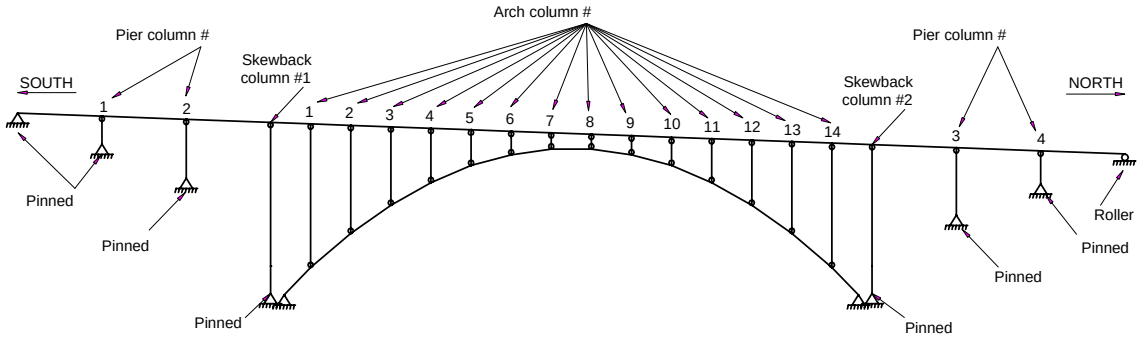

Figure 5.2 COLUMN rating model of pier, skewback, and arch columns.

Also, the boundary conditions at the south abutment and pier columns #1 and #4 needed to be changed from rollers to pinned supports in order to provide stability to the model. With the model given in Figure 5.2, the columns are subjected to pure axial loading (with no bending moment) and thus, are evaluated according to AASHTO Article 10.54.1.

In addition to the self-weight of the columns, the dead load applied to both the BEAM-COLUMN and COLUMN rating models included the weights of the floor system; wind bracing; barriers and utilities; and fencing. A detailed discussion of the dead loads can be found in Section 4.3 which covers the rating of the spandrel beam. Like the spandrel beam, the columns in the eastern arch rib plane control the capacity due to the position of the traffic lanes. Live-load distribution factors for the columns were also determined in the same manner as that of the spandrel beam; that is, using the lever rule for exterior beams (as specified in AASHTO Article 3.23.2.3) and live load reduction for multiple loaded traffic lanes (as specified in AASHTO Article 3.12.1). Hence, the live-load distribution factors for the columns in both rating models are the same as those tabulated in Table 4.6 for the eastern spandrel beam (see Section 4.3). A full listing of the rating calculations for the columns under AASHTO HS-20 truck loading is provided in Appendix A4.

5.2 Load Factor Rating Analysis

5.2.1 BEAM-COLUMN Model: Combined Axial Load and Bending

Since a two-dimensional model was used to evaluate the columns of the Omega Bridge, there is no bending moments generated in the out-of-plane direction. As a result, the columns were assumed to act as beam-column members in the plane of the arch rib (i.e., in-plane direction) and as pure column members in the out-of-plane direction. In reality, the columns are subjected to flexure perpendicular to the arch rib plane; however, the out-of-plane bending moments applied to the columns are generally smaller than those in the in-plane direction. Thus, the out-of-plane direction will not control the column capacity based on beam-column behavior. Furthermore, a three-dimensional analysis is required to properly evaluate the columns as beam-column members in the out-of-plane direction which was outside the scope of this study. In consequence, the evaluation of the columns under axial loading and bending moment is based on in-plane behavior. In the out-of-plane direction, the columns are treated as pure compression members (covered in Section 5.2.2).

Recall from AASHTO Article 3.8.2.1, the impact factor for a bridge member is a function of the loaded span length. For pier columns #2 and #3 and skewback columns #1 and #2, the loaded length equaled the span length of the spandrel beam in the approach spans as given below in the impact factor computation

$$I = \min\left(\frac{50}{L+125}, 0.30\right) = \min\left(\frac{50}{62+125}, 0.30\right) = \min(0.27, 0.30) = 0.27$$

Pier columns #1 and #4, closest to the abutments, are not subject to flexure since they are leaner columns and thus, were not evaluated as beam-column members. The capacity evaluation of these two columns was done based on pure column behavior which is discussed in Section 5.2.2. For the arch columns, numbered #1 through #14, the loaded span length was taken as two times the arch column spacing (i.e., 59 ft). This length was determined by influence line analysis of both axial compression and bending moment in the arch columns. In both analysis cases, the minimum distance between inflection points (i.e., locations of zero axial compression or bending moment on the influence line) was about two times the arch column spacing. Thus, using a loaded span length of 59 ft, the dynamic impact factor of the arch columns amounted to

$$I = \min\left(\frac{50}{L+125}, 0.30\right) = \min\left(\frac{50}{2 \text{ x } 29.5+125}, 0.30\right) = \min(0.27, 0.30) = 0.27$$

With no bracing between the columns in the arch rib plane (see Figure 5.1), the portion of the Omega Bridge above the arch line (i.e., columns and spandrel beam) was considered an unbraced or sway frame for analysis purposes. The arch rib is laterally supported on both ends with pin connections and thus, is not subject to sidesway; hence, the arch rib provided vertical and lateral support at the bottom of the arch columns. In an unbraced frame, lateral resistance is generally provided by rigid beam-column connections. For the Omega Bridge, lateral stiffness is provided by the connections between the columns and the spandrel beam as well as the fixed base

connections of the skewback columns and the connections between the arch columns and arch rib.

As specified in AASHTO Article 10.54.2.1, the capacity of bridge components under combined axial loading and bending shall satisfy interaction equations (10-155) and (10-156) given below:

$$\frac{P}{0.85A_s F_{cr}} + \frac{M}{M_u}\left(\frac{C}{1-\frac{P}{A_s F_e}}\right) \le 1 \qquad \text{AASHTO Equation (10-155)}$$

and

$$\frac{P}{0.85A_s F_y} + \frac{M}{M_p} \le 1 \qquad \text{AASHTO Equation (10-156)}$$

where P = maximum axial compression (due to dead load and live load plus impact); A_s = cross-sectional area of column; F_{cr} = critical buckling stress; M = maximum bending moment (due to dead load and live load plus impact); M_u = maximum flexural strength (amounted to the yield moment or F_yS for all the columns); C = equivalent moment factor; F_e = Euler Buckling stress; F_y = yield stress; and M_p = full plastic moment of the section or F_yZ. Note that M_u, F_e, and M_p are computed in the plane of bending (i.e., arch rib plane).

In beam-column analysis for unbraced frames, the maximum moment applied to a bridge member is generally expressed as $M = B_1 M_{nt} + B_2 M_{lt}$ where M_{nt} is the first

order moment assuming no lateral translation of the member ends (i.e., non-sway case) and M_{lt} is the first order moment due to lateral end translation (i.e., sway case). The moment amplification factors, B_1 and B_2, account for second order effects due to the displacement between member ends (i.e., P-δ effects) and due to lateral end translation (i.e., P-Δ effects), respectively, which are computed as follows:

$$B_1 = \frac{C}{1 - \frac{P}{A_s F_{e1}}} \geq 1$$

and

$$B_2 = \frac{1}{1 - \frac{\sum P}{\sum A_s F_{e2}}} \geq 1$$

where F_{e1} is the Euler Buckling stress for the non-sway case and F_{e2} is the Euler Buckling stress for the sway case. Note that separate B_1 factors are computed for all the columns of the frame while a single B_2 value applies to all the columns of the frame since second order effects in frames subject to lateral translation is a story phenomenon. It is therefore observed that AASHTO Equation (10-155) is meant to be applied directly to braced frames. For unbraced frames such as the Omega Bridge, the equation may be rewritten as follows to account for non-sway and sway effects

$$\frac{P}{0.85 A_s F_{cr}} + \frac{B_1 M_{nt} + B_2 M_{lt}}{M_u} \leq 1$$

The greatest difficulty in the evaluation of beam-columns is determining the maximum bending moment, $M = B_1M_{nt} + B_2M_{lt}$. To calculate B_1, the column ends are assumed to be restrained from lateral end translation. According to AASHTO Article 10.54.1.2, the effective length factor under braced conditions used to compute F_{e1} is specified as 0.75 for members with riveted-end conditions (i.e., arch and skewback columns) and 0.875 for members with pinned-end conditions (i.e., pier columns). The equivalent load factor, C, is computed according to AASHTO Article 10.54.2.2 using the equation $C = 0.6 + 0.4a$ where "a" is the ratio of the smaller to larger moment at the column ends; the value of "a" is positive for members in single curvature and negative for members in double curvature. Thus, the equivalent load factor for the pier columns is $C = 0.6$ since the moment at the pinned base is zero. The arch and skewback columns, on the other hand, have bending moments on both ends which are approximately equal in magnitude and act in the same direction (causing double curvature). The "a" ratio for the arch and skewback columns was conservatively taken as -0.5 (i.e., the smaller end moment is half in magnitude of the larger end moment) and thus, $C = 0.4$. Because of the small C values, the moment amplification factor for the unbraced condition (i.e., B_1) was equal to unity for all the columns under the different vehicular loads.

Contrary to B_1, B_2 is computed based on unrestrained lateral end translation of the column ends. As shown above, the denominator of the B_2 equation contains the term $\sum A_sF_{e2}$ which represents the total Euler Buckling resistance (of all the columns)

under unbraced conditions. Since the spandrel beam and arch rib were found to be significantly stiffer in flexure than the columns, the end conditions were taken to be fixed-pinned for the pier columns and fixed-fixed for the arch and skewback columns to compute F_{e2}; the top end of each of the columns was free to translate relative to the bottom end. These end conditions resulted in effective length factors equal to 2.0 for the pier columns and 1.2 for the arch and skewback columns as specified in AASHTO Appendix C. The two pier columns closest to the abutment (i.e., pier column #1 and #2 in Figure 5.1) are leaner columns and theoretically have an effective length factor equal to infinity and no axial capacity under unbraced conditions. As a result, these columns do not contribute to the overall sway buckling strength of the Omega Bridge.

Table 5.1 shows a sample computation of B_2 under HS-20 vehicular loading at the inventory rating level. Note the pier columns #1 and #2 were not included in the calculation for the reasons discussed above. As shown in the table, the value of B_2 is very close to unity since the total load acting on the columns under dead load and live load plus impact (i.e., $\sum P$) is small compared to the total elastic sidesway buckling strength (i.e., $\sum A_s F_{e2}$). This is true under all the vehicular loading cases at both the inventory and operating rating level.

Table 5.1 Sample calculation of sidesway moment amplification factor, B_2.

1. Frame strength calculation

Column	L (ft)	L (in)	K	P_{e2} (kips)
Pier col #2	41.2	494.4	2	1980
Pier col #3	47.4	568.8	2	1496
Skewback col #1	103.1	1237.2	1.2	4114
Skewback col #2	86.8	1041.6	1.2	5804
Arch col #1	99.1	1189.2	1.2	950
Arch col #2	73.1	877.2	1.2	1747
Arch col #3	51.4	616.8	1.2	3533
Arch col #4	34.2	410.4	1.2	7980
Arch col #5	20.5	246	1.2	22210
Arch col #6	11.7	140.4	1.2	68183
Arch col #7	6.9	82.8	1.2	196042
Arch col #8	5.8	69.6	1.2	277455
Arch col #9	8.5	102	1.2	129184
Arch col #10	15.1	181.2	1.2	40935
Arch col #11	26.7	320.4	1.2	13093
Arch col #12	41.7	500.4	1.2	5368
Arch col #13	61.2	734.4	1.2	2492
Arch col #14	85	1020	1.2	1292
Frame strength (kips)			$\sum P_{e2} =$	**783855**

2. Total frame force calculation

Total dead load (kips)	2510
HS20 live load plus impact (kips)	203
Frame force at inventory level (kips) $\sum P = 1.3 \times 2510 + 2.17 \times 203 =$	**3704**

3. Sidesway moment amplification factor calculation at inventory level

$$B_2 = \frac{1}{1 - \frac{\sum P}{\sum P_{e2}}} = \frac{1}{1 - \frac{3704}{783855}} = 1.005$$

With both the moment amplification factors equal to unity (i.e., $B_1 = 1$ and $B_2 = 1$), AASHTO Equation (10-155) becomes

$$\frac{P}{0.85A_s F_{cr}} + \frac{M_{nt} + M_{lt}}{M_u} \leq 1$$

where P is the maximum compressive load and $M_{nt} + M_{lt}$ is the maximum first order moment acting on the column under dead load and live load plus impact. In general, the longitudinal position of the vehicular load that causes the maximum axial force in a given column is not the same as that producing the maximum bending moment. For maximum axial compression, the truck is generally positioned straddling the column with axles on both of the adjacent spans. To maximize the bending moment, the truck is generally positioned in only one of the spans adjacent to the column. In order to simplify the analysis of the Omega Bridge columns, the largest magnitudes for axial force and bending moment from the design envelopes were used. This approach is conservative but reasonable since the influence line analysis showed that the critical truck locations for axial force and bending moment were in close proximity (i.e., within about 60 ft for the pier columns and 30 ft for the arch and skewback columns).

The final variable needed in the interaction equation is the critical buckling stress, F_{cr}, of the column which is specified in AASHTO Article 10.54.1.1 for inelastic and elastic buckling as

$$F_{cr} = F_y\left[1 - \frac{F_y}{4\pi^2 E}\left(\frac{KL_c}{r}\right)\right] \qquad \text{Inelastic Buckling}$$

$$F_{cr} = \frac{\pi^2 E}{\left(\frac{KL_c}{r}\right)^2}$$ Elastic Buckling

where E = modulus of elasticity (29000 ksi); K = effective length factor in the plane of buckling; L_c = length of the member between points of support; and r = radius of gyration in the plane of buckling. In basic frame analysis, the maximum slenderness ratio, $(KL_c/r)_{max}$, for in-plane or out-of-plane buckling is used to compute F_{cr}. For the Omega Bridge, however, in-plane buckling was not considered likely for three reasons. First, for sway buckling to occur, the columns would all have to buckle simultaneously as a story. This type of behavior is likely for rectangular framing where the columns all have about the same stiffness and applied loads. The Omega Bridge, on the other hand, is composed of columns having different end conditions, unsupported lengths, and axial loads. Under truck loading, only a single column is subjected to maximum loading; the remaining columns are subjected to axial loads below their largest magnitude (since the truck load is positioned to maximize the force in a discrete column) and thus, act to brace the most heavily loaded column. Second, there is only a limited amount of movement that can take place at the expansion joints (at the abutment ends) of the bridge. Once the expansion joint gap is exhausted, sway will be restrained to some degree by the abutment. Third, in the computation of B_2 (see Table 5.1), the total elastic sidesway buckling strength of the bridge columns (i.e., $\sum A_s F_{e2}$) was found to be large compared to the total applied compressive loads (i.e., $\sum P$). For these three major reasons, the columns were all

assumed to be braced in the in-plane direction and the critical buckling stress was determined based on nonsway in-plane buckling.

With support from the discussion given above, Equations (10-155) and (10-156) of the AASHTO Standard Specifications may now be written in terms of the factored dead load and live load (plus impact) as follows

$$\frac{P}{P_{cr}}+\frac{M}{M_u}=\frac{A_1P_D+A_2P_L}{0.85A_sF_{cr}}+\frac{A_1M_D+A_2M_L}{SF_y}\le 1 \quad \text{AASHTO Eq. (10-155)}$$

$$\frac{P}{P_y}+\frac{M}{M_p}=\frac{A_1P_D+A_2P_L}{0.85A_sF_y}+\frac{A_1M_D+A_2M_L}{ZF_y}\le 1 \quad \text{AASHTO Eq. (10-156)}$$

where P_D and P_L are the unfactored axial forces; M_D and M_L are the unfactored bending moments; and A_1 and A_2 are the load factors under dead load and live load (plus impact), respectively. Tables 5.2 through 5.6 gives the final interaction ratios for the pier columns (excluding the ones closest to the abutments), arch columns, and skewback columns computed based on AASHTO Equations (10-155) and (10-156) at the inventory and operating rating levels; the five tables correspond to the five different live loads. The interaction ratios are designated as IR_i at inventory and IR_o at operating; values less than one indicate satisfactory passing performance. Also reported in Tables 5.2 through 5.6 are the inventory (RF_i) and operating (RF_o) rating factors.

Table 5.2 Interaction ratios and rating factors for bridge columns under HS-20 design truck loading.

Column	AASHTO Eq. (10-155)				AASHTO Eq. (10-156)			
	IR_i	IR_o	RF_i	RF_o	IR_i	IR_o	RF_i	RF_o
Pier Col #2	0.87	0.59	1.18	1.97	0.79	0.53	1.33	2.21
Pier Col #3	0.76	0.53	1.42	2.36	0.69	0.48	1.60	2.68
Arch Col #1	0.80	0.54	1.30	2.16	0.67	0.45	1.59	2.66
Arch Col #2	0.93	0.62	1.10	1.83	0.81	0.54	1.29	2.15
Arch Col #3	1.02	0.68	0.98	1.64	0.90	0.60	1.13	1.89
Arch Col #4	1.07	0.72	0.93	1.55	0.95	0.63	1.06	1.77
Arch Col #5	1.17	0.77	0.83	1.39	1.04	0.69	0.95	1.59
Arch Col #6	1.21	0.80	0.80	1.34	1.08	0.71	0.92	1.53
Arch Col #7	1.08	0.70	0.91	1.52	0.97	0.63	1.04	1.73
Arch Col #8	0.92	0.59	1.10	1.83	0.83	0.54	1.23	2.06
Arch Col #9	1.19	0.78	0.82	1.36	1.06	0.70	0.93	1.56
Arch Col #10	1.26	0.83	0.76	1.27	1.13	0.74	0.87	1.45
Arch Col #11	1.17	0.76	0.84	1.40	1.04	0.68	0.96	1.59
Arch Col #12	1.10	0.72	0.90	1.50	0.98	0.64	1.03	1.71
Arch Col #13	0.98	0.65	1.02	1.71	0.86	0.57	1.19	1.98
Arch Col #14	0.79	0.52	1.31	2.19	0.68	0.45	1.55	2.59
Skewback Col #1	0.44	0.31	2.76	4.60	0.38	0.27	3.21	5.36
Skewback Col #2	0.45	0.32	2.63	4.39	0.40	0.28	3.03	5.06

Table 5.3 Interaction ratios and rating factors for bridge columns under TYPE 3 legal truck loading.

Column	AASHTO Eq. (10-155)				AASHTO Eq. (10-156)			
	IR_i	IR_o	RF_i	RF_o	IR_i	IR_o	RF_i	RF_o
Pier Col #2	0.66	0.46	1.69	2.82	0.60	0.42	1.90	3.17
Pier Col #3	0.59	0.42	2.03	3.38	0.53	0.39	2.30	3.83
Arch Col #1	0.61	0.42	1.85	3.09	0.51	0.35	2.26	3.78
Arch Col #2	0.70	0.48	1.56	2.61	0.61	0.42	1.83	3.06
Arch Col #3	0.76	0.52	1.39	2.32	0.68	0.47	1.60	2.68
Arch Col #4	0.80	0.54	1.32	2.20	0.71	0.49	1.50	2.51
Arch Col #5	0.88	0.60	1.18	1.96	0.79	0.54	1.35	2.24
Arch Col #6	0.91	0.62	1.13	1.89	0.81	0.55	1.30	2.16
Arch Col #7	0.80	0.54	1.29	2.16	0.72	0.48	1.47	2.45
Arch Col #8	0.68	0.45	1.56	2.61	0.61	0.40	1.76	2.93
Arch Col #9	0.89	0.61	1.15	1.92	0.80	0.54	1.32	2.20
Arch Col #10	0.94	0.64	1.07	1.79	0.84	0.57	1.23	2.05
Arch Col #11	0.87	0.58	1.19	1.98	0.78	0.52	1.35	2.26
Arch Col #12	0.82	0.55	1.27	2.13	0.73	0.49	1.46	2.43
Arch Col #13	0.73	0.50	1.46	2.43	0.65	0.44	1.69	2.82
Arch Col #14	0.59	0.40	1.87	3.12	0.51	0.35	2.21	3.69
Skewback Col #1	0.35	0.25	3.87	6.47	0.30	0.22	4.52	7.55
Skewback Col #2	0.35	0.26	3.71	6.19	0.31	0.23	4.27	7.13

Table 5.4 Interaction ratios and rating factors for bridge columns under TYPE 3S2 legal truck loading.

Column	AASHTO Eq. (10-155)				AASHTO Eq. (10-156)			
	IR_i	IR_o	RF_i	RF_o	IR_i	IR_o	RF_i	RF_o
Pier Col #2	0.85	0.57	1.22	2.04	0.77	0.52	1.37	2.29
Pier Col #3	0.74	0.51	1.48	2.46	0.67	0.47	1.67	2.79
Arch Col #1	0.74	0.50	1.43	2.38	0.63	0.42	1.73	2.90
Arch Col #2	0.87	0.58	1.19	1.99	0.76	0.51	1.40	2.34
Arch Col #3	0.95	0.63	1.07	1.79	0.84	0.56	1.24	2.06
Arch Col #4	0.98	0.65	1.02	1.71	0.87	0.58	1.17	1.96
Arch Col #5	1.07	0.71	0.92	1.54	0.95	0.64	1.06	1.77
Arch Col #6	1.10	0.73	0.89	1.48	0.98	0.66	1.02	1.71
Arch Col #7	1.02	0.66	0.98	1.64	0.91	0.59	1.12	1.87
Arch Col #8	0.87	0.56	1.17	1.96	0.78	0.50	1.33	2.22
Arch Col #9	1.09	0.72	0.90	1.51	0.97	0.65	1.04	1.73
Arch Col #10	1.15	0.76	0.84	1.41	1.03	0.68	0.97	1.62
Arch Col #11	1.07	0.70	0.92	1.54	0.95	0.63	1.06	1.77
Arch Col #12	1.02	0.67	0.98	1.63	0.91	0.60	1.12	1.87
Arch Col #13	0.92	0.61	1.11	1.85	0.81	0.54	1.28	2.14
Arch Col #14	0.74	0.49	1.43	2.38	0.64	0.42	1.69	2.82
Skewback Col #1	0.39	0.28	3.24	5.41	0.34	0.25	3.77	6.30
Skewback Col #2	0.40	0.29	3.10	5.18	0.36	0.25	3.57	5.95

Table 5.5 Interaction ratios and rating factors for bridge columns under TYPE 3-3 legal truck loading.

Column	AASHTO Eq. (10-155)				AASHTO Eq. (10-156)			
	IR_i	IR_o	RF_i	RF_o	IR_i	IR_o	RF_i	RF_o
Pier Col #2	0.90	0.60	1.13	1.89	0.82	0.55	1.28	2.13
Pier Col #3	0.78	0.54	1.37	2.29	0.70	0.49	1.56	2.60
Arch Col #1	0.77	0.52	1.36	2.27	0.65	0.44	1.65	2.75
Arch Col #2	0.90	0.61	1.13	1.89	0.79	0.53	1.33	2.22
Arch Col #3	0.98	0.66	1.02	1.70	0.87	0.58	1.18	1.97
Arch Col #4	1.02	0.67	0.98	1.64	0.90	0.60	1.13	1.88
Arch Col #5	1.11	0.73	0.89	1.48	0.98	0.66	1.02	1.70
Arch Col #6	1.14	0.76	0.86	1.43	1.01	0.67	0.99	1.65
Arch Col #7	1.06	0.69	0.94	1.56	0.94	0.62	1.07	1.79
Arch Col #8	0.91	0.59	1.11	1.85	0.82	0.53	1.26	2.10
Arch Col #9	1.12	0.74	0.87	1.45	1.00	0.66	1.00	1.67
Arch Col #10	1.19	0.78	0.81	1.36	1.06	0.70	0.94	1.56
Arch Col #11	1.11	0.73	0.89	1.48	0.99	0.65	1.02	1.70
Arch Col #12	1.06	0.70	0.93	1.56	0.94	0.62	1.07	1.79
Arch Col #13	0.96	0.63	1.05	1.75	0.84	0.56	1.22	2.03
Arch Col #14	0.77	0.51	1.36	2.26	0.66	0.44	1.60	2.67
Skewback Col #1	0.38	0.28	3.31	5.53	0.34	0.25	3.85	6.43
Skewback Col #2	0.39	0.28	3.18	5.31	0.35	0.25	3.65	6.09

Table 5.6 Interaction ratios and rating factors for bridge columns under FIRE special truck loading.

Column	AASHTO Eq. (10-155)				AASHTO Eq. (10-156)			
	IR_i	IR_o	RF_i	RF_o	IR_i	IR_o	RF_i	RF_o
Pier Col #2	0.88	0.59	1.16	1.94	0.80	0.54	1.31	2.19
Pier Col #3	0.77	0.53	1.40	2.34	0.69	0.48	1.59	2.65
Arch Col #1	0.81	0.54	1.29	2.15	0.68	0.45	1.57	2.63
Arch Col #2	0.93	0.62	1.09	1.82	0.81	0.55	1.28	2.13
Arch Col #3	1.03	0.68	0.97	1.62	0.91	0.60	1.12	1.87
Arch Col #4	1.07	0.71	0.92	1.54	0.96	0.63	1.05	1.76
Arch Col #5	1.17	0.78	0.83	1.38	1.05	0.69	0.94	1.58
Arch Col #6	1.21	0.80	0.80	1.33	1.08	0.71	0.91	1.52
Arch Col #7	1.09	0.71	0.90	1.51	0.98	0.64	1.02	1.71
Arch Col #8	0.93	0.60	1.09	1.82	0.84	0.54	1.22	2.04
Arch Col #9	1.19	0.78	0.81	1.36	1.06	0.70	0.93	1.56
Arch Col #10	1.27	0.83	0.76	1.26	1.13	0.74	0.86	1.44
Arch Col #11	1.17	0.76	0.83	1.39	1.05	0.68	0.95	1.58
Arch Col #12	1.11	0.72	0.89	1.48	0.98	0.64	1.02	1.70
Arch Col #13	0.99	0.65	1.01	1.69	0.87	0.57	1.17	1.96
Arch Col #14	0.80	0.53	1.30	2.17	0.69	0.45	1.54	2.57
Skewback Col #1	0.44	0.31	2.73	4.56	0.39	0.27	3.18	5.32
Skewback Col #2	0.45	0.32	2.61	4.35	0.40	0.28	3.00	5.01

These factors were determined by solving for the multiple of the live load effects (axial force and bending moment) that set the left part of the AASHTO equations equal to one as shown below. Contrary to the interaction ratios, the capacity check is confirmed when the rating factors exceed one.

$$\frac{A_1 P_D + A_2 P_L (RF)}{0.85 A_s F_{cr}} + \frac{A_1 M_D + A_2 M_L (RF)}{S F_y} = 1$$

$$\frac{A_1 P_D + A_2 P_L (RF)}{0.85 A_s F_y} + \frac{A_1 M_D + A_2 M_L (RF)}{Z F_y} = 1$$

5.2.2 COLUMN Model: Axial Loading

Using the COLUMN rating model, the second term of AASHTO Equation (10-155) that accounts for the bending moment effects in beam-column behavior goes away leaving the following equation

$$\frac{A_1 P_D + A_2 P_L (RF)}{0.85 A_s F_{cr}} = 1$$

This equation can now be solved for the rating factor, RF, which gives

$$RF = \frac{P_R - A_1 P_D}{A_2 P_L}$$

where $P_R = 0.85 A_s F_{cr}$ as specified by AASHTO Equation (10-150) for concentrically loaded compression members. It is important to note that the dead and live load axial forces, P_D and P_L, did not differ significantly between the BEAM-COLUMN and COLUMN rating models.

Table 5.7 lists the rating factors computed for the columns with the equation given above. No significant difference were found in the rating factors for the arch columns symmetrical about the centerline of the arch (i.e., arch columns #1 and #14, #2 and #13, etc.) so only one value is reported for each arch column pair. The same distribution factors and impact factors used in the beam-column analysis (based on braced conditions) were also used for the pure compression analysis. However, the effective length factors were conservatively taken as K = 2 (for in-plane buckling) for the pier columns located closest to the abutments which assumes fixed-free end conditions. For these two columns, the strength was controlled by in-plane buckling since the effective slenderness ratio was larger compared to out-of-plane buckling. This is reasonable considering the large stiffness of the spandrel beam and the rocker bearing at the base support. In the out-of-plane direction, the buckling strength of all the columns was computed assuming an effective length factor of K = 1. The columns were also assumed to be unsupported over their full length with bracing only at the top and bottom ends. This was true also for the skewback columns which had wind bracing at intermittent distances along their length; an effective length factor of unity for these columns assumes the pair buckles together. A discussion of the rating factors based on beam-column and column behavior is provided in the following section.

Table 5.7 Rating factors for bridge columns based on axial loading only.

Column	HS-20		TYPE 3		TYPE 3S2		TYPE 3-3		FIRE	
	RF_i	RF_o	RF_i	RF_o	RF_i	RF_o	RF_i	RF_o	RF_i	RF_o
Pier Col #1	3.28	5.48	4.68	7.82	3.49	5.83	3.32	5.54	3.24	5.41
Pier Col #2	3.35	5.59	4.77	7.96	3.61	6.03	3.46	5.77	3.31	5.52
Pier Col #3	3.26	5.44	4.64	7.74	3.51	5.86	3.37	5.62	3.22	5.37
Pier Col #4	3.19	5.32	4.55	7.59	3.39	5.66	3.22	5.38	3.15	5.25
Arch Col #1 and #14	2.69	4.48	3.72	6.21	3.65	6.10	4.03	6.72	2.67	4.46
Arch Col #2 and #13	3.41	5.70	4.72	7.89	4.70	7.84	5.19	8.66	3.40	5.67
Arch Col #3 and #12	3.93	6.56	5.45	9.09	5.41	9.04	5.99	9.99	3.92	6.54
Arch Col #4 and #11	4.20	7.01	5.81	9.70	5.78	9.65	6.39	10.66	4.18	6.98
Arch Col #5 and #10	4.33	7.23	6.00	10.01	5.97	9.96	6.59	11.01	4.32	7.20
Arch Col #6 and #9	4.38	7.31	6.07	10.13	6.03	10.07	6.67	11.13	4.37	7.29
Arch Col #7 and #8	4.40	7.34	6.09	10.17	6.06	10.11	6.69	11.17	4.38	7.31
Skewback Col #1	3.78	6.30	5.35	8.92	4.26	7.11	4.25	7.09	3.74	6.23
Skewback Col #2	4.56	7.60	6.45	10.77	5.14	8.58	5.13	8.56	4.51	7.52

5.3 Discussion of BEAM-COLUMN and COLUMN Rating Factors

Recall that in the BEAM-COLUMN model, the riveted connections as well as the base supports of the skewback columns were discretized as rigid connections; this approach resulted in the column rating factors shown in Tables 5.2 through 5.6. Contrary to the BEAM-COLUMN model, the column connections in the COLUMN model were idealized as pinned connections which significantly increased the rating factors (see Table 5.7). In Table 5.8, the inventory rating factors from the BEAM-COLUMN and COLUMN models (designated $RF_{i,b\text{-}c}$ and $RF_{i,col}$, respectively) are summarized.

Table 5.8 Inventory rating factors for bridge columns based on beam-column ($RF_{i,b-c}$) and column ($RF_{i,c}$) behavior.

Column	HS-20		TYPE 3		TYPE 3S2		TYPE 3-3		FIRE	
	$RF_{i,b-c}$	$RF_{i,col}$	$RF_{i,b-c}$	$RF_{i,col}$	$RF_{i,b-c}$	$RF_{i,col}$	$RF_{i,b-c}$	$RF_{i,col}$	$RF_{i,b-c}$	$RF_{i,col}$
Pier Col #1	N/A	3.28	N/A	4.68	N/A	3.49	N/A	3.32	N/A	3.24
Pier Col #2	1.18	3.35	1.69	4.77	1.22	3.61	1.13	3.46	1.16	3.31
Pier Col #3	1.42	3.26	2.03	4.64	1.48	3.51	1.37	3.37	1.40	3.22
Pier Col #4	N/A	3.19	N/A	4.55	N/A	3.39	N/A	3.22	N/A	3.15
Arch Col #1	1.30	2.69	1.85	3.72	1.43	3.65	1.36	4.03	1.29	2.67
Arch Col #2	1.10	3.41	1.56	4.72	1.19	4.70	1.13	5.19	1.09	3.40
Arch Col #3	0.98	3.93	1.39	5.45	1.07	5.41	1.02	5.99	0.97	3.92
Arch Col #4	0.93	4.20	1.32	5.81	1.02	5.78	0.98	6.39	0.92	4.18
Arch Col #5	0.83	4.33	1.18	6.00	0.92	5.97	0.89	6.59	0.83	4.32
Arch Col #6	0.80	4.38	1.13	6.07	0.89	6.03	0.86	6.67	0.80	4.37
Arch Col #7	0.91	4.40	1.29	6.09	0.98	6.06	0.94	6.69	0.90	4.38
Arch Col #8	1.10	4.40	1.56	6.09	1.17	6.06	1.11	6.69	1.09	4.38
Arch Col #9	0.82	4.38	1.15	6.07	0.90	6.03	0.87	6.67	0.81	4.37
Arch Col #10	0.76	4.33	1.07	6.00	0.84	5.97	0.81	6.59	0.76	4.32
Arch Col #11	0.84	4.20	1.19	5.81	0.92	5.78	0.89	6.39	0.83	4.18
Arch Col #12	0.90	3.93	1.27	5.45	0.98	5.41	0.93	5.99	0.89	3.92
Arch Col #13	1.02	3.41	1.46	4.72	1.11	4.70	1.05	5.19	1.01	3.40
Arch Col #14	1.31	2.69	1.87	3.72	1.43	3.65	1.36	4.03	1.30	2.67
Skewback Col #1	2.76	3.78	3.87	5.35	3.24	4.26	3.31	4.25	2.73	3.74
Skewback Col #2	2.63	4.56	3.71	6.45	3.10	5.14	3.18	5.13	2.61	4.51

The rating values reported for the BEAM-COLUMN model correspond to AASHTO Equation (10-155) which controlled the capacity for combined axial load and bending rather than (10-156). No rating values are given for pier columns #1 and #2 for the

BEAM-COLUMN model since these two columns are under axial compression only regardless of the connection stiffness.

For the BEAM-COLUMN model, the two pier columns (labeled #2 and #3 in Figure 5.1), the two skewback columns, and four arch columns (labeled #1, #2, #13, and #14 in Figure 5.1) had inventory ratings greater than 1 for all live loads. These eight columns are the ones located on the north and south ends of the Omega Bridge (four on each end) as shown in Figure 5.1. Arch column #8 (located at the apex of the arch rib) had rating values also exceeding 1 at inventory while those for arch column #3 were close to or greater than 1. Thus, these 10 columns were not critical to the bridge capacity. Note also that all the columns had inventory ratings exceeding 1 under TYPE 3 legal truck loading.

The inventory capacity ratings were smallest and equal to 0.80 and 0.76, respectively, for arch columns #6 and #10 under HS-20 and FIRE truck loading; hence, these two arch columns were the most critical. The next three arch columns with the lowest capacity ratings were #5, #9, and #11 which all had inventory ratings between 0.81 and 0.84, also under HS-20 and FIRE truck loading. The column group that followed was arch columns #4, #7, and #12 with inventory rating values between 0.89 and 0.93. From the rating analysis of the BEAM-COLUMN model, it was observed that arch columns #4 through #12 had much smaller axial forces than the pier and

skewback columns. However, the use of rigid connections caused large end moments in the arch columns which were the dominate effects in the interaction equation and decreased the rating factors.

Comparing the inventory rating factors between the BEAM-COLUMN and COLUMN models shows that bending of the columns significantly reduces their capacity. The rating factors of pier columns #2 and #3 decreased by a factor of 2 to 3 when treated as beam-columns rather the pure columns. For the arch columns, the reduction was as much as seven-fold for columns located at the top of the arch rib (i.e., the shorter columns) and between two-fold and three-fold for those located closer to the pinned ends (i.e., the longer columns). This behavior is reasonable since short columns have a high axial compressive strength when treated as a pure column. Furthermore, the two skewback columns experienced a decrease in rating factor between 1 and 2 when bending was considered. These observations suggest that flexure impacts the shorter columns more than it does the longer columns. Thus, when flexure is considered in the rating, the capacity of the short columns becomes much more critical; under axial loading only, short column capacity is not as much of a concern.

An important observation is that the moments applied at the column ends are directly proportional to the stiffness of the riveted connections and thus, the capacity ratings

are inversely proportional. The largest bending moments and smallest capacity ratings result when the connections are assumed completely rigid (i.e., BEAM-COLUMN model). Conversely, the moment magnitudes are equal to zero for pinned connections and results in the largest capacity ratings (i.e., COLUMN model) which overestimates the true column capacities. In actuality, the connection stiffness may be somewhere between fully rigid and pinned behavior which if modeled appropriately would improve the rating factors compared to the BEAM-COLUMN model which underestimates the column capacities. Due to the very wide range in the magnitudes of the rating factors between the BEAM-COLUMN and COLUMN models, it is very difficult to judge where the actual rating factors for the columns will fall. Field testing is recommended to determine a better estimate of the stiffness of the riveted connections and thus, more realistic rating factors. For safety purposes, it is recommended that the rating factors produced from the BEAM-COLUMN be used until a field test can be carried out.

In the summer of 2004, a terrestrial survey of the Omega Bridge was carried out by Lasergeomatics (a division of Bohannan-Huston, Inc. in Albuquerque, NM) using laser scanning techniques. As shown in Tables 5.9 and 5.10, results of the survey showed that a few arch columns were out-of-plumb with angular variations exceeding the AISC (American Institute of Steel Construction) erection tolerance of 1:500 specified in Section 7.13 of the Code of Standard Practice for Steel Buildings and Bridges (AISC, 2001). The columns with out-of-plumb ratios greater than the AISC

erection limit were primarily the shorter arch columns located in the central portion of the arch rib. For these columns, the angular variation was as high as 1:80. Incidentally, these short arch columns were also found to be the more critical columns when evaluated based on beam-column behavior. In addition, a high angular variation (equal to 1:220) was measured at the pier column closest to the south abutment on both the east and west arch rib plane.

Column misalignment can influence beam-column capacity in two major ways. First, it can reduce the total unbraced buckling strength of a frame since more deformation is needed to reach the bifurcation buckling load (i.e., the buckling load assuming plumb columns). However, this particular impact was not considered a concern since the sway buckling resistance of the Omega Bridge was shown to be quite large for several reasons (see discussion given in Section 5.2.1). In addition, the columns were not all misaligned in the same direction in the arch rib plane as shown in Tables 5.9 and 5.10; some lean in the north direction and some lean in the south direction. Since the tendency of the Omega Bridge is to sway in the north direction (due to the road alignment), the south-leaning columns would act to brace the north-leaning columns which would further increase the sway buckling resistance. Note that a decrease in the sway buckling resistance increases the moment magnification factor (i.e., B_2) for the unbraced condition. However, B_2 was left at unity for the Omega Bridge columns for reasons given above and in Section 5.2.1.

Table 5.9 Column alignments on east side of Omega Bridge.

Column	Column Length (ft)	N-S Direction*		E-W Direction*	
		Offset (ft)	Ratio	Offset (ft)	Ratio
Pier Col #1	15.47	-0.071	1:218	+0.039	1:397
Pier Col #2	38.20	+0.015	1:2547	-0.056	1:682
Skewback Col #1	102.92	+0.050	1:2058	+0.268	1:384
Arch Col #1	100.73	+0.028	1:3598	+0.315	1:320
Arch Col #2	75.01	-0.036	1:2084	+0.192	1:391
Arch Col #3	52.87	-0.042	1:1259	+0.097	1:545
Arch Col #4	35.02	-0.055	1:637	+0.056	1:625
Arch Col #5	21.57	-0.102	1:211	-0.010	1:2157
Arch Col #6	13.19	-0.169	1:78	-0.005	1:2638
Arch Col #7	7.57	+0.050	1:151	-0.020	1:379
Arch Col #8	5.98	-0.002	1:2990	-0.101	1:59
Arch Col #9	8.46	+0.024	1:353	+0.047	1:180
Arch Col #10	15.17	+0.012	1:1264	+0.085	1:178
Arch Col #11	26.21	-0.079	1:332	+0.047	1:558
Arch Col #12	42.28	-0.070	1:604	+0.049	1:863
Arch Col #13	61.42	-0.189	1:325	+0.046	1:1335
Arch Col #14	84.63	-0.164	1:516	-0.003	1:28210
Skewback Col #2	87.22	-0.104	1:839	+0.059	1:1478
Pier Col #3	45.89	+0.080	1:574	+0.038	1:1208
Pier Col #4	23.21	-0.025	1:928	-0.099	1:234

* – positive offset values designate North or East direction

Table 5.10 Column alignments on west side of Omega Bridge.

Column	Column Length (ft)	N-S Direction*		E-W Direction*	
		Offset (ft)	Ratio	Offset (ft)	Ratio
Pier Col #1	15.44	+0.072	1:214	+0.028	1:551
Pier Col #2	38.14	+0.007	1:5448	-0.113	1:337
Skewback Col #1	103.66	+0.044	1:2356	+0.214	1:484
Arch Col #1	97.86	-0.012	1:8155	+0.316	1:310
Arch Col #2	74.04	-0.075	1:987	+0.237	1:312
Arch Col #3	52.90	+0.008	1:6613	+0.116	1:456
Arch Col #4	35.26	-0.106	1:333	-0.039	1:904
Arch Col #5	21.06	+0.043	1:490	-0.007	1:3009
Arch Col #6	12.41	+0.004	1:3103	+0.006	1:2068
Arch Col #7	7.16	+0.029	1:247	+0.080	1:90
Arch Col #8	6.21	+0.062	1:100	+0.136	1:46
Arch Col #9	9.26	+0.045	1:206	+0.005	1:1852
Arch Col #10	16.26	-0.010	1:1626	+0.054	1:301
Arch Col #11	26.29	+0.040	1:657	+0.026	1:1011
Arch Col #12	42.18	-0.040	1:1055	+0.047	1:897
Arch Col #13	61.90	+0.960	1:64	-0.034	1:1821
Arch Col #14	85.02	+0.024	1:3543	+0.040	1:2126
Skewback Col #2	87.46	+0.005	1:17492	+0.064	1:1367
Pier Col #3	47.91	-0.087	1:551	-0.103	1:465
Pier Col #4	22.89	+0.029	1:789	+0.035	1:654

* – positive offset values designate North or East direction

The second key impact of column misalignment is that the first order moments at a column end may increase or decrease depending on which direction the column is leaning; recall that the columns lean in opposite directions in the arch rib plane as shown in Tables 5.9 and 5.10. The axial and shear forces of a column will also change but by a smaller amount compared to the change in first order moments. Since column offsets were found in the north-south and east-west direction, the first order force effects will change in both the in-plane and out-of-plane direction of the columns. As mentioned previously, bending at the column ends in the out-of-plane direction was ignored. Although the columns will be subjected to out-of-plane flexure due to the misalignment, these effects were not considered critical since the in-plane bending moments are larger in magnitude. With the exception of the skewback columns, the bending stiffness of the columns are the same in both the in-plane and out-of-plane directions; hence, the in-plane direction with the larger moments will control. Furthermore, the columns are adequately braced in the out-of-plane direction by cross-bracing between the skewback columns. Based on these observations, the effects of column misalignment discussed in the following paragraph focuses on in-plane behavior (i.e., in the arch rib plane).

To illustrate the potential impact of column misalignment on the load rating capacity, consider arch column #10 located on the east side of the Omega Bridge. As discussed earlier, this column had the lowest rating factor based on beam-column behavior. Table 5.9 shows the column to be out-of-plumb in the northern direction a distance of

0.012 ft or 0.14 in. The column is assumed to lean in the direction that increases the first order moment effects compared to the vertical column position. Table 5.11 shows the first order dead load and live load effects and the rating factors of arch column #10 with the column in a vertical position (i.e., offset distance = 0) and an inclined position (i.e., offset distance = 0.14 in.). The change in axial force caused by column misalignment was ignored and thus, the same axial forces determined beforehand with the columns vertical were also used for the inclined case. The increase in first order moments due to column misalignment was approximated by multiplying the axial column load and the offset distance. It is important to note that this approach provides only an estimate of the column misalignment effects. Evaluation of the actual impact of the column misalignment would require remodeling of the entire structure in the arch rib plane and including the measured inclination (direction and magnitude) of each individual column.

Table 5.11 Load rating of arch column #10 in vertical and inclined position.

Offset Distance (in)	Axial force due to Dead Load (kips)	Axial force due to Live Load (kips)	Moment due to Dead Load (kip-in)	Moment due to Live Load (kip-in)	AASHTO Eq. (10-155)		AASHTO Eq. (10-156)	
					RF_i	RF_o	RF_i	RF_o
0.00	101.3	47.0	115.5	219.3	0.76	1.27	0.87	1.45
0.14	101.3	47.0	130.1	226.1	0.73	1.21	0.84	1.39

As shown in Table 5.11, the rating factors computed by AASHTO Equations (10-155) and (10-156) for beam-column behavior decreased about 4% with the column

misaligned a distance of 0.14 in. However, this reduction in the load rating assumes that the column was out-of-plumb under dead and live load axial forces which may not be the case. If the effects of misalignment under dead load are neglected, the total change in moment under live load amounts to about 7 kip-ft (i.e., 226.1 – 219.3 kip-ft = 6.8 kip-ft) which is one-third the change caused by dead and live load combined (i.e., 130.1 – 115.5 + 6.8 kip-ft = 21.4 kip-ft). Under this scenario, the reduction in capacity ratings would be less than 4%.

Aside from the arch columns, another notable impact of the column misalignment has to do with the pier columns. As mentioned previously, these columns were analyzed as compression members since the bottom ends are rocker bearings and thus, there is no shear force or bending moment. This is true only if the columns are perfectly plumb. If the column is out-of-plumb, the axial load acts through an eccentricity equal to the offset distance which produces both shear force and bending moment in the column. Tables 5.9 and 5.10 showed the pier column closest to the south abutment to be out-of-plumb a distance of about 0.07 ft (0.85 in) which gave an angular variation of 1:215 exceeding the AISC erection tolerance of 1:500. Shear and flexure can also be produced if the rocker bearing does not permit free rotation at the bottom end of the column; in this case, shear and flexure result from the horizontal force that develops at the rocker bearing. In either of these two scenarios, the pier columns behave as beam-column members which as stated earlier decreases the

capacity rating compared to pure compression. As shown in Table 5.8, the pier columns closest to the abutment had rating factors comparable to the pier columns closest to the skewback columns based on column behavior. When beam-column behavior was used to evaluate the latter two columns, the inventory ratings exceeded unity. It is therefore anticipated that the pier columns closest to the abutments will also have inventory ratings greater than one, particularly if the moment effects are produced primarily from column misalignment rather than locking of the rocker bearing which will cause larger moments.

As illustrated by the examples given above, column misalignment can reduce the rating factor should the column lean in the direction which increases the first order moments; a more significant reduction in the capacity ratings will result with larger column offsets. Thus, it is recommended that the column misalignment (both direction and magnitude) continue to be monitored periodically by the LANL, particularly the arch columns; the procedure given in this section provides a simple approach to approximate the out-of-plumb effects on the capacity ratings. It is important to note that misalignment of the columns will only change the rating factors of the BEAM-COLUMN model; trivial changes will occur in the column rating factors of the COLUMN model because the axial force in the columns remain about the same and also, there is no bending moment in the columns since the ends are pinned.

CHAPTER 6

LOAD RATING OF ARCH RIB

6.1 Description of Rating Model

As discussed earlier in Chapter 2, the arch rib is a two-hinge parabolic arch with a span of 422.5 ft and a rise of 106.6 ft. Recall that riveted connections were provided between all the columns and the spandrel beam as well as between the arch columns and arch rib; however, the stiffness of these connections is not certain. Therefore, two separate models were developed to load rate the arch rib. Similar to the column evaluation approach presented in Chapter 5, rigid connections were applied at the column ends in the first arch rib model (designated RIGID model) while pinned connections were assumed in the second model (designated PINNED model). The RIGID and PINNED models are shown in Figures 6.1 and 6.2, respectively, which are identical to the BEAM-COLUMN and COLUMN models used to evaluate the columns (see Chapter 5). As shown in these two figures, the entire structure in the arch rib plane was modeled including the spandrel beam, columns and arch rib.

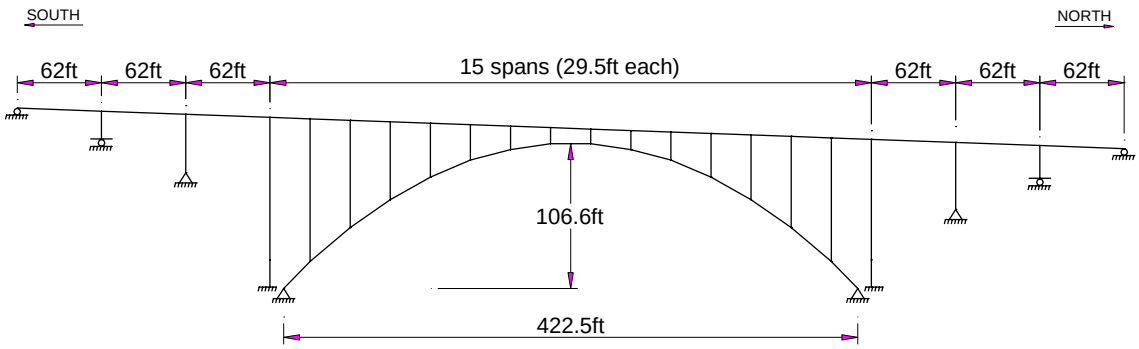

Figure 6.1 RIGID rating model of arch rib.

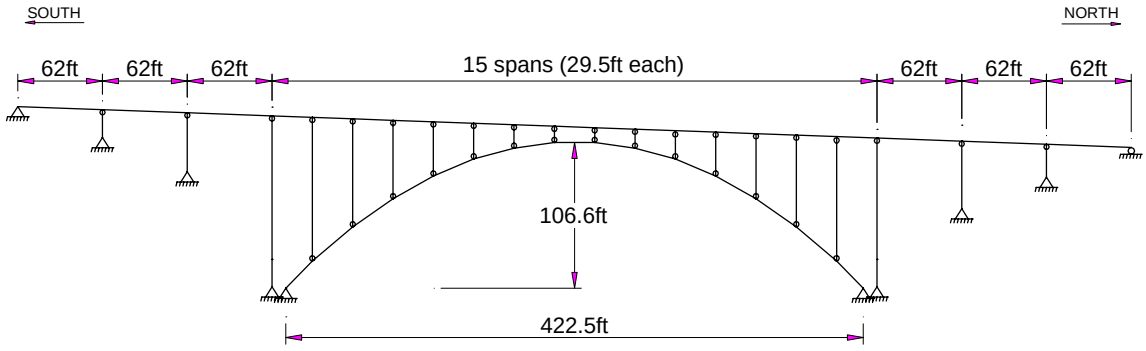

Figure 6.2 PINNED rating model of arch rib.

In the RIGID model, it is assumed that no relative rotation occurs between the connecting members (i.e., the original angle between the members is maintained). On the contrary, the PINNED model assumes that the columns are free to rotate relative to the connecting component (i.e., the spandrel beam or arch rib). In order to maintain structural stability of this model, however, a horizontal restraint was placed at the south abutment. The major difference between the two models is with regard to the forces transferred to the arch rib at the base of the arch columns. The RIGID model results in axial forces, bending moments, and shear forces at these locations while the PINNED model results in only axial forces. The reader is referred back to Section 5.1 for more discussion regarding these two modeling schemes.

The dead load that acts on the arch rib includes that applied to the arch columns (see Section 5.1) plus the self-weight of the arch rib and the wind bracing spanning between the arches. The live load impact factor amounted to

$$I = \min\left(\frac{50}{L+125}, 0.30\right) = \min\left(\frac{50}{4 \text{ x } 29.5+125}, 0.30\right) = \min(0.21, 0.30) = 0.21$$

for the arch rib according to AASHTO Article 3.8.2.1. In this computation, the loaded length (L) was taken as the distance between the two points on the influence lines where the ordinates were equal to zero. Influence line analysis showed the smallest distance to be equal to 4.5 times the distance between adjacent arch columns (i.e., 4.5 x 29.5 ft). In the end, a conservative decision was made to use 4 instead of 4.5 times the arch column spacing for the loaded length (i.e., 4 x 29.5 ft). As discussed in Chapter 4, the arch rib situated on the east side of the Omega Bridge is the most heavily loaded arch due to the location of the traffic lanes and thus, controls the arch capacity. For the eastern arch rib, the distribution factor (including multiple presence effects) is equal in magnitude to the one used to evaluate the eastern spandrel beam (see Table 4.6). Recall that the same distribution factor was also used to evaluate the columns (see Section 5.1). A full listing of the rating calculations for the arch rib under AASHTO HS-20 truck loading is provided in Appendix A5.

6.2 Load Factor Rating Analysis

According to AASHTO Articles 10.37 and 10.55, the capacity of the arch rib shall satisfy interaction equation (10-47) given below:

$$\frac{f_a}{F_a} + \frac{f_b}{F_b} \leq 1 \qquad \text{AASHTO Equation (10-47)}$$

where f_a = the computed axial stress (under dead load and live load plus impact); F_a = the allowable axial stress; f_b = the computed bending stress, including moment amplification, at the extreme fiber (under dead load and live load plus impact); and F_b = the allowable bending stress. In terms of axial forces, f_a may be expressed as

$$f_a = \frac{A_1 N_D + A_2 N_L}{A}$$

where N_D and N_L are the unfactored axial forces and A_1 and A_2 are the load factors under dead load and live load (plus impact). The variable A represents the cross-sectional area of the arch rib. Similarly to f_a, f_b may be rewritten in terms of the bending moments in the arch rib as follows

$$f_b = \frac{A_1 M_D + A_2 (M_L \times A_F)}{S}$$

where M_D and M_L are the unfactored, first-order bending moments under dead load and live load (plus impact); A_F is the amplification factor for the live load plus impact moment; and S is the section modulus of the arch rib at the extreme fiber. The amplification factor, A_F, is computed by AASHTO Equation (10-159) as shown below:

$$A_F = \frac{1}{1 - \frac{1.18T}{AF_e}} \qquad \text{AASHTO Equation (10-159)}$$

where T is the thrust at the quarter point (under dead and live load plus impact) and F_e is the Euler buckling stress, $\pi^2 E / (KL/r)^2$, of the arch rib. In terms of the dead and

live load (plus impact) thrusts, T_D and T_L, AASHTO Equation (10-159) may be rewritten as

$$A_F = \frac{1}{1 - \frac{1.18\,(A_1 T_D + A_2 T_L)}{A F_e}}$$

The effective slenderness ratio (i.e., KL/r) used to compute F_e employs L equal to one-half the arch rib length and r equal to the radius of gyration in the plane of bending; E is equal to the modulus of elasticity in the calculation of F_e. The effective length factor, K, depends on the rise-to-span ratio and the type of arch (see K values given in Table 6.1).

Table 6.1 Effective length factor (K) values for arch rib (AASHTO, 2002).

Rise to Span Ratio	3-Hinged Arch	2-Hinged Arch	Fixed Arch
0.1 – 0.2	1.16	1.04	0.70
0.2 – 0.3	1.13	1.10	0.70
0.3 – 0.4	1.16	1.16	0.72

The arch rib of the Omega Bridge is a 2-hinged arch with a rise-to-span ratio equal to 0.25 (i.e., 106.6 ft divided by 422.5 ft) which gave a K value equal to 1.10. The same KL/r ratio is also used to determine the allowable axial stress, F_a, which is computed by AASHTO Equation (10-160) as follows

$$F_a = \frac{F_y}{1.18}\left[1 - \frac{\left(\frac{KL}{r}\right)F_y}{4\pi^2 E}\right]$$ AASHTO Equation (10-160)

The allowable bending stress, F_b, is taken to be equal to F_y (i.e., the yield stress). In order to use AASHTO Equation (10-47) to evaluate the arch rib capacity, the web plates, stiffener angles, and flange plates of the arch rib must all satisfy the slenderness checks given in AASHTO Article 10.37. The slenderness limits are computed based on the axial and bending stress in the arch rib (under dead load and live load plus impact). Appendix A5 shows that all the slenderness requirements were satisfied for the five different rating vehicles.

Based on the discussion given above, AASHTO Equation (10-47) may be rewritten in terms of the dead load and live load (plus impact) effects as follows

$$\frac{N_D + N_L}{AF_a} + \frac{M_D + M_L\left(\frac{1}{1 - \frac{1.18(T_D + T_L)}{AF_e}}\right)}{SF_b} \le 1$$

For solid rib arches evaluated by the Load Factor Method, AASHTO Article 10.55 specifies the same load factors as the Allowable Stress Method (i.e., $A_1 = A_2 = 1$) at the inventory rating level. Similar to the beam-column analysis of the Omega Bridge columns (see Section 5.2.1), the left side of AASHTO Equation (10-47) given above

represents the interaction ratio at the inventory rating level, IR_i. The arch rib is shown to have adequate capacity when the interaction ratio is less than unity. The inventory rating factor, RF_i, may then be determined by solving the multiple of live load effects which sets the interaction ratio (at the inventory level) equal to 1 as shown below.

$$\frac{N_D + N_L(RF_i)}{AF_a} + \frac{M_D + M_L(RF_i)\left(\dfrac{1}{1 - \dfrac{1.18(T_D + T_L(RF_i))}{AF_e}}\right)}{SF_b} = 1$$

To determine the operating rating factor, RF_o, the inventory rating factor is simply multiplied by a factor 1.67; hence, $RF_i = RF_o / 1.67$ and the equation becomes

$$\frac{N_D + N_L(RF_o/1.67)}{AF_a} + \frac{M_D + M_L(RF_o/1.67)\left(\dfrac{1}{1 - \dfrac{1.18(T_D + T_L(RF_o/1.67))}{AF_e}}\right)}{SF_b} = 1$$

which may be resolved for RF_o.

Structural analysis results showed that the maximum axial force occurs at the supports and the maximum bending moment occurs at the quarter points of the arch rib. However, the location of the rating vehicle that produces the maximum axial force in the arch rib does not coincide with the location that produces the maximum bending moment. Thus, four separate loading cases (designated Case 1 through Case

4) for each rating vehicle were considered in both the RIGID and PINNED rating models as described below.

Case 1: N_{max} @ Point A, M_{max} @ Point C2, T @ Point E

Case 2: N_{max} @ Point B, M_{max} @ Point D2, T @ Point F

Case 3: M_{max} @ Point C1, N_{max} @ Point A, T @ Point E

Case 4: M_{max} @ Point D1, N_{max} @ Point B, T @ Point F

Cases 1 and 2 maximized the axial forces in the arch rib (on the south and north end, respectively) while Cases 3 and 4 maximized the bending moments (on the south and north half, respectively). The locations of points A, B, C1, C2, D1, D2, E, and F on the arch rib mentioned above are shown in Figure 6.3.

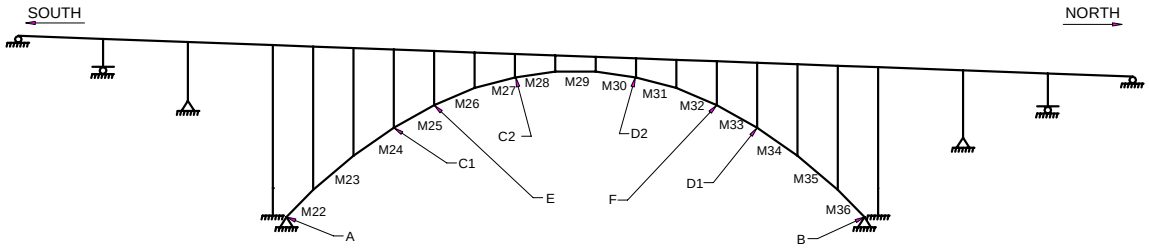

NOTES:
C1 : j end of element M24
C2 : j end of element M27
D2 : i end of element M31
D1 : i end of element M34
E : j end of element M25
F : i end of element M33
A : i end of element M22 (the south support of the arch)
B : j end of element M36 (the north support of the arch).

Figure 6.3 Critical locations of axial force and bending moment of arch rib.

Table 6.2 reports the inventory interaction ratio and the rating factors (inventory and operating) for the arch rib. Values are given for the RIGID and PINNED rating models of the arch rib under the different rating vehicles.

Table 6.2 Interaction ratio and rating factors for arch rib based on AASHTO Equation (10-47).

Rating Vehicle	Case	RIGID Model			PINNED Model		
		IR_i	RF_i	RF_o	IR_i	RF_i	RF_o
HS20	1	0.56	2.53	4.23	0.57	2.41	4.02
	2	0.55	2.60	4.34	0.57	2.36	3.94
	3	0.63	2.14	3.57	0.69	1.77	2.96
	4	0.61	2.20	3.67	0.68	1.81	3.02
TYPE 3	1	0.48	3.58	5.98	0.48	3.47	5.79
	2	0.47	3.73	6.23	0.48	3.48	5.81
	3	0.53	3.05	5.10	0.58	2.53	4.23
	4	0.52	3.13	5.23	0.56	2.58	4.31
TYPE 3S2	1	0.53	2.81	4.69	0.56	2.35	3.92
	2	0.52	2.88	4.81	0.55	2.36	3.95
	3	0.60	2.32	3.87	0.66	1.80	3.01
	4	0.59	2.38	3.98	0.65	1.84	3.07
TYPE 3-3	1	0.54	2.68	4.48	0.58	2.54	4.24
	2	0.51	2.96	4.95	0.57	2.56	4.27
	3	0.62	2.21	3.68	0.69	1.91	3.19
	4	0.60	2.26	3.78	0.67	1.95	3.25
FIRE	1	0.56	2.49	4.17	0.57	2.39	3.99
	2	0.55	2.56	4.28	0.57	2.40	4.01
	3	0.63	2.12	3.54	0.70	1.76	2.93
	4	0.62	2.18	3.63	0.68	1.79	2.99

6.3 Discussion of Rating Factors

As shown in Table 6.2, the rating factors for the RIGID model were larger in magnitude than those for the PINNED model. These results indicate that the arch rib has a lower capacity rating when the riveted connections are modeled as pinned rather than rigid, particularly for Case 3 and 4 which maximized the arch rib bending moments. This makes sense since the bending moments in the arch rib will decrease (thus, increasing the capacity rating) if bending moments are also carried by the bridge columns. Note that this is contrary to the column rating factors which showed smaller magnitudes when rigid connections were used and beam-column behavior was considered.

It is observed that the development of end moments in the bridge columns (at the riveted connections) helps the capacity rating of the arch rib but inhibits the capacity rating of the bridge columns. No significant difference was observed in the axial forces in the arch rib between the PINNED and RIGID models. In addition, the rating factors were about the same on the north and south half of the arch rib due to symmetry (i.e., Case 1 agreed with Case 2 and Case 3 agreed with Case 4). Only slight differences occurred due to the incline of the roadway. Of the four cases, Case 3 had the lowest rating factors (and largest interaction ratios) and thus, controlled the capacity of the arch rib. This was true for the two rating models of the arch rib and the five different rating vehicles. The Case 3 results for both the RIGID and PINNED model are repeated in Table 6.3.

Table 6.3 Interaction ratio and rating factors for arch rib based on AASHTO Equation (10-47) for Case 3.

Rating Vehicle	RIGID Model			PINNED Model		
	IR_i	RF_i	RF_o	IR_i	RF_i	RF_o
HS20	0.63	2.14	3.57	0.69	1.77	2.96
TYPE 3	0.53	3.05	5.10	0.58	2.53	4.23
TYPE 3S2	0.60	2.32	3.87	0.66	1.80	3.01
TYPE 3-3	0.62	2.21	3.68	0.69	1.91	3.19
FIRE	0.63	2.12	3.54	0.70	1.76	2.93

As mentioned before, the PINNED model has the smaller capacity ratings since the riveted connections were assumed to be pinned; this model underestimates the true capacity of the arch rib. On the other hand, the RIGID model is based on rigid connection behavior which results in an overestimate of the actual arch rib capacity for reasons discussed earlier. Similar to the bridge columns, the actual capacity ratings of the arch rib will be somewhere between the values for the pinned-connection and rigid-connection models. A field test could aid in obtaining a better estimate of the arch rib capacity. Nevertheless, the inventory rating values given in Table 6.3 are all greater than 1.75 (i.e., $IR_i > 1.75$) which shows that the arch rib has substantial capacity to indefinitely carry the five rating vehicles. These results are quite comforting considering the arch rib is a fracture critical element.

CHAPTER 7

SUMMARY AND CONCLUSIONS

7.1 Summary

7.1.1 Floor System

From the capacity evaluation of the floor system reported in Chapter 4, the smallest rating factors calculated for the stringers (see Table 4.3), floor beams (see Table 4.5), and spandrel beams (see Table 4.8) are repeated in Table 7.1. Figure 7.1 shows the critical locations of the floor system components. As shown in the figure, the critical section for the stringers is at the negative moment region (i.e., above floor beam FB#2). The two critical floor beams are FB#2 (located one bay from the abutment on the approach spans) and FB#6 (located above arch column #4 on the arch spans). There are two critical sections for the east spandrel beam; the negative moment region located above pier column #1 closest to the abutment and the positive moment region located at mid-span of the third approach span (i.e., at floor beam FB#3). Of the three floor system components, the floor beam controlled the capacity rating. Although the inventory rating of the floor beam at inventory level for the design load is smaller than one (i.e., $RF_i = 0.85$ for the HS-20 Truck), all the rating factors under legal loads are larger than one; thus, load posting of the Omega Bridge is not required based on the floor system capacity. Also note that the operating rating for the FIRE truck is larger than one and the smallest inventory rating is 0.88. This indicates that the floor system is safe for passing of the emergency vehicle.

Table 7.1 Controlling rating factors of the floor system.

Floor System Component	Design Load HS-20 Truck		Legal Load TYPE 3, TYPE 3S2 or TYPE 3-3 Truck		Permit Load FIRE Truck	
	RF_i	RF_o	RF_i	RF_o	RF_i	RF_o
Stringer	1.09	1.81	1.03	1.72	0.97	1.62
Floor Beam	0.85	1.14	1.13	1.89	0.88	1.47
Spandrel Beam	1.15	1.93	1.34	2.23	1.18	1.96

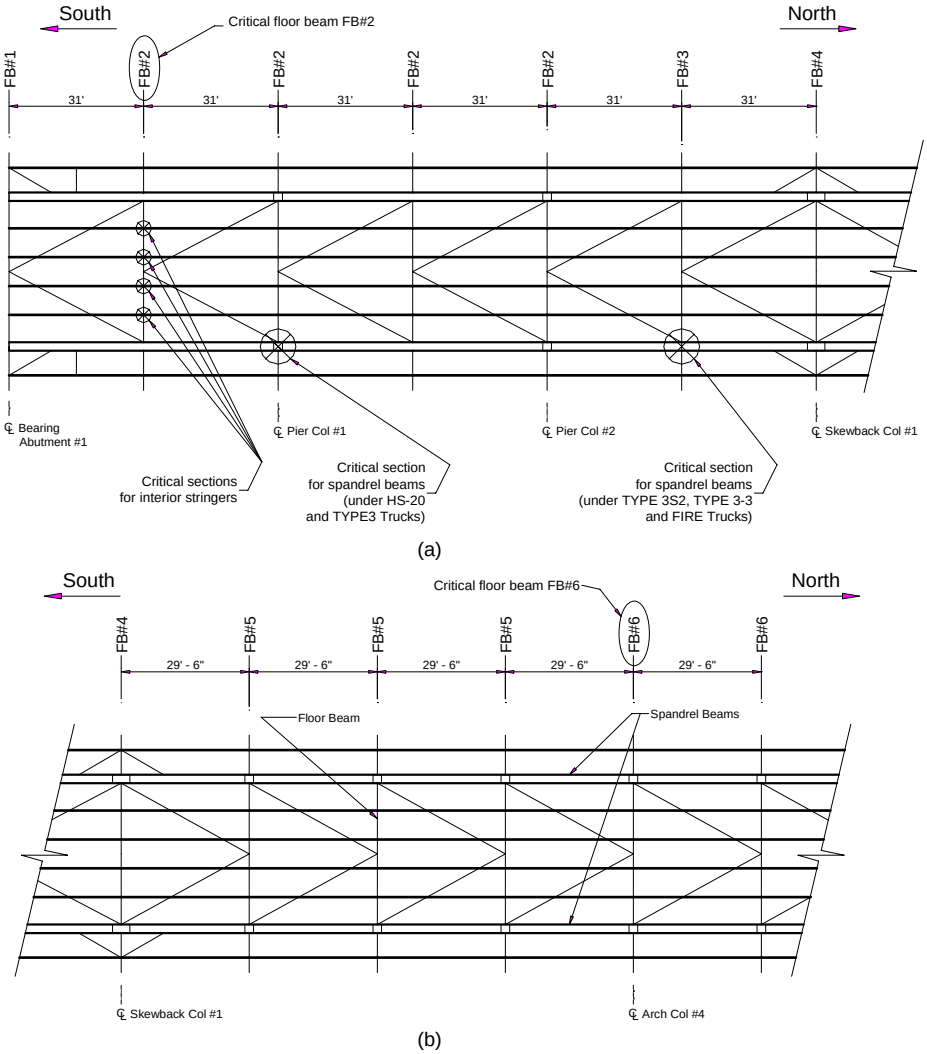

Figure 7.1 Critical locations of the floor system: (a) approach spans and (b) arch spans.

7.1.2 Columns

As discussed in Chapter 5, because of the uncertainty of the rotational connection stiffness at the column ends, two separate models were developed to obtain the rating factors for the columns. The BEAM-COLUMN model represented the most conservative case for the columns (i.e., small rating factors) while the COLUMN model represented the least conservative case (i.e., large rating factors). The lowest rating factors from Tables 5.2 through 5.6 in Chapter 5 for the BEAM-COLUMN model are repeated in Table 7.2. Figure 7.2 shows the locations of the critical columns (i.e., those having rating values smaller than unity at the inventory level) which included arch columns #3 – #6 and #9 – #12. Of these eight columns, arch column #10 had the smallest rating capacity rating. Thus, the rating factors for this critical column controlled the arch column capacity and are the ones reported in Table 7.2. As mentioned earlier, the rating factors produced from the BEAM-COLUMN model represent a lower bound of the column capacity; however, in the interest of safety it is recommended that they be used until the connection stiffness can be more accurately estimated. Based on the rating factors in Table 7.2, all the pier and skewback columns are satisfactory since their rating factors are larger than one at the inventory and operating levels. The rating factors for the arch columns at inventory level under design, legal and permit loads are all less than one. However, they are larger than one at the operating level for all the five rating vehicles and thus, no load posting is required. However, more frequent inspection of the columns than the two-year interval may be warranted as well as traffic monitoring for overloads.

Table 7.2 Controlling rating factors of the columns based on BEAM-COLUMN model.

Column	Design Load HS-20 Truck		Legal Load TYPE 3, TYPE 3S2 or TYPE 3-3 Truck		Permit Load FIRE Truck	
	RF_i	RF_o	RF_i	RF_o	RF_i	RF_o
Pier Column	1.18	1.97	1.13	1.89	1.16	1.94
Arch Column	0.76	1.27	0.81	1.36	0.76	1.26
Skewback Column	2.63	4.39	3.10	5.18	2.61	4.35

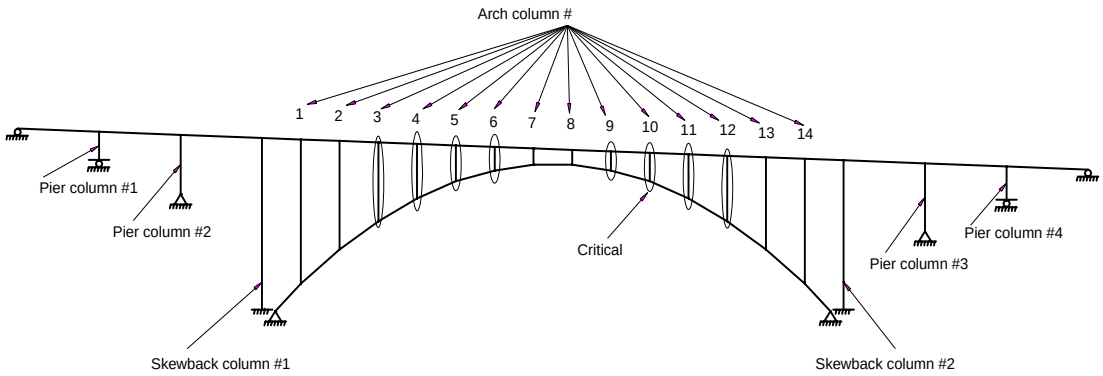

Figure 7.2 Critical locations of the columns.

7.1.3 Arch Rib

Table 7.3 shows the lowest rating factors for the arch rib taken from Table 6.3. Unlike the rating factors of the columns, the rating factors of the arch rib were not much different between the two separate connection models, RIGID and PINNED. Recall that the RIGID model assumed that the riveted connections at the column ends are completely rigid (similar to the BEAM-COLUMN model for the columns) and thus, provide full moment transfer. The PINNED model, on the other hand, assumed pinned connections (similar to the COLUMN model for the columns) and no moment

transfer. As shown in Table 7.3, all the rating factors for the arch rib were found to be larger than one at both the inventory and operating level, and thus the arch rib capacity is satisfactory.

Table 7.3 Controlling rating factors of the arch rib.

Model	Design Load HS-20 Truck		Legal Load TYPE 3, TYPE 3S2 or TYPE 3-3 Truck		Permit Load FIRE Truck	
	RF_i	RF_o	RF_i	RF_o	RF_i	RF_o
PINNED	1.77	2.96	1.80	3.01	1.75	2.93
RIGID	2.14	3.57	2.21	3.68	2.12	3.54

7.2 Conclusions

In general, the Omega Bridge is in satisfactory condition and no load posting is necessary but there are some concerns for the floor beams and the arch columns. Based on the lowest rating factors provided in this report (i.e., $RF_i = 0.76$ and $RF_o = 1.26$ for HS-20 and FIRE trucks), the arch columns are most critical and therefore, control the capacity of the Omega Bridge. However, if a better estimate of the rotational stiffness of the riveted connections is obtained, the arch columns may no longer be the critical components since the rating factors are inversely proportional to the column moments (i.e., connection stiffness ↓ rating factor ↑). In such a case, the floor beam capacity may become more critical than that of the columns. Future evaluation of the Omega Bridge under other vehicles should be based on the column rating values determined under legal loads (i.e., $RF_i = 0.81$ and $RF_o = 1.36$) until further study is carried out to improve the rating factors.

Recall that the floor beam dimensions did not satisfy the AASHTO (2002) compactness requirements and thus, it is recommended that the floor beams be inspected thoroughly for signs of instability. As discussed in Chapter 5, leaning of the columns may also reduce their capacity; thus, monitoring of the column out-of-plumb (both magnitude and direction) is suggested in future capacity rating of the bridge. Load testing along with 3-D finite element analysis is also recommended to refine the calculation of the rating factors. From a load test, the rotational stiffness of the column-end connections and the load distribution to each bridge component could be determined more accurately and thus, provide a better evaluation of the structure. Using the actual stiffness of the riveted connections and the load distribution found from field testing, a 3-D finite element model can be developed and calibrated to the test data. Recall that the column rating factors, which controlled the bridge capacity, increase if the connection stiffness at the column ends decreases. Conversely, the rating factors of the spandrel beams and arch ribs will decrease. However, the spandrel beam and arch rib rating factors will converge to the rating values for the case of pinned connections. Hence, a better estimate of the connection stiffness will not change the final rating factors of the other components (i.e., stringers, floor beams, spandrel beams, arch ribs) since they were conservatively calculated. Finally, a calibrated finite element model can also be used to evaluate the effects of other loads (e.g., temperature, settlement, seismic) on the Omega Bridge capacity.

REFERENCES

American Association of State Highway and Transportation Officials (AASHTO). (1994). *Manual for Condition Evaluation of Bridges*, 2nd Edition, Washington, DC.

American Association of State Highway and Transportation Officials (AASHTO). (1996). *Standard Specifications for Highway Bridges*, 16th Edition, Washington, DC.

American Association of State Highway and Transportation Officials (AASHTO). (2002). *Standard Specifications for Highway Bridges*, 17th Edition, Washington, DC.

American Association of State Highway and Transportation Officials (AASHTO). (2003). *Manual for Condition Evaluation and Load and Resistance Factor Rating (LRFR) of Highway Bridges*, Washington, DC.

American Association of State Highway and Transportation Officials (AASHTO). (2004). *LRFD Bridge Design Specifications*, 3rd Edition, Washington, DC.

American Institute of Steel Construction (AISC). (2001). *Manual of Steel Construction: Load and Resistance Factor Design*, 3rd Edition, Chicago, IL.

Merrick & Company. (1989). "Feasibility Study: Los Alamos Canyon Bridge Deck Replacement." *Report prepared for Los Alamos National Laboratory*, Los Alamos National Laboratory, Los Alamos, NM.

Minervino, C., Sivakumar, B., Moses, F., Mertz, D., and Edberg, W. (2004). "New AASHTO Guide Manual for Load and Resistance Factor Rating of Highway Bridges." *ASCE Journal of Bridge Engineering*, Vol. 9, No. 1, pp. 43-54.

Taly, N. (1998). "Chapter 10. Inspection, Evaluation, Rehabilitation, and Maintenance of Bridges." *Design of Modern Highway Bridges*, McGraw-Hill Inc., New York, pp. 1156-1162.